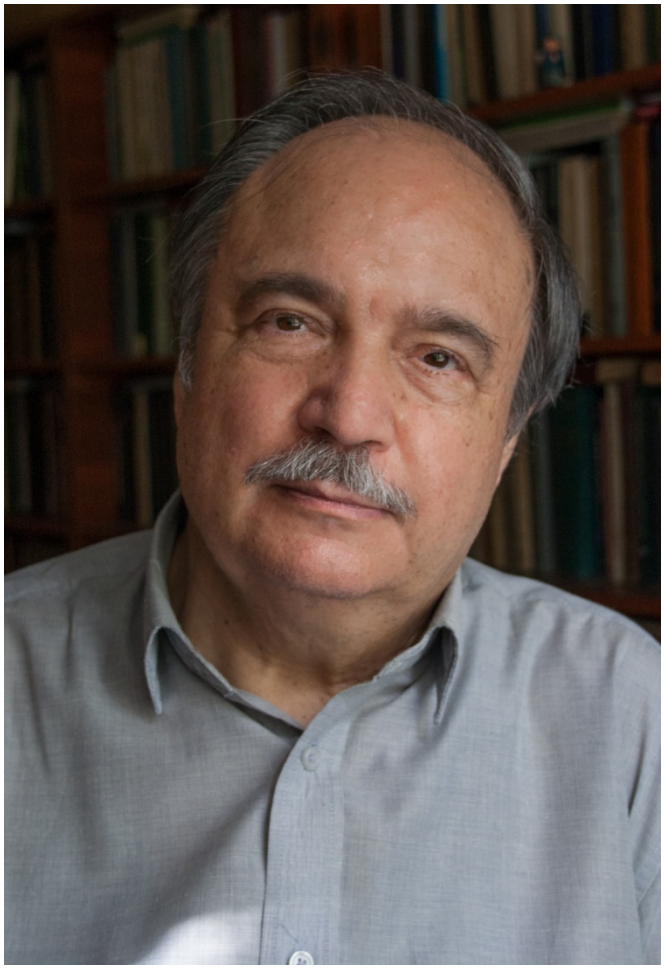
INTERNATIONAL SCIENTIFIC JOURNAL

MATHEMATICAL MODELING

YEAR I ISSUE 3/2017 ISSN (PRINT) 2535-0986
ISSN (WEB) 2603-2929

Published by
SCIENTIFIC-TECHNICAL UNION of MECHANICAL ENGINEERING - INDUSTRY 4.0
Sofia, BULGARIA



Уважаемые коллеги!

Задача нашего журнала – предоставить возможность широкой научной общественности познакомиться с новыми идеями и исследованиями теоретического и прикладного характера из разных областей научного творчества, но объединенных общим языком описания – языком математики. Использование этого языка позволяет лучше осознать единство и взаимозависимость различных, на первый взгляд, явлений и процессов. Мы надеемся, что наш журнал поможет молодым исследователям научиться грамотно излагать свои мысли, а также сможет подсказать им новые направления для творческого поиска. Мы надеемся также, что журнал сможет стать ареной содержательных профессиональных дискуссий, ибо, как хорошо известно, «в споре рождается истина». Со своей стороны, мы сделаем все от нас зависящее, чтобы создать для авторов комфортные и объективные условия общения с Редакционной коллегией. Успехов!

Dear colleagues!

Our journal is aimed to provide an opportunity for the wide-range scientific community to get acquainted with new ideas in theoretic and applied research, in various areas of scientific creativity, united by a common language - the language of mathematics. This language is able to clarify an understanding of the unity and interdependence of phenomena and processes, which initially are seemed to be different. We hope that our journal could be helpful for young researchers, who want to learn how to express correctly their thoughts, and also show them new directions of creativity. We hope that our journal will become an arena for meaningful professional discussions, cause, as it’s well known, "Discussio mater veritas est". For our part, we will do our utmost to create comfortable and objective conditions for communication of authors with the Editorial Board. Good luck!

Andrei Firsov



INTERNATIONAL EDITORIAL BOARD

EDITOR I CHIEF	
Prof. ANDREY FIRSOV Peter the Great St.Petersburg Polytechnic University	RU

Members:		
Abilmazhin Adamov, Prof.	L.N.Gumilyov Eurasian National University	KZ
Alexander Guts, Prof.	Omsk State University	RU
Alexei Zhabko, Prof.	Saint Petersburg State University	RU
Andrey Markov, Prof.	Baltic State Technical University	RU
Andrii Matviichuk, Prof.	Kyiv National Economics University	UA
Andrzej Nowakowski, Prof.	University of Lodz	PL
Anton Makarov, Dr.	Saint Petersburg State University	RU
Armands Gricans, Assoc. Prof.	Daugavpils University	LV
Artūras Dubickas, Prof.	Vilnius University	LT
Avinir Makarov, Prof.	Saint Petersburg State University of Industrial Technologies and Design	RU
Christo Boyadjiev, Prof.	Institute of Chemical Engineering, BAS	BG
Daniela Marinova, Dssoc. Prof.	Technical University of Sofia	BG
Dimitrios Poulakis, Prof.	Aristotle University of Thessaloniki	GR
Evgeniy Smirnov, Assoc. Prof.	Volgograd State Technical University	RU
Giovanni Borgioli, Assoc. Prof.	University of Florence	IT
Haskiz Coskun, Prof.	Karadeniz Technical University of Trabzon	TR
Idilia Bachkova, Prof.	University of Chemical Technology and Metallurgy	BG
Igor Anufriev, Assoc. Prof.	Peter the Great St.Petersburg Polytechnic University	RU
Irena Stojkovska, Prof.	Ss. Cyril and Methodius University in Skopje	MK
Ivana Štajner-Papuga, Prof.	University of Novi Sad	RS
Kanagat Aldazharov, Assoc. Prof.	Kazakh Economics University	KZ
Karl Kunisch, Prof.	University of Graz	AT
Mahomed Agamirza ogly Dunyamalyev, Prof.	Azerbaijan Technical University	AZ
Marius Giuclea, Prof.	The Bucharest University of Economics Studies	RO
Mihail Okrepilov, Prof.	D.I. Mendeleyev Institute for Metrology (VNIIM)	RU
Milena Racheva, Assoc. Prof.	Technical University of Gabrovo	BG
Mohamed Kara, Dr.	Ferhat Abbas Sétif 1 University	DZ
Mohamed Taher El-mayah, Prof	MTI University	EG
Neli Dimitrova, Prof.	Institute of Mathematics and Informatics, BAS	BG
Nina Bijedic, Prof.	Dzemal Bijedic University of Mostar	BA
Oleg Obradović, Prof.	University of Montenegro	ME
Olga Pritomanova, Assoc. Prof.	Oles Honchar Dnipropetrovsk National University	UA
Özkan Öcalan, Prof.	Akdeniz University of Antalya	TR
Paşc Găvruţă, Prof.	Politehnic University of Timisoara	RO
Pavel Satrapa, Assoc. Prof.	Technical University of Liberec	CZ
Pavel Tvrdík, Prof.	Czech Technical University in Prague	CZ
Pavlina Yordanova, Assoc. Prof.	Shumen University	BG
Petr Trusov, Prof.	Perm State Technical University	RU
Rannveig Björnsdóttir, Prof.	University of Akureyri	IS
Roumen Anguelov, Prof.	University of Pretoria	ZA
Sándor Szabó, Dr. Prof.	University of Pécs	HU
Sashko Martinovski, Assoc. Prof.	St. Kliment Ohridski University of Bitola	MK
Sergey Bosnyakov, Prof.	Moscow Institute of Physics and Technology	RU
Sergey Kshevetskii, Prof.	Immanuel Kant Baltic Federal University	RU
Snejana Hristova, Prof.	University of Plovdiv	BG
Svetlana Lebed, Assoc. Prof.	Brest State Technical University	BY
Tomasz Szarek, Prof.	University of Gdansk	PL
Valeriy Serov, Prof.	University of Oulu	FI
Vasily Maximov, Prof.	Saint Petersburg State University of Industrial Technologies and Design	RU
Ventsi Rumchev, Prof.	Curtin University, Perth	AU
Veronika Stoffová, Prof.	University of Trnava	SK
Veselka Pavlova, Prof.	University of National and World Economy	BG
Viorica Sudacevschi, Assoc. Prof.	Technical University of Moldova	MD
Vladimir Janković, Prof.	University of Belgrade	RS
Vladislav Holodnov, Prof.	Saint Petersburg State Institute of Technology	RU
Vyacheslav Demidov, Prof.	Saint Petersburg State University of Industrial Technologies and Design	RU
Yordan Yordanov, Assoc. Prof.	University of Sofia	BG
Yuriy Kuznetsov, Prof.	Nizhny Novgorod State University	RU
Zdenka Kolar - Begović, Prof.	University of Osijek	HR

INTERNATIONAL SCIENTIFIC JOURNAL

MATHEMATICAL MODELING

PUBLISHER:

SCIENTIFIC TECHNICAL UNION OF MECHANICAL ENGINEERING "INDUSTRY 4.0"

108, Rakovski Str., 1000 Sofia, Bulgaria
tel. (+359 2) 987 72 90,
tel./fax (+359 2) 986 22 40**,**
office@stumejournals.com
www.stumejournals.com

ISSN (PRINT) 2535-0986
ISSN (WEB) 2603-2929
YEAR I, ISSUE 3 / 2017

EDITOR IN CHIEF:

Prof. D.Sc. ANDREY FIRSOV
Peter the Great St.Petersburg Polytechnic University, Russia

C O N T E N T S

THEORETICAL FOUNDATIONS AND SPECIFICITY OF MATHEMATICAL MODELLING

ABOUT THE PROBLEM OF DATA LOSSES IN REAL-TIME IOT BASED MONITORING SYSTEMS
Prof. Alieksieiev V. PhD., Prof. Gaiduchok O. PhD. 121

PARAMETRIC INDUCED INSTABILITIES OF BOSONS IN MAGNETAR'S CRUST
Prof. Dr. Dariescu M.-A., PhD. student Mihu D.-A., Prof. Dr. Dariescu C. 123

ON THE USE OF CONFORMING AND NONCONFORMING RECTANGULAR FINITE ELEMENTS FOR EIGENVALUE APPROXIMATIONS
Assoc. Prof Racheva M. Dsc., Prof. Andreev A. Dsc. 127

MATHEMATICAL MODELLING OF TECHNOLOGICAL PROCESSES AND SYSTEMS

A VARIATIONAL SOLUTION OF THE SCHRÖDINGER EQUATIONS IN AN INHOMOGENEOUS COULOMB FIELD
Freinkman B., Polyakov S., Tolstov I. 131

MODELING OF ELECTRONIC STATES OF A SINGLE DONOR IN MIS-STRUCTURE USING THE FINITE DIFFERENCE METHOD
M.Sc. Levchuk E.A., Prof. Lemeshevskii S.V. PhD., Prof. Makarenko L.F. PhD 134

MATHEMATICAL MODEL OF SUSTAINABLE INTEGRATED BIOETHANOL SUPPLY CHAINS
Eng. Dzhelil Y., Prof. DSc Ivanov B., Eng. Ganev E., Assoc. Prof. PhD Dobrudzhaliev D. 138

ENERGY AND EXERGY ANALYSIS OF SEA WATER PUMP FOR THE MAIN CONDENSER COOLING IN THE LNG CARRIER STEAM PROPULSION SYSTEM
PhD. Mrzljak Vedran, Student Žarković Božica, PhD Student Eng. Poljak Igor 144

THE PECULIARITIES OF THE METALLURGICAL DESIGN DEVELOPED THROUGH PROJECT MANAGEMENT PRINCIPLES
Prof.Tontchev N., Assoc. Prof. Dimitrov D. Prof. Hai Hao 148

ELECTRIC POWER SYSTEMS MODELING AND EDUCATION: HYDRO POWER STATIONS MODELING FRAMEWORK
M.Sc. Trashlieva V., M.Sc. Radeva T. PhD. 152

MATHEMATICAL MODELLING OF SOCIO-ECONOMIC PROCESSES AND SYSTEMS

THE SUBJECTIVE MODEL OF RATIONAL CHOICE IN MULTI-AGENT SYSTEMS
Gennady PavlovichVinogradov 155

MATHEMATICAL MODELLING OF SOCIO-ECONOMIC PROCESSES AND SYSTEMS

ILLUSTRATION OF MODEL CREATION ON EXAMPLE OF APPROXIMATIONS TO THE STEADY STATE CURRENT OF CHEMICAL CYCLIC PROCESSES
Assoc. Prof. Dimitrov A.G. PhD. 159

STOCHASTIC COMPUTER SIMULATION OF THE IONIC DIFFUSION THROUGH BIOLOGICAL TISSUES UNDER THE EFFECT OF DIRECT ELECTRICFIELD
MSc. Fawzy HM, Associate Prof. Dr. Salem NM, Prof. Dr. El Sheikh SM and Prof. Dr. El-Messiery MA. 163

ABOUT THE PROBLEM OF DATA LOSSES IN REAL-TIME IOT BASED MONITORING SYSTEMS

Prof. Alieksieiev V. PhD.[1], Prof. Gaiduchok O. PhD.[1]
Lviv Polytechnic National University, Lviv, Ukraine [1]

Vladyslav.I.Alieksieiev@lpnu.ua

Abstract: *Fast growing market of IoT devices revealed a number of complex problems. Among these problems, there is a problem of data losses caused by data package losses or delays while its transition from sensor to server. As anticipated, there are a number of businesses relying on easy opportunity to build real-time monitoring systems using modern software and IoT hardware solutions. Although the growing reliability of contemporary communication networks one can find the problem of making decision about lost or delayed data packages. Current research is dedicated to building an algorithm for compensation of gaps in data series to support real-time monitoring systems with appropriate artificially generated values. Cases of applicability of the algorithm were also studied and discussed.*

Keywords: DATA LOSSES, DATA SERIES, TIME SERIES, IOT, COMPENSATION ALGORITHM

1. Introduction

An IoT growth allowed designing some new platforms for supporting business both with surveillance tools and analytics software applications. Three key features of such platforms are:

- Device – a remote computer like Raspberry Pi or any of its alternatives [1] or some custom hardware device that may include a set of sensors (business solution may consist of a whole network of such devices).
- Internet – any kind of Internet wireless connection via Wi-Fi, GPRS, 3G/4G or anything else supplied with mobile network [2] (business solution may combine different types of Internet service providers to establish connection).
- Cloud – any popular IoT platform [3] to store and process big data.

If one adds some software solution to provide data analytics to that IoT platform than it becomes a powerful business tool supporting real-time monitoring. There is a number of companies developing their own platforms or exploiting powerful cloud services to provide their client with such platform as a reliable business solution.

However, practical use of such system reveals some serious problems. One of most important problem is the problem of lost or delayed data packages. It is obvious that real-time monitoring faces vulnerability to data losses. The data losses or at least delays in package deliveries via Internet over mobile networks is an ordinary problem. Such data losses may cause fake alerts about hardware failures or, otherwise, hide a real failure or a critical state. This means the correct functioning of the whole solution requires some reliable analytical decision about current state of remote device.

2. Prerequisites and means for solving the problem

Let us assume that data packages should come to server within a fixed period of time t_p. This can be any value appropriate for particular business logic. For example, it can be a quarter of an hour – receiving packages every 15 minutes. Again, depending on observed business area we can define a critical time for monitoring and accuracy of alerts. Now we will not discuss the accuracy of data and the actual method or frequency of sensors gathering some values. Thus, we assume that each one sensor gives us a single value across the period of t_p. This value is sent to our server within a single data package (there can be a set of values – one for each sensor in the remote device).

As we analyze some value, than we can assume a range of "good" and "bad" values for normal state and failure state. For example, the range $v_{\min} \le v \le v_{\max}$ can be defined to indicate normal state and values outside of this range can be considered as failure state. For the purpose of analysis of the need of invoking an alert, we can simplify these values to Boolean value: TRUE for normal state, FALSE for failure state. We also need one more value to indicate missing value (package loss) – NULL can be an appropriate one for that state.

Next, we are to define the number of lost packages to consider device to go offline and the size of a "window" to display the current state in the real-time monitoring system. The exact values depend on peculiarities of observed processes and can be defined experimentally. For the purpose of our research, let us assume these values ($N_{offline}$ and N_{window}) to be interdependent:

$$N_{offline} / N_{window} = k \in (0, 1] \quad (1)$$

The k value can describe system sustainability or vulnerability to data losses (with consider to the "window" width). k=1 means sustainable system, and $k \to 0$ means vulnerable system. To be clear we can consider the k value as a measure of customer requirement of data losses vulnerability.

The easiest conditions to make decision about system state (normal or failure) are in case with no data losses. We can use simple probability calculation to find whether system should indicate normal state (n_{true} and n_{false} are the numbers of TRUE and FALSE values among all N_{window} values in the "window" of observation, so that $N_{window} = n_{true} + n_{false}$):

$$n_{true} / N_{window} = 1 - n_{false} / N_{window} > 0.5 \quad (2)$$

Condition "> 0.5" is expected to be strict to be sure that most values indicates the normal state. Table 1 lists some common examples for definition of state indicator according to analysis of sensor values within predefined "window" (N_{window} = 8).

Table 1*: Examples of state definition in case without data losses (N_{window}=8).*

State indicator	Set of values							
Failure	F	F	F	F	F	F	F	F
Failure	F	F	T	F	T	F	F	T
Failure	F	F	F	F	T	T	T	T
Normal	T	T	F	F	T	T	T	F
Normal	T	T	T	T	T	T	T	T

In case of data losses, it looks unclear how to make a reliable decision about current state. On one hand, uncertainty can be ignored, but this will yield mistakes in indication the state. On the other hand, replacement of lost data with artificially generated value is possible, but we cannot be definitely sure about accuracy of the result. Table 2 shows examples of situations, when data loss obstructs ability to indicate system state.

Table 2*: Examples of uncertainty caused by data losses (N_{window}=8, F – FALSE, T – TRUE, N – NULL).*

State indicator	Set of values							
Unknown	F	N	T	N	F	N	T	F
Unknown	N	N	N	N	N	N	F	T
Unknown	N	N	N	N	T	T	T	T
Unknown	N	N	F	F	T	T	N	N
Unknown	T	T	F	F	N	T	T	F
Unknown	T	T	F	T	F	F	N	N

There is a number of algorithms based on calculation of some kind of average values – arithmetic mean or moving average [4, p.153]. However, such approach usually uses only previous data and does not "cover" gaps. Considering trends in data series with moving average "on-the-fly" can be a good method to replace data losses of the last package. Nevertheless, we cannot rely on several artificially generated values to cover new loss. The best way is to store gaps (for example, as a NULL values) and use some other algorithm to cover gaps later.

Another way to fill in the gap is to use some regression model or prediction technique [5, p.279]. For example, one may use simple linear regression or logistic regression model to cover gaps in our time series. Trying to make it better, we can even use polynomial or spline regression models [6, p.166]. Considering these methods, one can mention a high complexity for its implementation. This means that these methods will not fit the requirement of "on-the-fly" data processing, particularly in case of "big data" volumes.

Finally, we can define a couple of requirements for constructing an appropriate algorithm to cover gaps in time series caused by data losses:

- Simplicity – the algorithm should be easy to implement and fast enough to be used "on-the-fly".
- Reliability – the algorithm should give a reliable approximation for each lost value as the most probable value.

3. Solution of the examined problem

First, we are to determine key concept for the algorithm, to fit all above mentioned requirements and limitations: *a lost package value can be replaced with a dominant value of neighbouring packages*. Both with a common sense of this concept we should assume to keep the quantitative majority concept of eq. (2). In the case of missing values presented with its number n_{null} we can rewrite (2) as

$$n_{true} / (N_{window} - n_{null}) = 1 - n_{false} / (N_{window} - n_{null}) > 0.5 \qquad (3)$$

Here, the number of values in the "window" fits the condition $N_{window} = n_{true} + n_{false} + n_{null}$. We should also mention, that $n_{null} < N_{offline}$ is the rule to consider device staying online. Now we can search the way to determine that dominant value to cover gap.

Second, we are to determine known patterns of data losses presented in terms of Boolean values and most appropriate replacement for each missing value. Table 3 lists examples of patterns containing three packages (these cases are obvious according to eq. (3)).

***Table 3**: Example of 3-package pattern (F – FALSE, T – TRUE, N – NULL).*

Replacement	Set of values (X for F or T)						
N→X	N	X	X	…			
N→X	…		X	N	X	…	
N→X	…				X	X	N

Next, in Table 4, we list examples of patterns containing four packages (these patterns were formed excluding the subset of patterns similar to smaller patterns in Table 3).

***Table 4**: Example of 4-package pattern (F – FALSE, T – TRUE, N – NULL).*

State indicator	Set of values (X for F or T and Y for *Not*{X})						
N→X	N	X	Y	X	…		
N→X	N	Y	X	X	…		
N→X	Y	N	X	X	…		
N→X	…		X	N	Y	X	…
N→X	…				X	X	N	Y
N→X	…				X	Y	X	N
N→X	…				X	X	Y	N

Here and in further patterns, we use a general extension to the right rule – "*first step right, next step left*" – and in case of reaching the border of the "window" we can use extension to the free border (left or right accordingly). The rule of extension allows us find easily the dominant value to fit the majority concept. It is important here to remember, that we place packages like time series – from the left to the right. This assumption means we have latest values closer to the right border of the "window" and this is why we should use extension to the right rule. Therefore, this is how we accomplish not only implementation of majority concept, but also consider the influence of the latest state (unlike to most of moving average algorithms).

In some cases a "collision" can happen – the state of emerging new gap instead of value during extension procedure and reaching both borders of the "window". The collision state means repetitive need of extension while gap cover is impossible. To avoid such difficulties in case of collision we use propagation rule – "*replace all nulls with major value (if can be found) or last value (if there is no major value), when number of meaning values exceeds number of nulls*" – and in case of majority of nulls, we can consider device to be offline.

4. Results and discussion

Now let us formalize description of the algorithm for compensation of gaps in data series:

1. Define a "window" width N_{window} with respect to $N_{offline}$ and transition to "offline" state.
2. Use (2) to make decision when there are no gaps.
3. Following extension to the right rule – "*first step right, next step left*" – use (3) to make decision when there are gaps.
4. Use propagation rule – "*replace all nulls with major or last value, when number of meaning values exceeds number of nulls*" – in case of a "collision".

Such kind of algorithm allows covering all the gaps. It is simple enough to be used the same easily both at back-end or front-end solutions to supply appropriate values in customer's real-time IoT based monitoring system. Certainly, it is more likely to utilize the algorithm at front-end to lower the load of servers.

For the purpose of greater accuracy, one can choose between different kinds of moving averages (as a common solution for considering missing values), regressions models (as a common predictive solution) and various approximation techniques (like polynomial or spline).

5. Conclusion

The described algorithm for compensation of data losses fits all requirements of implementation simplicity and reliability. The level of computation efforts and complexity of the algorithm are relevant to arithmetic mean calculations. Simultaneously, the algorithm considers latest values (unlike the moving average techniques). The influence of latest values is crucial for indicating current system state. Considering the initial conditions for the problem and a specific time series, the algorithm appears to be the most adequate and reasonable solution.

6. Literature

1. 10 Best Raspberry Pi and Pi 2 Alternatives. // Beebom.com. – April 18, 2017. – https://beebom.com/raspberry-pi-and-pi-2-alternatives/
2. Global State of Mobile Networks (February, 2017) // OpenSignal, Inc. – February 6, 2017. – https://opensignal.com/reports/2017/02/global-state-of-the-mobile-network
3. Top 20 IoT Platforms in 2018./ Santosh Singh // Internet of Things Wiki – March 8, 2016 – https://internetofthingswiki.com/top-20-iot-platforms/634/
4. Allen B. Downey. Think Stats. — O'Reily, 2015. – 225 p.
5. Head First Data Analysis. — O'Reily, 2009. – 488 p.
6. Peter Bruce and Andrew Bruce. Practical Statistics for Data Scientists. — O'Reily, 2017. – 317 p.

PARAMETRIC INDUCED INSTABILITIES OF BOSONS IN MAGNETAR'S CRUST

Prof. Dr. Dariescu M.-A.[1], PhD. student Mihu D.-A.[1], Prof. Dr. Dariescu C.[1]
Alexandru Ioan Cuza University of Iasi, Romania
E-mail: marina@uaic.ro, denisa.mihu0@gmail.com

Abstract: *In the present work, we are discussing the Klein--Gordon equation describing relativistic spinless particles evolving in the (stationary) magnetar's crust. With the wave function expressed in terms of Mathieu's functions, we compute first-order transition amplitudes, pointing out the role of the strong magnetic induction in transitions to states which may be characterized by values of the model's parameters in instability bands.*
KEYWORDS*: KLEIN-GORDON EQUATION, MATHIEU'S EQUATION, BESSEL FUNCTIONS, PERTURBATION THEORY, MAGNETARS*

1. Introduction

In 1992, Duncan and Thompson introduced the term of magnetar for a type of neutron star with massively boosted magnetic fields whose decay powers the emission of high-energy electromagnetic radiation [1]. The configuration of the background field inside has been extensively worked out and is not unique. Inspired by some previous investigations [2-4], we are assuming a radial magnetic induction, parallel to the surface of a plane slab with finite thickness in the *z*-direction.

As for the matter content, in the magnetar's crust and core, one may expect the existence of various particles, including boson condensates, which might have a significant influence on the star properties. In this respect, the kaons are seen as best candidates, besides nucleons and leptons [5, 6].

In the present work, we are extending our previous results on boson's wave function, solution to the Klein-Gordon equation [3, 4]. Thus, within a perturbative approach, we are discussing special cases for parameters' ranges which are leading to non-trivial quantization laws and to a favored distribution of the magnetic field inside the crust, corresponding to a high probability of transitions.

With reference to the Mathieu's equation, challenging aspects that surround the interest around it and its solutions are more and more invoked as a solid motivation as these manifest in a rich manner, both theoretically – mostly, from algebraic point of view – and practically, i.e. from the applicative side. Concerning the latter, the range of physical situations in which Mathieu functions appear is extremely extended, from elastic wave equations worked in elliptical boundary geometries as it is the case of resonators or waveguides, the motion of quantum particles in a periodic type potential or the stability of floating vessels for harmonious coherent waves of various frequencies and swings [7], to some modern applications as the physics of a capacitor microphone, ferromagnetic substance manifesting elastic oscillations [8], the particle's behavior in different systems of electromagnetic traps [9] or the quantum dynamics of the electrons within the free electron lasers (FEL) [10].
From algebraic point of view, manipulating Mathieu functions is not at all an easy task. The algebra behind the Mathieu functions is extremely intricate, still admitting a range of unsolved mathematical and computational issues. For instance, if we take into account the convergence of Mathieu functions, some authors report slow convergence or the lack of convergence of specific representations of Mathieu functions [11]. Some codes [12], which led to results with single-precision accuracy (7 decimal places), proved to respond negatively to the action of extending them to get a double-precision accuracy (15 decimal places).

An ardent area of research on Mathieu functions focuses on deriving expressions for the dependence of the *Characteristic Exponent* γ on the Mathieu equation parameters, α,β. Due to the physical significance of the Characteristic Exponent, which proves to be intimately connected to the wavelike nature of the physical phenomena modelled by the Mathieu equation, finding relations of the form $\gamma=\gamma(\alpha,\beta)$ constitutes an outstanding mathematical approach. In literature, relations of this type written in power series of β, can be found both for integer [13, 14] and noninteger values of γ [15].

We point out that the literature is pretty rich in treating specific algebraic aspects of Mathieu functions and the main difficulties within the computational analysis [16, 17, 18, 19, 20].

To put it concisely, developing packages for calculating Mathieu functions and operating with them represents an instigation for the modern research being an open territory for algebraic and computational explorations.

2. Magnetic field configuration in the crust

Let us consider, besides the vertical induction B_z, a radial component parallel to the surface of the slab and vanishing at $z=0$ and $z=L$, of the form $B_\rho=b(t)\sin(\kappa z)$ [3, 4]. Working in cylindrical coordinates, the potential component

$$A_\varphi=\frac{B_0}{\kappa}exp\left[-\frac{\kappa^2}{\sigma}t\right]cos(\kappa z) \tag{1}$$

is generating the following electromagnetic field configuration

$$E_\varphi=-\frac{\partial A_\varphi}{\partial t}=\frac{\kappa B_0}{\sigma}exp\left[-\frac{\kappa^2}{\sigma}t\right]cos(\kappa z)$$
$$B_\rho=-\frac{\partial A_\varphi}{\partial z}=B_0 exp\left[-\frac{\kappa^2}{\sigma}t\right]sin(\kappa z)$$
$$B_z=\frac{1}{\rho}A_\varphi=\frac{B_0}{\kappa\rho}exp\left[-\frac{\kappa^2}{\sigma}t\right]cos(\kappa z) \tag{2}$$

which also satisfy the Maxwell equations.

In the following, we are assuming that the time variable is much less the *characteristic time*, $t\ll\tau=\sigma/\kappa^2\sim 1\,Myr$, which is comparable to the average Ohmic timescale, so that the exponential function in (2) can be set to one. However, soon after the crust

forms, the magnetic field is freezing and such objects can be treated as being stationary, with poloidal and toroidal fields of the same order of magnitude [21, 22].

In order to study the semi-classical behavior of the charged scalar field, we start with the Klein-Gordon equation

$$\left[\eta^{ij} D_i D_j - m_0^2\right]\Phi = 0, \tag{3}$$

where the gauge derivatives are expressed in terms of the four-potential components as $D_i = \partial_i - iqA_i$.

For the essential component

$$A_\varphi = \frac{B_0}{\kappa}\cos(\kappa z), \tag{4}$$

the Klein-Gordon equation, in cylindrical coordinates,

$$\left[\Delta - \partial_t^2 - m_0^2\right]\Phi = \frac{2iq}{\rho} A_\varphi \frac{\partial\Phi}{\partial\varphi} + q^2 A_\varphi^2 \Phi,$$

with the variables separation

$$\Phi = \phi(\rho, z) e^{im\varphi} e^{-i\omega t}, \tag{5}$$

leads to the following differential equation for $\phi(\rho,z)$,

$$\frac{1}{\rho}\frac{\partial}{\partial\rho}\left(\rho\frac{\partial\phi}{\partial\rho}\right) + \frac{\partial^2\phi}{\partial z^2} + \left[\omega^2 - m_0^2 - \frac{m^2}{\rho^2} - \left(\frac{qB_0}{\kappa}\right)^2 \cos^2(\kappa z)\right]\phi = -\frac{2mqB_0}{\kappa\rho}\cos(\kappa z)\phi. \tag{6}$$

By identifying the potential operator

$$\hat{V} = -\frac{2mqB_0}{\kappa\rho}\cos(\kappa z), \tag{7}$$

the equation (6) gets the standard form employed in the Perturbation Theory, $\hat{\mathbf{D}}\phi = V\phi$, where $\phi = \psi + \chi$.

The zero-order equation

$$\frac{1}{\rho}\frac{\partial}{\partial\rho}\left(\rho\frac{\partial\psi}{\partial\rho}\right) + \frac{\partial^2\psi}{\partial z^2} + \left[\omega^2 - m_0^2 - \frac{m^2}{\rho^2} - \left(\frac{qB_0}{\kappa}\right)^2 \cos^2(\kappa z)\right]\psi = 0$$

for $\psi(\rho,z) = F(\rho)T(z)$, splits into the following system

$$\frac{d^2F}{d\rho^2} + \frac{1}{\rho}\frac{dF}{d\rho} + \left[\omega^2 - m_0^2 - p_z^2 - \frac{m^2}{\rho^2}\right]F = 0, \quad \text{(a)}$$

$$\frac{d^2T}{dz^2} + \left[p_z^2 - \frac{1}{2}\left(\frac{qB_0}{\kappa}\right)^2 - \frac{1}{2}\left(\frac{qB_0}{\kappa}\right)^2 \cos(2\kappa z)\right]T = 0. \quad \text{(b)} \tag{8}$$

The first equation in (8) is satisfied by the Bessel functions

$$F_m(\rho) = J_m(P\rho), \text{ with } P \equiv \sqrt{\omega^2 - m_0^2 - p_z^2}, \tag{9}$$

while the second one can be identified with the Mathieu-type equation [23]

$$y'' + \left[\alpha - 2\beta\cos(2\zeta)\right]y = 0, \tag{10}$$

of parameters

$$\alpha = \frac{p_z^2}{\kappa^2} - \frac{1}{2}\left(\frac{qB_0}{\kappa^2}\right)^2, \quad \beta = \frac{1}{4}\left(\frac{qB_0}{\kappa^2}\right)^2, \tag{11}$$

and variable $\zeta = \kappa z$. The general solutions of the equation (10),

$$T(\alpha, \beta, \zeta) = \{MathieuC[\alpha, \beta, \zeta], MathieuS[\alpha, \beta, \zeta]\} \tag{12}$$

have been discussed in detail in our previous papers [3, 4], especially with respect to their stability. In general, the Mathieu's functions are of the form $f(z) = e^{i\gamma z}u(z)$, where the Mathieu Characteristic Exponent (MCE), γ, may be real or imaginary, depending on the values of the model parameters.

Nevertheless, we find worth stressing some interesting mathematical properties of these solutions. Thus, the even and odd solutions, can be written as the Fourier series [23]

$$MathieuC = ce_{2n} = \sum_{j=0}^{\infty} A_{2j}^{2n}(\beta)\cos(2j\zeta) \tag{13.a}$$

$$MathieuS = se_{2n+1} = \sum_{j=1}^{\infty} B_{2j+1}^{2n+1}(\beta)\sin((2j+1)\zeta) \tag{13.b}$$

In explicit calculations, one may employ the periodic expressions of the Mathieu's functions (13.a), valid in the first order in β

$$ce_0(z,\beta) = \sum_{j=0}^{\infty} A_{2j}^0(\beta)\cos(2jz) = A_0^0 + \sum_{j=1}^{\infty} A_{2j}^0(\beta)\cos(2jz)$$
$$= \frac{1}{\sqrt{2}}\left[-1 + J_0\left(\sqrt{\beta}exp(-iz)\right) + J_0\left(\sqrt{\beta}exp(iz)\right)\right]$$
$$\approx \frac{1}{\sqrt{2}}\left[1 - \frac{\beta}{2}\cos(2z) + \ldots\right]$$

$$ce_2(z,\beta) = \sum_{j=0}^{\infty} A_{2j}^2\cos(2jz) = A_0^2 + A_2^2\cos(2z) +$$
$$+ \sum_{j=1}^{\infty} A_{2(j+1)}^2(\beta)\cos(2(j+1)z)$$
$$= \frac{\beta}{4} + \frac{4}{\beta}\left[J_2\left(\sqrt{\beta}exp(-iz)\right) + J_2\left(\sqrt{\beta}exp(iz)\right)\right]$$
$$\approx \cos(2z) + \frac{\beta}{12}(3 - \cos(4z)) + \ldots$$

where $J_n\left(\sqrt{\beta}exp(\pm iz)\right)$ are the Bessel functions and we have used the formulas [24]

$$A_{2j}^0 \approx \frac{2(-1)^j}{(j!)^2}\left(\frac{\beta}{4}\right)^j A_0^0; \quad A_{2(j+1)}^2 \approx \frac{2(-1)^j}{j!(j+2)!}\left(\frac{\beta}{4}\right)^j;$$
$$A_0^0 = \frac{1}{\sqrt{2}}; \quad A_0^2 = \frac{\beta}{4}.$$

3. First-order transition amplitude

With the wave function

$$\psi_m = J_m(P\rho)T(\alpha,\beta,\zeta)e^{im\varphi}e^{-i\omega t}, \tag{14}$$

one may compute the one may compute the azimuthal current density component, of quantum origin, which is sustaining the magnetization current,

$$j_\varphi = -\frac{iq}{\rho}\left(\psi_m^*\partial_\varphi\psi_m - \psi_m\partial_\varphi\psi_m^*\right) - 2q^2|\psi_m|^2 A_\varphi$$
$$= 2qJ_m^2|T|^2\left[\frac{m}{\rho} - \frac{qB_0}{\kappa}\cos(\kappa z)\right].$$

In the transition amplitude

$$\mathcal{A} = \int \psi^*_{m'} V \psi_m \rho d\rho d\varphi dz dt = -\frac{4\pi m b}{\kappa} I_1 I_2 \quad (15)$$

where $b \equiv qB_0$, the first integral can be written in terms of the hypergeometric function F_{12} as [23]

$$I_1 = \int_0^\infty J_m(P'\rho) J_m(P\rho) d\rho = \frac{1}{P'}\left(\frac{P}{P'}\right)^m \frac{\Gamma(m+1/2)}{\sqrt{\pi}\Gamma(m+1)} F_{12}\left[\frac{1}{2}, m+\frac{1}{2}, m+1, \left(\frac{P}{P'}\right)^2\right], \quad (16)$$

with $P' > P$. Once we fix the quantum number m, the integral above is expressed as a combination of *EllipticE* and *EllipticK* functions, of variable $(P/P')^2$.

The second integral in (15), i.e.

$$I_2 = \int T^*(\alpha', \beta, \kappa z) \cos(\kappa z) T(\alpha, \beta, \kappa z) dz, \quad (17)$$

should be analyzed for specific ranges of the particle momentum along *Oz*.

For small values of the parameter β, the theory of the Mathieu's functions is well understood. The characteristic values $\alpha_n(\beta)$ are important since they yield periodic solutions and they separate the regions of stability. The resonance condition $\alpha_n \approx n^2$ leads to the momentum quantization relation

$$p_z^2 \approx n^2\kappa^2 + \frac{b^2}{2\kappa^2}, \quad (18)$$

and to a quantized variable in the Bessel functions (9), i.e.

$$P_n^2 = \omega^2 - m_0^2 - \frac{b^2}{2\kappa^2} - n^2\kappa^2. \quad (19)$$

For the particle momentum along *Oz* in the first band of instability

$$\kappa^2 - \frac{b^2}{4\kappa^2} < p_z^2 < \kappa^2 + \frac{3b^2}{4\kappa^2}, \quad (20)$$

the imaginary part of the MCE comes into play, $Im(\gamma) \approx \beta/2$, being responsible for the exponentially growing of the oscillatory wave functions.

By inspecting the stability chart of the Mathieu's functions, one can notice that, for increasing β, the stable regions situated between the characteristic curves $\alpha_n(\beta)$ become more and more narrow and their width is decreasing exponentially to practically discrete eigenvalues. For $\beta > 1$, one has a broad resonance and the solutions (12) are oscillating (along *Oz*) much faster than the electromagnetic field components, the ratio between the frequencies being $\sqrt{\beta} = b/(2\kappa^2)$.

In the case of a magnetar, whose magnetic field is extremely strong, $B_0 \approx 10^{10} - 10^{12}\,(T)$, the parameter β, proportional to the square of the magnetic induction, gets very large values. Thus, for $0 < \alpha < \beta$, i.e.

$$\frac{b^2}{2\kappa^2} < p_z^2 < \frac{3}{4}\frac{b^2}{\kappa^2}, \quad (21)$$

one has to use the following asymptotic expansion for the characteristic values [25]

$$\alpha_n \approx -2\beta + 2(2n+1)\sqrt{\beta}. \quad (22)$$

In our case, the above relation turns into

$$\alpha_n = \frac{b}{\kappa^2}\left[(2n+1) - \frac{b}{2\kappa^2}\right], \quad (23)$$

leading to the Landau-type quantization law for the particle momentum along *Oz*

$$p_z^2 \approx (2n+1)b, \quad (24)$$

and to a quantized variable in the Bessel functions computed with

$$P_n^2 = \omega^2 - m_0^2 - (2n+1)b. \quad (25)$$

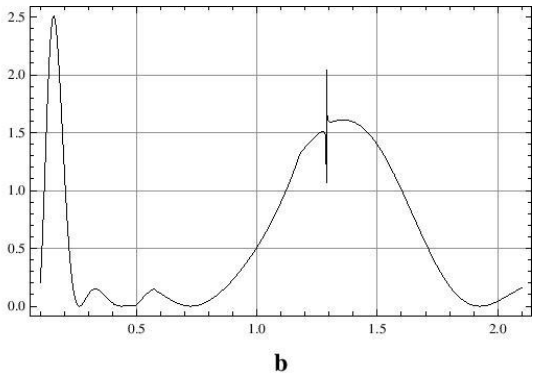


fig. 1 The absolute value of (17) as a function of $b = b/\kappa^2$

In the figure 1, for the transition between $n = 2$ and $n' = n+1$, we are giving, in dimensionless units, the graphical representation of the absolute value of (17), as a function of the parameter $b = b/\kappa^2$ b, characterizing the strength of the magnetic field inside the crust, for a given κ. For both α_n and α_{n+1} positive quantities computed with (23), one may notice the peaks separated by zero minima, corresponding to high probabilities and zero probabilities, respectively.

Let us point out that, for an electron with the momentum along *Oz* given by (24), the distance between the corresponding energy levels is $W = \sqrt{2hqB_0c^2} \approx 1.06\,(MeV)$, for $B_0 = 10^{10}\,(T)$. This ultra-relativistic particle promoted from the level with $n = 0$ to the one with $n = 1$ can produce, by de-excitation photons which will directly convert to electron-positron pairs.

Thus, one may compute only transitions between $n = 0$ and $n' = 1$, for which the characteristic values are given by

$$\alpha_0 \approx \frac{b}{\kappa^2}\left[1 - \frac{b}{2\kappa^2}\right];\ \alpha_1 \approx \frac{b}{\kappa^2}\left[3 - \frac{b}{2\kappa^2}\right], \quad (26)$$

and one can find similar peaks and minima as in the figure 1.

For $\beta \to \infty$, the oscillatory behavior of the Mathieu functions happen in a shrinking neighborhood of $\kappa z = \zeta = \pi/2 + O(\beta^{-1/2})$. In explicit calculations, it is very useful to express the Mathieu function $MathieuC[\alpha_n, \beta, \zeta]$ in terms of parabolic cylinder functions and their derivatives, of variable $t = 2\sqrt{h}\cos\zeta$, with $h = \sqrt{\beta}$, as [25]

$$MathieuC \approx C_n \left\{ D_n(t) \sum_s \frac{A_s(t)}{h^s} + D_n'(t) \sum_s \frac{B_s(t)}{h^s} \right\},$$

where

$$D_n' = \frac{n}{2} D_{n-1} - \frac{1}{2} D_{n+1},\ C_n \approx \left[\frac{\pi\sqrt{\beta}}{2(n!)^2} \right]^{1/4}$$

and the first terms of the polynomials $A_s(t)$ and $B_s(t)$ are

$$A_0 = 1,\quad A_1(t) = \frac{t^2}{2^6} = \frac{\sqrt{\beta}}{2^4} cos^2\zeta,$$

$$B_1(t) = \frac{1}{2^5}\left[t^3 - (2n+1)t \right] \approx \frac{\beta^{3/4}}{4} cos^3\zeta.$$

4. Conclusions

Within a perturbative approach, in the present paper, we are dealing with the Klein-Gordon equation, describing the bosons evolving in the (stationary) magnetar's crust, endowed with the electromagnetic configuration (2). The solution to the zero-order equation, expressed in terms of Bessel and Mathieu functions, is used for computing first-order transition amplitudes, for physically important ranges of model's parameters.

The width of the resonance bands are solely controlled by the parameter β in (11), which is characterizing the magnitude and the distribution of the magnetic field inside the crust.

A special attention is given to ultra-relativistic particles in ultra-strong magnetic field ($\beta > \alpha > 0$), when the particle momentum along *Oz* is satisfying the quantization law (24). The probability of the transition between two adiacent n values is discussed for different ranges of the model's parameters $b = qB_0$ and κ, characterizing the magnitude and the distribution of the magnetic field inside the crust. Thus, for $b/\kappa^2 < 2n+1$, a series of peaks, corresponding to high probabilities, can be noticed in the figure 1.

Finally, we mention that for particles moving in an ultra-strong magnetic field so that the α parameter defined in (11) is negative, the amplitude function is exponentially growing along *Oz* and there is only a narrow interval for the particle momentum p_z, i.e. $|\alpha| < \beta^2/2$, meaning

$$\frac{1}{2}\left(\frac{b}{\kappa}\right)^2 - \frac{1}{32\kappa^2}\left(\frac{b}{\kappa}\right)^4 < p_z^2 < \frac{1}{2}\left(\frac{b}{\kappa}\right)^2 \quad (27)$$

which corresponds to a stable region in the Ince-Strutt diagram [26]. The present work can be extended in several directions, as for example to consider instead of the Klein-Gordon equation, the Dirac equation for relativistic fermions, leading to Mathieu's functions of complex variable and parameters [27].

These situations are very challenging and they are rarely discussed in literature. The existing packages written in MAPLE and MATHEMATICA are insufficient and some routines have been recently developed in [28]. It is worth to mention that the first study which considered a purely imaginary β parameter ($\beta = is,\ s \in \mathbb{R}$) was initiated by Mulholland and Goldstein [29] who deduced an approximative law governing the position of branching points in terms of a quadric growth. The authors detected the first branching point to be. $s_0 \approx 1.47$. For a more detailed analysis on the branching points we recommend [30, 31].

Acknowledgement

This work was supported by a grant of Minister of Research and Innovation, CNCS - UEFISCDI, project number PN-III-P4-ID-PCE-2016-0131, within PNCDI III.

References

[1] Duncan R. C. and Thompson C., Astrophys. J. 392 (1992) L9
[2] Wareing C. J. and Hollerbach R., Astron. Astrophys. 508 (2009) L39;
[3] Dariescu M. A., Dariescu C. and Buhucianu O., Chinese Phys. Lett. 28 (2011) 010303;
[4] Dariescu C. and Dariescu M. A., Mod. Phys. Lett. A 26 (2011) 1245;
[5] Kaplan D. B. and Nelson A. E., Phys. Lett. B 175 (1986) 57;
[6] Nelson A. E. and Kaplan D. B., Phys. Lett. B 192 (1987) 193;
[7] Allievi A. and Soudack A., Int. J. Control 51 (1990) 139;
[8] Phelps III F. M., Hunter J. H., Jr ., Am. J. Phys. 34 (1966) 533;
[9] Ruby L., Am. J. Phys. 64 (1996) 39;
[10] Procida L., Lee H. –W., Opt. Commun. 49 (1984) 201;
[11] Erricolo D., IEEE Antennas Wireless Propagat. Letters 2 (2003) 58;
[12] Zhang, S. J., J. M. Jin, Computation of Special Functions, New York, Wiley (1996);
[13] Hill G. W., Acta Math. 8, 1 (1886) 1;
[14] Campbell, R., Theorie Generale de l'Equation de Mathieu Paris, Masson and Co. (1955);
[15] Tamir T., Wang H. C., National Bureau of Standards – B. Mathematics and Mathematical Physics 69B (1965) 101;
[16] Erricolo D., Uslenghi P. L. E., Elnour B., Electromagnetics, vol. 26 (2006) 57;
[17] Frenkel D. and Portugal R., J.Phys. A: Math. Gen. 34 (2001) 3541;
[18] Toyama N. and Shogen K., IEEE Trans. on Antennas and Propagation AP-32 (1984) 537;
[19] Kokkorakis G. C., Roumeliotis J. A., Mathematics of Computation 70 (2000) 1221;
[20] Alhorgan F. A., ACM Trans. on Math. Software (TOMS) 26 (2000) 390;
[21] Rheinhardt M. and Geppert U., Phys. Rev. Lett. 88 (2002) 101103;
[22] Braithwaite J. and Spruit H., Astron. Astrophys. 450 (2006) 1097;
[23] Gradshteyn, I. S., and I. M. Ryzhik, Table of Integrals, Series and Products, New York, Academic Press (1965);
[24] http://dlmf.nist.gov.;
[25] Ogilvie K.and Olde Daalhuis A. B., Sigma 11 (2015) 095;
[26] Simakhinaa S. V. and Tierb C., Applied Mathematics and Computation 162 (2005) 639;
[27] Dariescu M. A., Dariescu C., Mod. Phys. Lett. A 28 (2013) 1350157;
[28] Blose E. N. et al., Phys. Rev. A 91 (2015) 012501;
[29] Mulholland H. P., Goldstein S., Phil. Mag. 8 (1929) 834;
[30] Hunter C. et al., Stud. Appl. Math. 64 (1981) 113.

ON THE USE OF CONFORMING AND NONCONFORMING RECTANGULAR FINITE ELEMENTS FOR EIGENVALUE APPROXIMATIONS

Assoc. Prof Racheva M. Dsc.[1], Prof. Andreev A. Dsc.[1,2],
Technical University of Gabrovo, Bulgaria [1]
Institute of Information and Communication Technologies – BAS, Bulgaria [2]

milena@tugab.bg

Abstract: *The paper deals with some combinations of conforming and nonconforming rectangular finite elements in order to obtain two-sided bounds of eigenvalues, applied to second-order elliptic opertor. The aim is to use the lowest possible order finite elements. Namely, the combination of serendipity conforming and rotated bilinear nonconforming elements is considered in details. This work continues some recent researches of the authors concerning eigenvalue approximations. Computational aspects of the used algorithm are also discussed. Finally, results from numerical experiments are presented.*

Keywords: RECTANGULAR FINITE ELEMENTS, CONFORMING/NONCONFORMING ELEMENTS, EIGENVALUE APPROXIMATION, TWO-SIDED BOUND

2010 Mathematical Subject Classification: 65N25, 65N30

1. Introduction and Preliminaries

We consider a bounded polygonal domain Ω in R^2 with boundary $\Gamma=\partial\Omega$. Given an integer $m\geq 0$, we use the Sobolev space $H^m(\Omega)$ with a norm $\|\cdot\|_{m,\Omega}$ and $(\cdot,\cdot)$ denotes the $L_2(\Omega)$ – inner product.

Consider the following weak form eigenvalue model problem: Find a number $\lambda\in R$ and a function $u\in V\equiv H_0^1(\Omega), \|u\|_{0,\Omega}=1$ such that

$$a(u,v)=\lambda(u,v), \quad \forall v\in V, \tag{1}$$

where

$$a(u,v)=\iint_{\Omega}\nabla u\cdot\nabla v\,dx\,dy \quad \forall u,v\in V.$$

This problem has a countable sequence of real and positive eigenvalues $0<\lambda_1\leq\lambda_2\leq\ldots$ and the corresponding eigenfunctions $u_1,u_2,\ldots$ satisfy $(u_i,u_j)=\delta_{ij}, i,j\geq 1$.

Let $\{\tau_h\}$ be a family of a rectangulations of Ω which satisfies the usual regularity conditions (see [1]), i.e. there exists a constant $\sigma>0$ such that $h_K/\rho_K\leq\sigma$, where h_K is the diameter of the rectangle $K\in\tau_h$ and ρ_K being the diameter of the largest circle contained in *K*. Then we denote $h=\max\limits_{K\in\tau_h} h_K$.

So, we introduce a conforming finite element space $V_h\subset V$ based on the partition τ_h. Then, the corresponding approximation of (1) is: Find a number $\lambda_h\in R$ and a function $u_h\in V_h$, $\|u_h\|_{0,\Omega}=1$ such that

$$a(u_h,v_h)=\lambda_h(u_h,v_h), \quad \forall v_h\in V_h. \tag{2}$$

For second- and fourth-order self-adjoint elliptic operator the eigenvalues computed using standard conforming finite element method (FEM) are always above the exact ones. This fact comes from minimum-maximum charachterization of the eigenvalues (see for example [2]). So that, it is an important and nontrivial problem to find methods giving lower bounds of the eigenvalues [3]. Herein, we claim a contribution to this specific field. More precisely, this paper is an extension of the authors' research done in [4] and [5].

First, let us consider nine-point conforming rectangular finite element. For any test function *v* and $K\in\tau_h$ the degrees of freedom which we will use are (see Fig. 1(a)) $v(a_j)$ and $\frac{1}{|l_j|}\int_{l_j} v(s)ds$ and $\frac{1}{|K|}\int_K v(x,y)dx\,dy$, where $a_j, j=1,2,3,4$ are the vertices and $l_j, j=1,2,3,4$ are the edges of *K*.

Then, the finite element space V_h is defined by (see [6]):

$$V_h=\left\{v\in H^1(\Omega): v_{|K}=span\left\{1,x,y,xy,x^2,y^2,x^2y,xy^2,x^2y^2\right\}\right\}.$$

We can use also eight-point serendipity conforming finite element (see Fig. 1(b)). In this case:

$$V_h=\left\{v\in H^1(\Omega): v_{|K}=span\left\{1,x,y,xy,x^2,y^2,x^2y,xy^2\right\}\right\}.$$

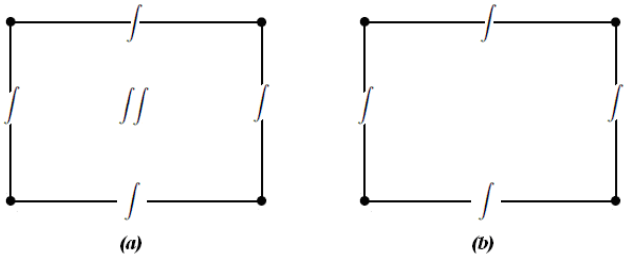


Fig. 1 *(a) 9-point rectangle; (b) 8-point serendipity rectangle*

Now we introduce non-conforming finite element spaces $\tilde{V}_h$ related to the same partition τ_h. We also introduce mesh-dependent bilinear form

$$a_h(u,v)=\sum_{K\in\tau_h} a_K(u,v), \quad u,v\in V,$$

where

$$a_K(u,v)=\iint_K \nabla u\cdot\nabla v\,dx\,dy.$$

Obviously, in case of conforming FEM, $a(\cdot,\cdot)$ and $a_h(\cdot,\cdot)$ coincide.

The space $\tilde{V}_h$ consists of Rannacher-Tourek (i.e. rotated bilinear) nonconforming finite elements denoted by Q_1^{rot} (Fig. 2(a)). Its degrees of freedom are the integral values at the edges of rectangle. An another case for construction of the space $\tilde{V}_h$ is to use the extension of Rannacher-Tourek element (so-called extended rotated bilinear element) denoted by EQ_1^{rot}. The degrees of freedom for this element are the integral values at the edges of the rectangle and the integral value over the rectangle (see Fig. 2(b)).

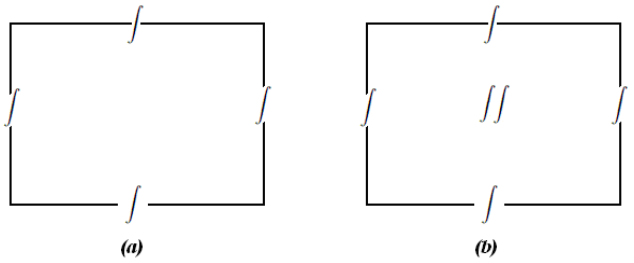


Fig. 2 *(a)* Q_1^{rot} *nonconforming element; (b)* EQ_1^{rot} *nonconforming element*

Let us define a so-called "nonconforming interpolation operator" $\tilde{i}_h : V \to \tilde{V}_h$ such that

$$a_h(v - \tilde{i}_h v, \tilde{v}_h) = 0, \ \forall v \in V, \tilde{v}_h \in \tilde{V}_h. \tag{3}$$

2. Main Result

Our result is based on determining a couple of finite element spaces $(V_h, \tilde{V}_h)$ which verify two sided bounds of eigenvalues λ using the following algorithm:

Algorithm

1. Find (λ_h, u_h) from (2) by means of conforming finite element space V_h;
2. Construct nonconforming space $\tilde{V}_h$ from V_h by eliminating some degrees of freedom in such a way that after obtaining of $\tilde{i}_h u_h \in \tilde{V}_h$ the condition (3) to be fulfilled;
3. Calculate the number $\tilde{\Lambda}_h = a_h(\tilde{i}_h u_h, \tilde{i}_h u_h)$ which approximates the exact eigenvalues λ asymptotically from below.

The case when V_h consists of nine-point quadratic conforming finite elements and $\tilde{V}_h$ contains EQ_1^{rot}-elements is proved by the authors in [4] (see Theorem 1). Later on, we will use the same notations as in [4].

Here, our aim is to prove the validity of the algorithm when V_h use the eight-point serendipity elements and $\tilde{V}_h$ -- Q_1^{rot}-nonconforming elements, respectively.

Thus the nonconforming finite element space is defined by (see [6]):

$$\tilde{V}_h = \left\{ v \in L_2(\Omega) : v_{|K} = span\left\{1, x, y, x^2 - y^2\right\} \right\}.$$

Also, for any $v \in V$:

$$\int_{l_j} \tilde{i}_h v(s)\, ds = \int_{l_j} v(s)\, ds, \tag{4}$$

with edges $l_j, j = 1,2,3,4$.

Introducing the notation $|v_h|_h^2 = a_h(v_h, v_h)$ for any $v_h \in V + \tilde{V}_h$, for our considerations, it is enough to assume the following interpolation inequality for $v \in V$:

$$\left| \tilde{i}_h v - v \right|_h \geq C h^{3/2}. \tag{5}$$

The following theorem contains a main result of the paper.

Theorem 1. Let (λ_h, u_h) be an approximation of the exact eigenpair (λ, u) obtained from (2) by means of eight-point serendipity elements. It the inequality (5) is valid, the number

$$\tilde{\Lambda}_h = a_h(\tilde{i}_h u_h, \tilde{i}_h u_h)$$

approximates λ from below when h is small enough, so that two-sided bounds of λ are obtained:

$$\tilde{\Lambda}_h \leq \lambda \leq \lambda_h. \tag{6}$$

Proof. We adopt the following notations for partial derivatives:

$$\partial_x \bullet = \frac{\partial \bullet}{\partial x}, \partial_y \bullet = \frac{\partial \bullet}{\partial y} \text{ and so on.}$$

Let $v_h \in \tilde{V}_h$ and $v \in V$. Then

$$\begin{aligned} a_h(\tilde{i}_h v - v, v_h) &= \sum_{K \in \tau_h} \iint_K \nabla(\tilde{i}_h v - v) \cdot \nabla v_h \, dx\, dy \\ &= \sum_{K \in \tau_h} \iint_K \left(\partial_x (\tilde{i}_h v - v) \partial_x v_h + \partial_y (\tilde{i}_h v - v) \partial_y v_h \right) dx\, dy. \end{aligned} \tag{7}$$

We choose K_0 to be a fixed reference rectangle. Then the result on arbitrary $K \in \tau_h$ will be transformed from K_0 using an affine transformation.

The equations of the edges of K_0 are:

$$l_{1;3} : y - y_0 = \mp \frac{h_2}{2}; \ l_{2;4} : x - x_0 = \pm \frac{h_1}{2},$$

where (x_0, y_0) is the center of K_0 (Fig. 3) and $h = \sqrt{h_1^2 + h_2^2}$.

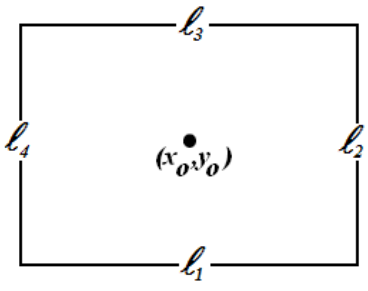


Fig. 3 *Rectangular reference element* K_0

Having in mind that $\tilde{V}_h$ is an incomplete biquadratic polynomial space on K_0, we can write

$$v_h(x,y)=v_h(x_0,y_0)+(x-x_0)\partial_x v_h(x_0,y_0)+(y-y_0)\partial_y v_h(x_0,y_0)$$

$$+\frac{1}{2}(x-x_0)^2\partial_{xx}v_h(x_0,y_0)+\frac{1}{2}(y-y_0)^2\partial_{yy}v_h(x_0,y_0).$$

Then obviously

$$\partial_x v_h(x,y)=\partial_x v_h(x_0,y_0)+(x-x_0)\partial_{xx}v_h(x_0,y_0),$$

$$\partial_y v_h(x,y)=\partial_y v_h(x_0,y_0)+(y-y_0)\partial_{yy}v_h(x_0,y_0).$$

Using Q_1^{rot} -element we have

$$\partial_{xx}v_h=-\partial_{yy}v_h=const. \qquad (8)$$

Applying the properties (4), from (7) we obtain

$$\iint_{K_0}\partial_x\left(\tilde{i}_h v-v\right)\partial_x v_h\,dx\,dy=\partial_x v_h(x_0,y_0)\left(\int_{l_2}-\int_{l_4}\right)\left(\tilde{i}_h v-v\right)dy$$

$$+h_1\,\partial_{xx}v_h\left(\int_{l_2}-\int_{l_4}\right)\left(\tilde{i}_h v-v\right)dy-\iint_{K_0}\left(\tilde{i}_h v-v\right)\partial_{xx}v_h\,dx\,dy$$

$$=-\iint_{K_0}\left(\tilde{i}_h v-v\right)\partial_{xx}v_h\,dx\,dy.$$

In the same manner,

$$\iint_{K_0}\partial_y\left(\tilde{i}_h v-v\right)\partial_y v_h\,dx\,dy=-\iint_{K_0}\left(\tilde{i}_h v-v\right)\partial_{yy}v_h\,dx\,dy.$$

Finally, from (8) it follows that

$$\iint_{K_0}\nabla\left(\tilde{i}_h v-v\right)\cdot\nabla v_h\,dx\,dy=0 \quad \text{for any } v_h\in\tilde{V}_h$$

and the relation (3) is proved for the element Q_1^{rot}.

Now, having in mind that $\|u_h\|_{0,\Omega}=1$, from (3) it follows

$$a_h\left(\tilde{i}_h u_h-u_h,\tilde{i}_h u_h-u_h\right)=a_h\left(\tilde{i}_h u_h,\tilde{i}_h u_h\right)-2\,a_h\left(\tilde{i}_h u_h,u_h\right)$$

$$+\,a_h(u_h,u_h)=a_h(u_h,u_h)-a_h\left(\tilde{i}_h u_h,\tilde{i}_h u_h\right)=\lambda_h-\tilde{\lambda}_h,$$

consequently

$$\lambda_h-\tilde{\lambda}_h=\left|\tilde{i}_h u_h-u_h\right|_h^2\geq 0.$$

Considering that λ_h is a conforming approximation of λ by means of serendipity rectangular finite element [2], we have

$$0\leq\lambda_h-\lambda\leq C\|u_h-u\|_{1,\Omega}^2\leq C_1\left(h^{2-\delta}\right)^2,$$

where δ is a small positive number.

Moreover, from (5) we obtain asymptotically the inequality

$$\lambda-\tilde{\lambda}_h=\lambda-\lambda_h+\lambda_h-\tilde{\lambda}_h=-(\lambda_h-\lambda)+\left|\tilde{i}_h u_h-u_h\right|_h^2$$

$$\geq -C_1 h^{4-2\delta}+C_2 h^3\geq 0.$$

Thus, (6) is proved.

■

3. Numerical Results

The numerical experiments and the resulting approximations of eigenvalues given in this section verify and confirm the validity, reliability and effectiveness of the proposed algorithm.

For purpose of demonstration of the method we propose, we solve the problem (1) on square domain $\Omega=[0,\pi]\times[0,\pi]$.

This choice we have made because of the fact that in this case the exact eigenvalues are known and are equal to $s_1^2+s_2^3$, $s_1,s_2=1,2,3,...$ So that, $\lambda_1=2;\lambda_2=5;\lambda_3=5;...$

For our numerical implementation we divide the domain Ω into N^2 squares, *N = 4; 8; 12; 16; 20*. Thus the mesh parameter *h* is equal to $\frac{\pi\sqrt{2}}{N}$.

We solve the variational discrete problem (2) using conforming quadratic rectangular (9-point) finite elements for V_h (see Fig. 1(a)). As a result, we obtain the approximate eigenvalues λ_h, which give upper bounds for the corresponding exact eigenvalues and the approximate eigenfunctions u_h which we interpolate. Interpolation is done by means of EQ_1^{rot} -nonconforming finite element space (Fig. 2(b)). Obtaining the intepolants $\tilde{i}_h u_h\in\tilde{V}_h$ and calculating the numbers $\tilde{\lambda}_h=a_h(\tilde{i}_h u_h,\tilde{i}_h u_h)$ we get lower bounds for the exact eigenvalues. The results from our numerical experiment for the first three eigenvalues are give in Table 1 and Table 2, respectively.

Table 1: *Approximations of the exact eigenvalues obtained after finite element implementation by means of 9-point conforming rectangular quadratic finite elements*

	$\lambda_{1,h}$	$\lambda_{2,h}$	$\lambda_{3,h}$
N = 4	2.001024281	5.030616274	5.032574099
N = 8	2.000065532	5.002110541	5.004469411
N = 12	2.000013002	5.000450150	5.002890554
N = 16	2.000004120	5.000165987	5.0026355170
N = 20	2.000001689	5.000087946	5.002571064
Exact eigenvalues	2	5	5

Table 2: *Approximations of the exact eigenvalues obtained after nonconforming EQ_1^{rot} – interpolation*

	$\tilde{\lambda}_{1,h}$	$\tilde{\lambda}_{2,h}$	$\tilde{\lambda}_{3,h}$
N = 4	1.902219920	4.655142682	4.656420455
N = 8	1.974624003	4.901823878	4.903948840
N = 12	1.988641719	4.955268267	4.957598338
N = 16	1.993595054	4.974626877	4.977033035
N = 20	1.995896103	4.983705600	4.986147765
Exact eigenvalues	2	5	5

Next, for the same model problem we demonstrate the efficiency of the proposed algorithm for more simple finite elements.

We solve the variational discrete problem (2) using eight-point serendipity conforming finite elements for V_h (Fig. 1(b)). As a result we obtain the approximate eigenvalues λ_h giving upper bounds for the corresponding exact eigenvalues and the approximate eigenfunctions u_h which we interpolate. Interpolation is done by means of Q_1^{rot}-nonconforming finite element space (Fig. 2(a)). Obtaining the intepolants $\tilde{i}_h u_h \in \tilde{V}_h$ and calculating the numbers $\tilde{\Lambda}_h = a_h(\tilde{i}_h u_h, \tilde{i}_h u_h)$ we get lower bounds for the exact eigenvalues. The results from our numerical experiment for the first three eigenvalues are give in Table 3 and Table 4, respectively.

Table 3: *Approximations of the exact eigenvalues obtained after finite element implementation by means of 8-point serendipity conforming rectangular finite elements*

	$\lambda_{1,h}$	$\lambda_{2,h}$	$\lambda_{3,h}$
N = 4	2.001091866	5.032026684	5.032037751
N = 8	2.0000664317	5.002126594	5.004493905
N = 12	2.000066432	5.000451611	5.002891734
N = 16	2.000004134	5.000166314	5.002635721
N = 20	2.000001692	5.000088072	5.002571117
Exact eigenvalues	2	5	5

Table 4: *Approximations of the exact eigenvalues obtained after nonconforming Q_1^{rot} – interpolation*

	$\tilde{\Lambda}_{1,h}$	$\tilde{\Lambda}_{2,h}$	$\tilde{\Lambda}_{3,h}$
N = 4	1.881513965	4.124185537	4.124191017
N = 8	1.949450862	4.748511061	4.750459845
N = 12	1.977322992	4.885339250	4.887582856
N = 16	1.987202566	4.934933147	4.937289058
N = 20	1.999994922	4.979244596	4.980117042
Exact eigenvalues	2	5	5

The approximate values in Table 1 and Table 3 are greater than the exact ones and the sequences $\{\lambda_{j,h}\}, j=1,2,3$ obtained when the mesh parameter *h* decreases are decreasing. This is a reasonable and expected numerical result, because of the fact that conforming finite element methods are used [2].

On the part of the nonconforming interpolation implementation, from the approximations of the eigenvalues given in Table 2 and Table 4, respectively, it is clear that the resulting approximation of the exact eigenvalues is from below. When the mesh parameter *h* decreases, the sequences $\{\tilde{\Lambda}_{j,h}\}, j=1,2,3$ are increasing and go to the corresponding exact eigenvalue.

As it is well-known from the theoretical point of view, nine-point and eight-point conforming finite elements give similar results concerning the error estimates (Table 1 and Table 3). As a consequence of this, as well as from the fact that Q_1^{rot} and EQ_1^{rot} - nonconforming finite elements give one and the same convergence order, the results in Table 2 and Table 4 are also similar.

3. Conclusions

The proposed algorithm gives lower and upper bounds of the eigenvalues simultaneously – only to solve by conforming FEM the eigenvalue problem once and additionally to apply a nonconforming interpolation to the conforming solution is needed.

In this paper use of more simple and convenient finite elements is proposed, proved theoretically and demonstrated.

Acknowledgements This work was partially supported by the Technical University of Gabrovo under grant D1703E/2017.

References

1. P.G. Ciarlet, The Finite Element Method for Elliptic Problems. North-Holland, Amsterdam, New York, Oxford, 1978.
2. I. Babuška, J. Osborn, Eigenvalue Problems, In Handbook of Numerical Analysis, Vol. II, (Eds. P. G. Lions and Ciarlet P.G.), Finite Element Methods (Part 1) North-Holland, Amsterdam, 641-787, 1991.
3. Y.D. Yang, Z.M. Zhang, F.B. Lin: Eigenvalue approximation from below using nonconforming finite elements, Science China, Mathematics (2010), Vol. 53 No. 1, 137-150.
4. A. B. Andreev, M. R. Racheva, A new algorithm for two-sided eigenvalue approximation, Comp. rend. Acad. bulg. Sci. 70, 1207 – 1214, No 9, 2017.
5. M.R. Racheva , A.B. Andreev: Numerical Aspects for Obtaining Two-sided Bounds of Eigenvalues. International Scientific Journal "Science. Business. Society", 3, Scientific Technical Union of Mechanical Engineering, 2017, ISSN:2367-8380, 104-107
6. S. Brenner, L.R. Scott: The Mathematical Theory for Finite Element Methods, New York, Springer-Verlag, 1994.

A VARIATIONAL SOLUTION OF THE SCHRÖDINGER EQUATIONS IN AN INHOMOGENEOUS COULOMB FIELD

Freinkman B., Polyakov S., Tolstov I.
Keldysh Institute of Applied Mathematics of RAS – Moscow, Russia
E-mail: freink@newmail.ru, polyakov@imamod.ru, tolstov_ilya@inbox.ru

Abstract: The present work is devoted to computer modeling of the emission processes from the surface of graphene. The pivotal obstacle for emission is a model of the unperturbed emission surface. The hydrogen-like atom model is one of the useful approaches describing the states of the emission surface. In [1] this model was used considering ion screening in the Brandt model [2]. To calculate the ground state of the electron, we used the variational solution of the Schrodinger equation, based on the minimization of the potential energy of an electron in the field of a homogeneous ion. However, the field of the screened singly ionized carbon atom in the Brandt model is not homogeneous. Therefore, it was shown in [3] that it is possible to obtain a binding energy error of up to 40% when using only the external screening parameter without taking into account the inhomogeneity. In this paper, we consider the effect of the ion screening parameter in the Brandt model λ and the algorithm for determining it by minimizing the total energy of the electron interaction in s state in two parameters: the effective ion charge and the ion screening parameter. The obtained solution of the Schrödinger equation is used to calculate the ground state of a hydrogen-like carbon atom in a graphene lattice at zero temperature and is compared with the results of [2, 4].
KEYWORDS: GRAPHENE, PSEUDOPOTENTIAL OF A HYDROGEN-LIKE ATOM, COMPUTER SIMULATION FOR GRAPHENE LATTICE

1. Introduction

The present work is devoted to computer modeling of the emission processes from the surface of graphene - a perspective material for micro- and nanoelectronic devices. The pivotal obstacle for emission is a model of the unperturbed emission surface, determining the theoretical spectrum and the emission threshold current. One of the approaches to describe the states of the emission surface is the hydrogen-like atom model, which is used for light elements of the periodical table. In [1], a lattice of hydrogen-like atoms with a screened ion in the Brandt model was used to calculate the ground state of atoms of the graphene surface [2]. To calculate the ground state of an electron, the Schrödinger equation was solved by minimization of the potential energy of the electron in the ion field, which assumes homogeneity of the ion field. However, the field of the shielded singly ionized carbon atom in the Brant model is not homogeneous. Therefore, it was shown in [3] that using only the external screening parameter without taking into account the inhomogeneity, it is possible to obtain a binding energy error of up to 40%, which is unacceptable even for qualitative theory. In this paper, we consider the influence of the ion screening parameter in the Brant model λ and the algorithm for determining it by minimizing the total energy of the electron interaction in s state in terms of two parameters: the effective ion charge and the ion screening parameter. The obtained solution of the Schrodinger equation is used to calculate the ground state of a hydrogen-like carbon atom in a graphene lattice at zero temperature. The obtained solution is compared with the results of [2, 4].

2. Prerequisites and means for solving the problem

In [1], for the variational solution of the Schrödinger equation for an electron in a hydrogen-like atom, the method of determining the wave function in a given field was used [6]. This technique is based on minimizing the discrepancy of the difference between the total energy of an electron in a known ion field and the effective field

$$\tilde{U}_i(r) = \frac{q}{r} + A \qquad (1)$$

for which a self-similar solution of the Schrodinger equation is known, depending on the parameters of this field. For the ground state of a hydrogen-like carbon atom, this leads to a minimization of the functional

$$J_s(q,\lambda) = \int_0^\infty \psi_{2s}^2(x)\left[U_i(r,\lambda) - \frac{q}{r}\right]x^2 dx + \frac{q^2}{2n^2} + A,$$
$$\psi_{2s}^2(r) = \left(1 - \frac{x}{2}\right)^2 \exp(-x), \quad x = \frac{2q}{n}r. \qquad (2)$$

In this case, it is implicitly assumed that the field is uniform over *r*. However, the field of the screened ion in the Brandt-Kitagawa model is not uniform:

$$U_i(r) = \frac{1}{r} + \frac{Z-1}{r}\exp\left(-\frac{r}{\lambda_i}\right), \quad \frac{\partial}{\partial r}U_i(r) \neq kU_i(r). \qquad (3)$$

According to the virial theorem, the average total energy of the finite motion of an electron in the Coulomb field is related to the average kinetic and mean potential energy by the equation

$$\bar{E} = -\bar{T}, \quad \bar{U} = 2\bar{E}. \qquad (4)$$

Using the expression for the mean kinetic energy in a nonuniform field [5], we obtain the distribution of the total energy of the bound electron in an inhomogeneous field ion:

$$E(r) = \frac{r}{2}\frac{\partial}{\partial r}U_i(r) + U_i(r). \qquad (5)$$

Fig. 1 shows the distribution of the total energy of an electron with and without an accounting of the inhomogeneity of this field. As can be seen from the figure, the inhomogeneity of the field appears mostly near the nucleus. Therefore, taking into account the distribution of the probability density in s and p states, the influence of the field inhomogeneity on the binding energy of the electron with the ion will be larger for the electron in the s state than in the p state.

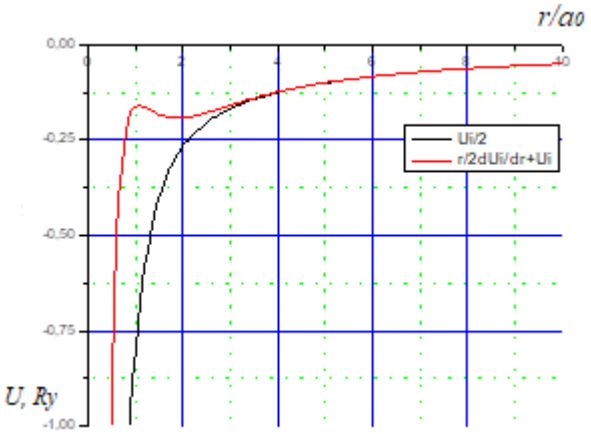


Fig. 1. *Comparison of the distribution of the total energy along the radius for a finite motion of an electron*

in the field of the singly charged carbon ion in the Brandt model without and taking into account the inhomogeneity of the field.
Therefore, in an arbitrary field ion at solving the problem of variations on the characterization of the effective uniform field should be based on minimizing the total energy of the finite electron motion in a particular quantum state. The effective charge of the ion - q, and the external screening parameter - λ, are determined by the following system of nonlinear equations:

$$\frac{\partial}{\partial q}\left\{\int_0^\infty \psi_{2s}^2(x)\left[U_i(r,\lambda)-\frac{q}{r}\right]x^2dx+\frac{q^2}{2n^2}\right\}\Bigg|_{q=q_m}=0$$
$$A=-\int_0^\infty \psi_{2s}^2(x)\left[U_i(r,\lambda)-\frac{q_m}{r}\right]x^2dx-\frac{q_m^{22}}{2n^2} \quad (6)$$

The hypothesis adopted by us was realized with the help of a numerical solution of the problem (6).

3. Solution of the examined problem

Figures 2a and 2b show numerical solutions of this problem for an electron in the s state with and without consideration for the inhomogeneity of the ion field for different values of the internal screening parameter λ of the ion in the Brandt model.

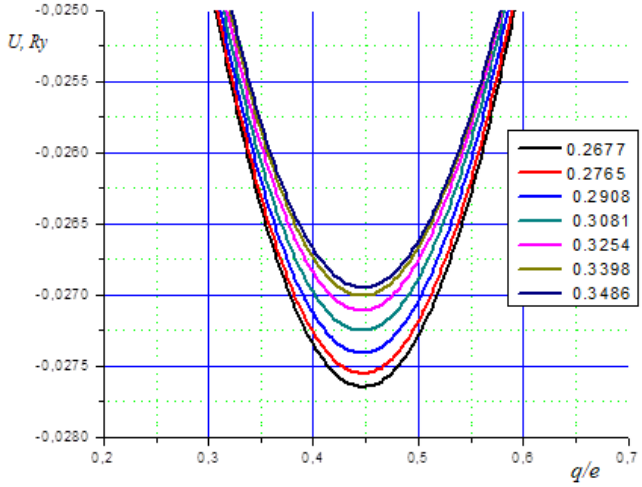


Fig. 2a *Numerical solution of the variational task for an electron in the s state taking into account the inhomogeneity of the ion field.*

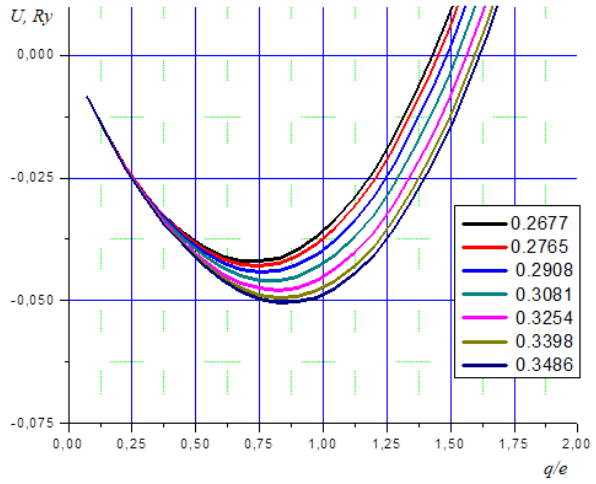


Fig. 2b *Numerical solution of the variational task for an electron in the s state without taking into account the inhomogeneity of the ion field. Different lines explain different values of screening parameter λ*

Comparison of these solutions shows that the lowest value of the effective charge of the ion q and the external screening potential of the atom *A* will be when the heterogeneity of the ion field is considered.

4. Results and discussion

For comparison, Fig. 3 shows the solution of this task using the previously used method of the variational solution of the Schrodinger equation [1, 6].

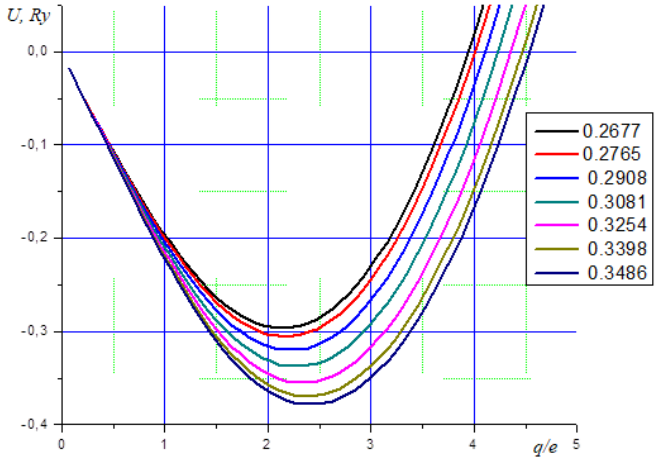


Fig. 3 *The variational solution of the Schrödinger equation by the method [6].*

Comparison of this solution with previous ones shows that the effective charge of the ion and the screening parameter of the atom are much higher and the binding energy exceeds the ionization potential of carbon. It can be assumed that these discrepancies go from the fact that the method of the variational solution of the Schrödinger equation [6] is more suitable for atoms with a large number of valence electrons.

An analysis of the dependence of the solution of the variational task on the parameter of the internal screening λ of an ion in the Brandt model is shown in Fig. 4.

It is interesting to note that the optimal value of λ is close to its value for a neutral atom in the Brandt model.

Figure 5 compares the obtained distribution of the field of a hydrogen-like atom along the radius with analogous distributions in [2,4].

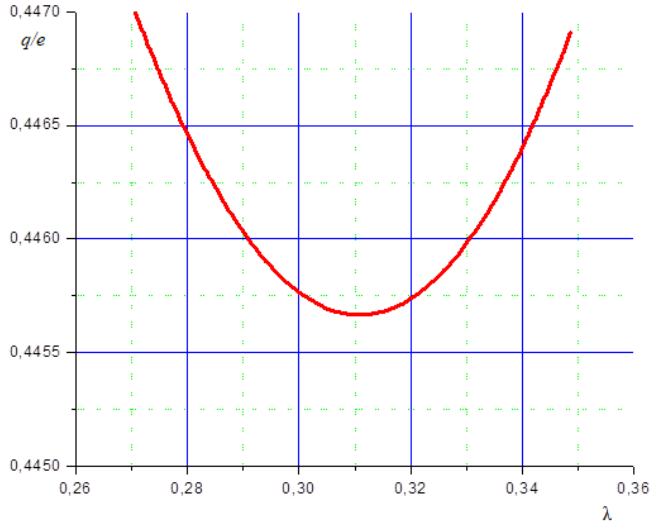


Fig. 4 *Dependence of the effective charge of an ion on the parameter of the internal screening of the ion λ in the Brandt model.*

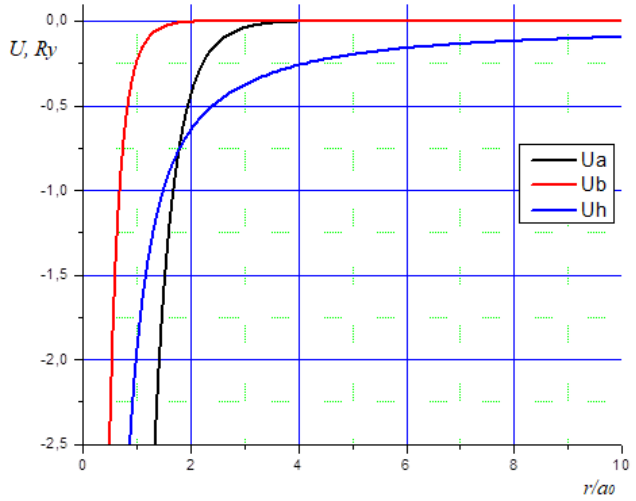


Fig. 5 *Comparison of the distribution of the field along the radius of a hydrogen-like atom with similar distributions in [2,4].*

It can be seen that the distribution of the field of the hydrogen-like atom is allocated between the distributions near the nucleus in other models and it decreases much more slowly in the distance.
When considering these results, it should be noted that the model Brandt atom is surrounded by an electron gas, but only the effect of neighboring atoms is taken into account in the model Abrahamson.
Because in the future we will be interested in the ground state of a hydrogen atom in the lattice of graphene, then the profiles of the potential distribution between two lattice sites in these models were calculated.

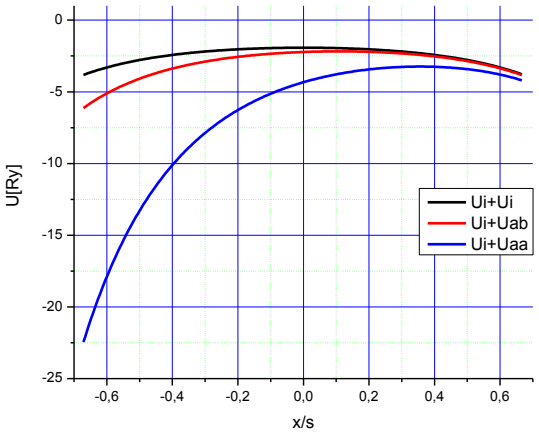


Fig. 6 *Potential well for a weakly bound electron accounting the field of an ion or atom at an adjacent graphene lattice site.*

Figure 6 shows that in the Abrahamson model the potential well is unnaturally deep while in the Brandt model it is close to the atom and the surrounding ion.

5. Conclusion

The problems of modeling the emission processes from the graphene surface are considered. To describe the states of the emission surface at zero temperature, we used a hydrogen-like atom model, taking into account the screening of the ion in the Brandt model. To calculate the ground state of an unbound electron located in a graphene lattice site, we used the variational solution of the Schrödinger equation. It corresponds to a minimum of the total interaction energy of an unbound electron in the s state with the corresponding lattice ion. In numerical experiments, minimization was carried out in two parameters: the effective ion charge and the ion screening parameter. However, we restricted ourselves to the first iteration of the minimization of the energy functional, since it is assumed hereinafter account of the influence of the field in the immediate environment of the atoms of the electron energy with the ion in the lattice site. Our calculations showed that in the considered model it is important to take into account the inhomogeneity of the field produced by the screened lattice ion.
The work was supported by Russian Fund for Basic Research (Project No. 17-01-00973-a

6. References

1. B.G. Freinkman. Pseudo-potential atom model for carbon one in graphen lattice // Matematicheskoe modelirovanie, 2015, v. 27, No. 7, p. 122-128 (in Russian).
2. W. Brandt, and M. Kitagawa. Effective stopping-power charges of swift ions in condensed matter // Phys. Rev. , 1982, v. B25, n. 9, p. 5631-5637.
3. Tolstov I., Freinkman B., Polyakov S. Variation solution of the Shrodinger eqiation in an inhomogeneous central field as applied to emission problems / Mathematical modeling and computational physics (MMCP'2017): Abstracts of International Conference (2017 July 3-7, Dubna, Russia). - Dubna: JINR, 2017. - p. 54.
4. A.A. Abrahamson. Born-Mayer-type interatomic potential for neutral ground-state atoms with Z = 2 to 105 // Phys. Rev., 1969, v. 178, p. 76-79.
5. Fok V.A., Nachala kwantovoi mekhaniki (Introduction to quantum mechanics) (Moscow, 1974)
6. A.F. Nikiforov, I.G. Novikov, V.B. Uvarov. Kvantovo-statisticheskie modeli vysokotemperaturnoi plasmy. – M.: Fizmatlit, 2000 (in Russian).

MODELING OF ELECTRONIC STATES OF A SINGLE DONOR IN MIS-STRUCTURE USING THE FINITE DIFFERENCE METHOD

M.Sc. Levchuk E.A.[1], Prof. Lemeshevskii S.V. PhD.[2], Prof. Makarenko L.F. PhD [1]
Faculty of Applied Mathematics and Computer Science – Belarusian State University, Belarus [1]
Institute of Mathematics, National Academy of Sciences of Belarus, Belarus [2]

liauchuk.alena@gmail.com

Abstract: *Numerical modeling of electronic state evolution due to external electric field in the structure metal-insulator-semiconductor with solitary donor center is carried out. Considering a nanometer disc-shaped gate as a source of the electric field, the problem for the Laplace equation in infinite multilayered medium is solved to determine the gate potential. The energy spectrum of a bound electron is calculated from the problem for the stationary Schrödinger equation. Finite difference schemes are constructed to solve both the problems. Difference scheme for the Schrödinger equation takes into account cusp condition for the wave function at the donor location. To solve the problem for the Laplace equation, asymptotic boundary conditions for approximating the potential at large distances from the gate are proposed. On the basis of calculation results, a controlling parameter is suggested, which allows to determine the localization of electron wave function regardless of insulator thickness and permittivity.*

Keywords: FINITE DIFFERENCE METHOD, MIS-STRUCTURE, NANOGATE, SCHRÖDINGER EQUATION, ENERGY LEVEL, NUMERICAL MODELING

1. Introduction

The sensitivity of the electrical, optical, and magnetic properties of semiconductors to doping impurities is widely used to create various semiconductor devices. Reducing the physical size of the devices led to the need for taking into account quantum effects in the design and optimization of modern semiconductor structures [1]. Moreover, the achievements in technology of manufacturing nanoscale structures have made it possible to construct devices with only one impurity atom in the working region [2]. Designing of such devices requires additional fundamental studies devoted to the quantum mechanical modeling of their physical properties.

There are several proposals of using single impurity atoms to physically realize qubits, which can be based on the nuclear spin of a phosphorus impurity in silicon [3], the electron spin of a bound electron [4] or its charge [5]. These proposals stimulated the appearance of a number of papers devoted to modeling the electronic states of a donor near semiconductor surface (see [6-13]). The main attention was paid to the control of the donor electron density with an external electric field when the critical characteristic of the system under study was the critical field [9-10] or the critical potential at the gate [6], which corresponds to the relocation of the wave function of the donor electron into the gate area.

Taking into account all the features of the system (the finite size of the gate, the presence of a dielectric layer of nonzero thickness, the difference between the dielectric permittivities of semiconductor and insulator layers) requires solving the problem for the Laplace equation in a multilayered medium. As a result, it becomes necessary to use numerical methods, in particular, the finite difference method (FDM), which had shown its effectiveness in solving similar problems [14]. Attempts of applying FDM for modeling quantum mechanical effects in nanoscale structures with single donors were made in Refs. [15-16]. However, in these papers, the structures with confining potential of a simple form were considered, that does not require solving the problem for the Laplace equation.

The aim of this paper is to develop an algorithm for the numerical simulation of electronic states in a metal-insulator-semiconductor (MIS) structure with a single donor in the gate region based on sequential solution of the problems for the Laplace equation and the stationary Schrödinger equation. To calculate the gate potential, wave functions, and energy levels, FDM is used. The results of FDM calculations are compared with the results obtained with the finite element method (FEM).

2. Formulation of the problem

We consider a singly charged donor located in semiconductor at a distance z_0 from the semiconductor-insulator interface. An external electric field is created by an infinitely thin disc-shaped gate of diameter d and potential Φ_0. The insulator layer, separating the gate from the semiconductor, is located in the area $-t_{ox} < z < 0$. The donor and the center of the gate are positioned on the Oz axis.

According to the effective mass approach, the energy E and the electron wave function Ψ for states with zero projection of the orbital angular momentum on the Oz axis are described with the problem for the stationary Schrödinger equation (in cylindrical coordinates):

$$\left(\hat{T}+\hat{V}\right)\Psi = E\Psi, \qquad \rho > 0,\ z > 0, \tag{1}$$

where $\hat{T}$ is a kinetic energy operator, $\hat{V}$ is a potential energy operator.

In Eq. (1), we use effective Bohr radius as a unit of length

$$a^* = \frac{4\pi\varepsilon_0\varepsilon_2\hbar^2}{m^* e^2} \tag{2}$$

and effective Rydberg as a unit of energy

$$Ry^* = \frac{\hbar^2}{2m^*\left(a^*\right)^2} = \frac{1}{4\pi\varepsilon_0\varepsilon_1}\frac{e^2}{2a^*}, \tag{3}$$

where m^* is electron effective mass in semiconductor, ε_1 is dielectric permittivity of semiconductor. The potential is measured in units of Ry^*/e, respectively.

In Eq. (1), the kinetic energy operator $\hat{T}$ is defined as

$$\hat{T} = -\frac{1}{\rho}\frac{\partial}{\partial\rho}\left(\rho\frac{\partial}{\partial\rho}\right) - \frac{\partial^2}{\partial z^2}, \tag{4}$$

The potential energy operator is the sum

$$\hat{V} = \hat{V}_D + \hat{V}_{D'} + \hat{V}_{sim} + \hat{V}_G,$$

where $\hat{V}_D$ is the interaction between the electron and the donor

$$\hat{V}_D = -\frac{2}{\sqrt{(z-z_0)^2+\rho^2}}, \tag{5}$$

$\hat{V}_{D'}$, $\hat{V}_{sim}$ are the interactions of the electron with the donor image and electron image respectively [12]:

$$\hat{V}_{D'} = -\frac{2Q^*}{\sqrt{(z+z_0)^2+\rho^2}} + \\ + \frac{8\varepsilon_1\varepsilon_2}{(\varepsilon_1+\varepsilon_2)^2}\frac{\varepsilon_3-\varepsilon_2}{\varepsilon_3+\varepsilon_2}\sum_{k=1}^{\infty}\frac{\left(P^*\right)^{k-1}}{\sqrt{(z+z_0+2kt_{ox})^2+\rho^2}}, \quad (6)$$

$$\hat{V}_{sim} = \frac{Q^*}{2z} - \frac{2\varepsilon_1\varepsilon_2}{(\varepsilon_1+\varepsilon_2)^2}\frac{\varepsilon_3-\varepsilon_2}{\varepsilon_3+\varepsilon_2}\sum_{k=1}^{\infty}\frac{\left(P^*\right)^{k-1}}{z+kt_{ox}}, \quad (7)$$

where dielectric permittivity of the medium $\varepsilon(\rho,z)$ is

$$\varepsilon(\rho,z) = \begin{cases} \varepsilon_1, & (\rho,z)\in(0,+\infty)\times(0,+\infty) = D_1; \\ \varepsilon_2, & (\rho,z)\in(0,+\infty)\times(-t_{ox},0) = D_2; \\ \varepsilon_3, & (\rho,z)\in(0,+\infty)\times(-\infty,-t_{ox}) = D_3; \end{cases} \quad (8)$$

$$Q^* = \frac{\varepsilon_1-\varepsilon_2}{\varepsilon_1+\varepsilon_2}; \qquad P^* = Q^*\frac{\varepsilon_3-\varepsilon_2}{\varepsilon_3+\varepsilon_2}. \quad (9)$$

Operator $\hat{V}_G = -u(\rho,z)$ describes the electron potential energy in external field, where gate potential $u(\rho,z)$ is solution of the following problem:

$$\frac{1}{\rho}\frac{\partial}{\partial\rho}\left(\rho\varepsilon\frac{\partial u}{\partial\rho}\right)+\frac{\partial}{\partial z}\left(\varepsilon\frac{\partial u}{\partial z}\right)=0, \quad \rho>0, \quad -\infty<z<+\infty, \quad (10)$$

$$\left.\frac{\partial u}{\partial\rho}\right|_{\rho=0}=0, \quad (11)$$

$$u\to 0 \quad \text{as} \quad z\to\pm\infty, \quad \rho>0, \quad (12)$$

$$u\to 0 \quad \text{as} \quad \rho\to+\infty, \quad -\infty<z<+\infty. \quad (13)$$

At the semiconductor boundary, an infinitely high potential barrier is assumed, which allows to set the boundary condition for the wave function in the form

$$\Psi\big|_{z=0}=0. \quad (14)$$

For bound states:

$$\Psi\to 0 \quad \text{as} \quad \rho\to\infty, \quad z\to\infty. \quad (15)$$

At points on the axis $\rho=0$ outside the donor location, the wave function must be continuously differentiable, so

$$\left.\frac{\partial\Psi}{\partial\rho}\right|_{\rho=0}=0, \quad z\neq z_0. \quad (16)$$

At the donor location, condition (16) is not satisfied, since the potential becomes infinite at this point. Using a method described in [11], one can obtain the following condition

$$\left.\left(\frac{\partial\Psi}{\partial\rho}+\Psi\right)\right|_{\rho=0}=0, \quad z=z_0. \quad (17)$$

3. Calculation of the gate potential

For numerical calculation of the gate potential, the unbounded domain $\rho>0$, $-\infty<z<+\infty$, on which the problem is posed, was replaced by a bounded domain $0<\rho<L_\rho$, $-L_{z3}<z<L_{z1}$. The conditions on the boundary of this domain were set using the assumption that at large distances the gate potential can be approximately assumed to be equal to the potential of the point charge q located in the center of the gate. This potential has been found using Fourier-Bessel transform [18]:

$$v_1(\rho,z) = \frac{q}{\pi\varepsilon_0}\frac{\varepsilon_2}{(\varepsilon_2+\varepsilon_3)(\varepsilon_2+\varepsilon_1)}\sum_{k=0}^{\infty}\frac{\left(P^*\right)^k}{\sqrt{(z+t_{ox}(2k+1))^2+\rho^2}},$$

$$v_2(\rho,z) = \frac{q}{2\pi\varepsilon_0(\varepsilon_2+\varepsilon_3)}\left(\sum_{k=0}^{\infty}\frac{\left(P^*\right)^k}{\sqrt{(z+t_{ox}(2k+1))^2+\rho^2}} - \right. \\ \left. -\sum_{k=0}^{\infty}\frac{Q^*\left(P^*\right)^k}{\sqrt{(z-t_{ox}(2k+1))^2+\rho^2}}\right),$$

$$v_3(\rho,z) = \frac{q}{4\pi\varepsilon_0\varepsilon_3}\left(\frac{2\varepsilon_3}{\varepsilon_2+\varepsilon_3}\frac{1}{\sqrt{(z+t_{ox})^2+\rho^2}} - \right. \\ \left. -\frac{4\varepsilon_2\varepsilon_3}{(\varepsilon_2+\varepsilon_3)^2}\sum_{k=1}^{\infty}\frac{Q^*\left(P^*\right)^{k-1}}{\sqrt{(z-t_{ox}(2k-1))^2+\rho^2}}\right).$$

After differentiation we get the boundary conditions:

$$\left.\left(\frac{\partial u_1}{\partial z}-\frac{1}{v_1}\frac{\partial v_1}{\partial z}u_1\right)\right|_{z=L_{z1}}=0, \quad \rho>0, \quad (18)$$

$$\left.\left(\frac{\partial u_3}{\partial z}-\frac{1}{v_3}\frac{\partial v_3}{\partial z}u_3\right)\right|_{z=-L_{z3}}=0, \quad \rho>0, \quad (19)$$

$$\left.\left(\frac{\partial u_k}{\partial\rho}-\frac{1}{v_k}\frac{\partial v_k}{\partial\rho}u_k\right)\right|_{\rho=L_\rho}=0, \quad -\infty<z<+\infty, \quad k=1,2,3. \quad (20)$$

Difference scheme for the problem (10) – (11), (18) – (20) was constructed on the grid Ω_L, which is defined as follows:

$$\omega_\rho = \left\{\rho_i = ih_\rho: \quad h_\rho = \frac{L_\rho}{N_\rho}, \quad i=\overline{0,N_\rho}\right\},$$

where h_ρ is a grid step, N_ρ is a number of nodes on ρ direction,

$$\omega_z^{(1)} = \left\{z_j^{(1)} = jh_z^{(1)}: \quad h_z^{(1)} = \frac{L_{z1}}{N_z^{(1)}}, \quad j=\overline{0,N_z^{(1)}}\right\},$$

$$\omega_z^{(2)} = \left\{z_j^{(2)} = jh_z^{(2)} - t_{ox}: \quad h_z^{(2)} = \frac{t_{ox}}{N_z^{(2)}}, \quad j=\overline{0,N_z^{(2)}-1}\right\},$$

$$\omega_z^{(3)} = \left\{z_j^{(3)} = -L_{z3} + jh_z^{(3)}: \quad h_z^{(3)} = \frac{L_{z3}-t_{ox}}{N_z^{(3)}}, \quad j=\overline{0,N_z^{(3)}-1}\right\},$$

$h_z^{(k)}$ is a grid step, $N_z^{(k)}$ is a number of nodes on z direction. Then

$$\Omega_L = \omega_\rho\times\left(\omega_z^{(1)}\cup\omega_z^{(2)}\cup\omega_z^{(3)}\right).$$

The values of the potential in grid nodes are denoted as

$$y_{ij}^{(k)} = u_k(\rho_i, z_j^{(k)}), \quad k=1,2,3.$$

As a result, we get the following difference scheme [14]:

$$\frac{1}{\rho_i}\left(\rho_{i+1/2}y_{\bar{\rho}}^{(k)}\right)_\rho + y_{\bar{z}z}^{(k)} = 0, \quad k=1,2,3. \quad (21)$$

$$\varepsilon_k\frac{y_{i,1}^{(k)}-y_{i,0}^{(k)}}{h_z^{(k)}} - \varepsilon_{k+1}\frac{y_{i,0}^{(k)}-y_{i,N_z^{(k+1)}-1}^{(k+1)}}{h_z^{(k+1)}} + \frac{\varepsilon_k h_z^{(k)}+\varepsilon_{k+1}h_z^{(k+1)}}{2}\times \\ \times\frac{\rho_{i+1/2}\left(y_{i+1,0}^{(k)}-y_{i,0}^{(k)}\right)-\rho_{i-1/2}\left(y_{i,0}^{(k)}-y_{i-1,0}^{(k)}\right)}{\rho_i h_\rho^2}=0, \quad (22)$$

$$k=1: \quad i=\overline{1,N_\rho-1}; \qquad k=2: \quad i=\overline{N_d+1,N_\rho-1}.$$

$$\frac{y_{1,j}^{(k)}-y_{0,j}^{(k)}}{h_\rho} + \frac{h_\rho}{4}\frac{y_{0,j+1}^{(k)}-2y_{0,j}^{(k)}+y_{0,j-1}^{(k)}}{\left(h_z^{(k)}\right)^2}=0, \quad (23)$$

$$j=\overline{1,N_z^{(k)}-1}, \quad k=1,2,3.$$

$$y_{i,0}^{(2)} = \Phi_0, \quad i=\overline{0,N_d}, \quad (24)$$

where $N_d = \left[d/2h_\rho \right]$. Conditions (18) – (20) are approximated with the second order using additional points outside the computational domain and Eqs. (21) – (22).

4. Numerical solving of the Schrödinger equation

As in the case of potential computation, the problem for the Schrödinger equation has been solved on the finite domain $0 < \rho < L_\rho$, $0 < z < L_{z1}$. Since there is an exponential decay of the wave function at infinity, zero boundary conditions for the wave function were set on the boundary of the computational domain, i.e. the boundary condition (15) has been replaced with the conditions:

$$\Psi\big|_{z=L_{z1}} = 0, \quad \Psi\big|_{\rho=L_\rho} = 0. \tag{25}$$

The solution of the Schrödinger equation has been constructed on a grid:

$$\Omega_S = \omega_\rho \times \omega_z^{(1)}.$$

Denoting the values of the wave function at the grid nodes as

$$w_{ij} = \Psi(\rho_i, z_j^{(1)})$$

we get the following difference scheme:

$$-\frac{1}{\rho_i}\left(\rho_{i+1/2} w_\rho\right)_{\bar{\rho}} - w_{\bar{z}z} + V_{ij} w = E_h w, \tag{26}$$

$$w_{i,0} = 0, \quad i = \overline{0, N_\rho}, \tag{27}$$

$$w_{i,N_z^{(1)}} = 0, \quad i = \overline{0, N_\rho}, \tag{28}$$

$$w_{N_\rho, j} = 0, \quad j = \overline{1, N_z^{(1)} - 1}, \tag{29}$$

where E_h is approximate energy value, $V_{ij} = \hat{V}(\rho_i, z_j^{(1)})$.

To increase the order of approximation of the boundary condition (16), the difference approximation of the Schrödinger equation (1) on the axis $\rho = 0$ is used. As a result, we get

$$w_\rho + \frac{h_\rho}{4}\left(w_{\bar{z}z} - V_{0j} w + E_h w\right) = 0, \quad j \neq j_0, i = 0, \tag{30}$$

where $(0, j_0)$ is the node corresponding to the donor location. The value of the wave function at the donor location can be found from the second order approximation for the condition (17):

$$3w_{0,j_0} = 4w_{1,j_0} - w_{2,j_0} + 2h_\rho w_{0,j_0}. \tag{31}$$

5. Error estimation

The error of calculating the energy will be different when the electron is in the gate region and when it is located in the region near the donor. In the first case, both the error in calculating the potential and the error of the solution of the Schrodinger equation affect the accuracy of energy calculation.

To estimate the error in calculating the potential, arising from setting conditions (18) – (20) on the boundaries of computational domain, we consider a test problem in which an infinitely thin disc is in a homogeneous medium or on the boundary of two homogeneous media. In this case, the exact analytic expression for the potential is known [18]. Calculations of the gate potential using FDM have been carried out for three model problems with different conditions on the boundaries of the computational domain. In the first problem, the value of the potential at the boundary is assumed to be zero, in the second problem, the potential on the boundary is exact [18] and, in the third problem, conditions (18) – (20) are set on the boundary. The solutions obtained in all three cases were compared with the exact value of the potential in the integral norm on the domain $0 < \rho < 10a^*$, $-10a^* < z < 10a^*$. Calculations for gate diameter $d = 6a^*$, $L = L_\rho = L_{z1} = L_{z3}$ in range from $10a^*$ to $40a^*$ and grid step $h = h_\rho = h_z^{(k)} = 0.1$ have shown that the use of the conditions (18) – (20) instead of exact boundary conditions does not increase relative energy error even for small computational domains. On the contrary, when using zero boundary conditions on the boundary of the computational domain, the computational error increases sufficiently: the relative error at $L = 10a^*$ with zero boundary conditions is more than twenty much greater than the corresponding error for the problem with exact boundary conditions.

We consider the case, when the electron is localized on the donor, in the absence of external gate field and image charges. Then, at the donor location, the potential in the Schrödinger equation has a singularity, which can lead to additional errors. In order to verify the effect of condition (17) on the accuracy of the calculations, the dependences of the donor ground state energy on the grid step in the problem with condition (17) and with condition (16) at the donor location were calculated (Fig. 1). As one can see from Fig. 1, the use of the condition (16) at the location of the donor leads to the appearance of additional fluctuations in the error caused by the relative position of the donor location ($\rho = 0$, $z = z_0$) with respect to the grid. Thus, the use of conditions (17) has a significant effect on the accuracy of the computations.

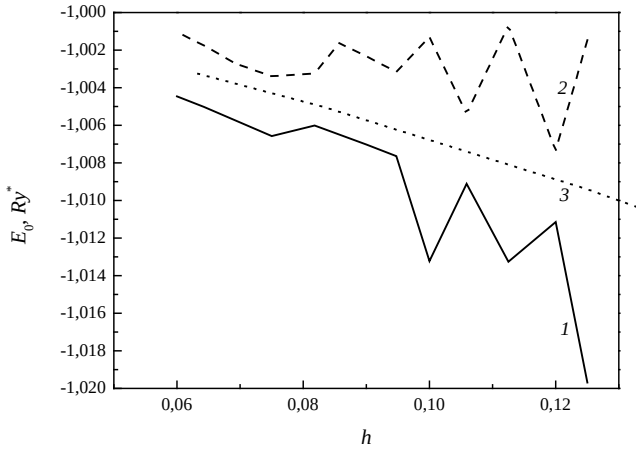


Fig. 1 *The effect of non-analyticity of the potential on calculation resutls of the energies of the ground state (E_0), for the distance from the donor to the semiconductor surface $z_0 = 8a^*$, at zero gate potential and neglecting image charges; h is the grid step. The curves 1, 2 are calculated using FDM and FEM, respectively, with conditions (16) at the donor location, the curve 3 is calculated using FDM with condition (17).*

6. Results and discussion

One of the main characteristics of the structure under study is the value of the external electric field at which relocation of electron wave function from the donor to the near-gate region takes place. We denote corresponding critical gate potential as Φ_{0C}. The critical potential depends on a number of parameters of the system: the size of the gate, the position of the donor, the dielectric constant of the media, and the thickness of the dielectric layer.

It had been shown in [19] that the critical field corresponds to a minimum of the difference between the energies of the first excited and ground states ($E_1 - E_0$). Therefore, to determine Φ_{0C} it is sufficient to calculate the energy values of two states, which essentially simplifies the problem.

Dependences of the critical potential on the thickness of the dielectric layer are shown in Fig. 2. As one can see from the figure, the critical potential increases with increasing thickness of the dielectric faster for smaller values of ε_2, e.g., for $t_{ox} = 2a^*$ (≈ 6.3 nm in silicon) $\Phi_{0C} \approx 231$ mV for $\varepsilon_2 = 3.8$ and $\Phi_{0C} \approx 95$ mV for $\varepsilon_2 = 34.2$. This means that when an insulator with a lower dielectric permittivity is used, the device requires a larger potential at the gate, which additionally increases the probability of dielectric breakdown.

It had been shown in [19] that at zero insulator thickness the redistribution of the ground state wave function depends only on the potential difference between the point of the donor location and semiconductor surface and does not depend on the position of the donor. An analogous dependence also takes place for a nonzero dielectric thickness. We consider the value $\Delta\Phi$ which is the potential difference between the donor and the semiconductor surface:

$$\Delta\Phi = \Phi(0, z_0) - \Phi(0,0),$$

where

$$\Phi(\rho, z) = \hat{V}_G(\rho, z) + \hat{V}_D(\rho, z) + \hat{V}_{sim}(\rho, z).$$

Correspondingly, we introduce the value of $\Delta\Phi_C$ which is the critical potential difference. The calculations show (Fig. 2) that the value of $\Delta\Phi_C$ is practically independent of the thickness and material of the dielectric. This allows us to use the results of calculations of the critical potential difference for a zero thickness of the dielectric in modeling of structures with an arbitrary thickness of the insulating layer.

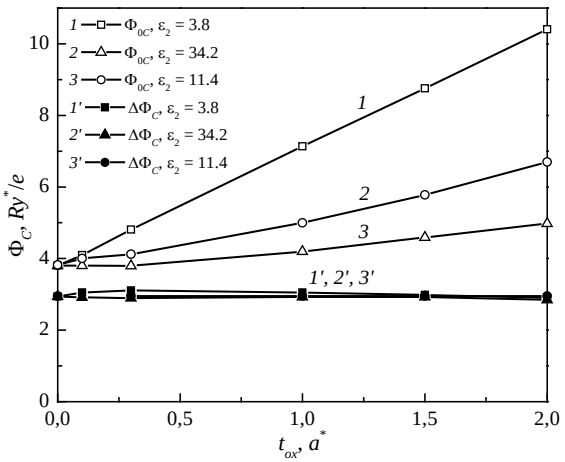


Fig. 2 *The dependences of the critical potential (Φ_{0C}) and critical potential difference ($\Delta\Phi_C$) on dielectric thickness for different dielectric constants of the insulating layer; $d = 6a^*$, $z_0 = 8a^*$, $\varepsilon_1 = 11.4$, $\varepsilon_3 = 1$.*

7. Conclusion

Numerical simulation of the electronic structure of a metal-insulator-semiconductor in the presence of a near-surface donor has been carried out. To calculate the gate potential and solve the problem for the stationary Schrödinger equation, a difference scheme has been proposed. A method to approximate the boundary conditions at infinity at calculations of the gate potential has been proposed. It has been found that the use of the proposed boundary conditions makes it possible to significantly reduce errors in calculated potential as compared with the use of zero conditions at the boundaries of calculation domain.

Using the suggested difference schemes, the dependences of the ground and first excited state energies of the donor on the field of disc-shaped gate in a three-layered medium have been obtained. On the basis of these dependences, the critical potential of the gate has been calculated, at which the electron density of the ground states is relocated from the donor to the gate region. It has been found that the critical potential difference between the donor and the semiconductor surface is the controlling parameter when describing the functioning of the device, since it practically does not depend on the thickness and permittivity of the dielectric layer.

References

1. Asenov, A., A.R. Brown, J.H. Davies, S. Kaya, G. Slavcheva. Simulation of intrinsic parameter fluctuations in decananometer and nanometer-scale MOSFETs. – IEEE transactions on electron devices, vol. 50, no. 9, 2003, pp. 1837-1853.

2. Koenraad, P.M., M.E. Flatte. Single dopants in semiconductors. – Nature materials, vol. 10, no. 2, 2011, p. 91.

3. Kane, B.E. A silicon-based nuclear spin quantum computer. – Nature (London), vol. 393, no. 6681, 1998, pp. 133-137.

4. Vrijen, R., E. Yablonovitch, K. Wang, H.W. Jiang, A. Balandin, V. Roychowdhury, T. Mor, D. DiVincenzo. Electron-spin-resonance transistors for quantum computing in silicon-germanium heterostructures. – Physical Review A, vol. 62, no. 1, 2000, p. 012306.

5. Hollenberg, L.C.L., A.S. Dzurak, C. Wellard, A.R. Hamilton, D.J. Reilly, G.J. Milburn, R.G. Clark. Charge-based quantum computing using single donors in semiconductors. – Physical Review B, vol. 69, no. 11, 2004, p. 113301.

6. Smit, G.D.J., S. Rogge, J. Caro, T.M. Klapwijk. Gate-induced ionization of single dopant atoms. – Physical Review B, vol. 68, no. 19, 2003, p. 193302.

7. Kettle, L.M., H.S. Goan, S.C. Smith, C.J. Wellard, L.C. Hollenberg, C.I. Pakes. Numerical study of hydrogenic effective mass theory for an impurity P donor in Si in the presence of an electric field and interfaces. – Physical Review B, vol. 68, no. 7, 2003, p. 075317.

8. MacMillen, D.B., U. Landman. Variational solutions of simple quantum systems subject to variable boundary conditions. II. Shallow donor imputities near semiconductor interfaces: Si, Ge. – J. Chem. Phys, vol. 80, no. 2, 1984, pp. 1691-1702.

9. Calderon, M.J., B. Koiller, S. Das Sarma. Quantum control of donor electrons at the Si-SiO_2 interface. – Physical Review Letters, vol. 96, no. 9, 2006, p. 096802.

10. Calderon, M.J., B. Koiller, S. Das Sarma. External field control of donor electron exchange at the Si/SiO_2 interface. – Physical Review B, vol. 75, no. 12, 2007, p. 125311.

11. Slachmuylders, A.F., B. Partoens, F.M. Peeters, W. Magnus. Effect of a metallic gate on the energy levels of a shallow donor. – Appl. Phys. Lett., vol. 92, no. 8, 2008, p. 083104.

12. Hao, Y.L., A.P. Djotyan, A.A. Avetisyan, F.M. Peeters. Shallow donor states near a semiconductor-insulator-metal interface. – Physical Review B, vol. 80, no. 3, 2009, p. 035329.

13. Nikolyuk, V.A., I.V. Ignatiev. The energy structure of quantum dots induced in quantum wells by a nonuniform electric field. – Semiconductors, vol. 41, no. 12, 2007, pp. 1422-1429.

14. Samarskii, A.A. The theory of difference schemes, New York, CRC Press, 2001.

15. Souza, G.V.B., A. Bruno-Alfonso. Finite-difference calculation of donor energy levels in a spherical quantum dot subject to a magnetic field. – Physica E, vol. 66, 2015, pp. 128-132.

16. Galeriu, C., L.L.Y. Voon, R. Melnik, M. Willatzen. Modeling a nanowire superlattice using the finite difference method in cylindrical polar coordinates. – Comp. Phys. Commun., vol. 157, no. 2, 2004, pp. 147-159.

17. Bingel, W.A. A physical interpretation of the cusp conditions for molecular wave functions. – Theoretica Chimica Acta, vol. 8, no. 1, 1967, pp. 54-61.

18. Smythe, S. Static and dynamic electricity, New York, Hemisphere Publishing, 1988.

19. Levchuk, E.A., L.F. Makarenko. On controlling the electronic states of shallow donors using a finite-size metal gate. – Semiconductors, vol. 50, no. 1, 2016, pp. 89-96.

MATHEMATICAL MODEL OF SUSTAINABLE INTEGRATED BIOETHANOL SUPPLY CHAINS

Eng. Dzhelil Y., Prof. DSc Ivanov B., Eng. Ganev E., Assoc. Prof. PhD Dobrudzhaliev D.
Bulgarian Academy of Sciences, Institute of Chemical Engineering, 1113 Sofia, BULGARIA,
E-mail: unzile_20@abv.bg, bivanov1946@gmail.com, evgeniy_ganev@abv.bg, dragodob@yahoo.com

Absract: *This paper focuses on designing mathematical model a integrated bioethanol supply chain (IBSC) that will account for economic and environmental aspects of sustainability. A mixed integer linear programming model is proposed to design an optimal IBSC. Bioethanol production from renewable biomass has experienced increased interest in order to reduce Bulgarian dependence on imported oil and reduce carbon emissions. Concerns regarding cost efficiency and environmental problems result in significant challenges that hinder the increased bioethanol production from renewable biomass. The model considers key supply chain activities including biomass harvesting/processing and transportation. The model uses the delivered feedstock cost, energy consumption, and GHG emissions as system performance criteria. The utility of the supply chain simulation model is demonstrated by considering a biomass supply chain for a biofuel facility in Bulgarian scale. The results show that the model is a useful tool for supply chain management, including selection of the optimal bioethanol facility location, logistics design, inventory management, and information exchange.*

KEYWORDS*: BIOETHANOL SUPPLY CHAIN, MATHEMATICAL MODEL, ECONOMIC AND ENVIRONMENTAL ASPECTS*

1. Introduction

Production and use of biofuels are promoted worldwide. Their use could potentially reduce emissions of greenhouse gases and the need for fossil fuels [1]. Accordingly, the European Union imposes a mandatory target of 10% biofuels by 2020 [2]. These fuels are produced from biomass. Their use for energy purposes has the potential to provide important benefits. Burning them releases such amount of CO_2 as was absorbed by the biomass in its formation [3]. Another advantage of biomass is its availability in the world due to its variety of sources. Despite the advantages of biomass with increasing quantities of biofuels to achieve the objectives of the European Union, this is accompanied by growing quantities of waste products. These wastes are related to the lifecycle of biofuels from crop cultivation, transportation, production to distribution and use. The main liquid biofuels are bioethanol and biodiesel. Depending on the raw material used, production is considered in three generations.

The first generation used as feedstock crops containing sugar and starch to produce bioethanol, and oilseed crops to produce biodiesel [4]. In the production of biodiesel, the advantage of these materials is that they can be grown on contaminated and saline soils, as the process does not affect the fuel production. The drawback is that they raise issues related to their competitiveness in the food sector. These materials also have a negative impact in terms of the quantity of water consumed. This is related to their cultivation that requires significant amounts of water resources. Excessive use of fertilizers, pesticides and chemicals to grow them also leads to accumulation of pollutants in groundwater that can penetrate into water courses and thus degrade water quality.

According to the second generation, bioethanol is produced by using as raw material waste biomass (agricultural and forest waste) [5], i.e. lignocellulose which is transformed into a valuable resource as bioethanol. Biofuel production second generation is an excellent way to deal with increasingly restrictive national and European regulations in this area and the use of organic waste for energy production and fertilizer as a byproduct. Logistics and use of these materials can be challenging due to the fact that they are usually dispersed. Another disadvantage from an environmental perspective is the need for further purification and processing.

The third generation comprises production from microalgae which occur as promising feedstock for biofuel production. The advantage of this biomass is that it is a year-round production and does not compete with the food industry.

The main technologies for production of bioethanol are fermentation, distillation and dehydration [6]. The wastes of biofuels are divided into production and performance. The technological waste is produced mainly in the creation of products that occur as waste production. The management of these wastes is related to their reduction, recovery and disposal. These guidelines are united in the idea of acquiring more sophisticated production processes. Efforts are focused on the use of new sources of raw materials, new processes, and new ways of realization of the side products. The use of by-products as raw materials for other production closes cycle in the supply chain, reducing the price of obtaining fuel. Operational waste associated with gases and emissions released during operation and the burning of biofuels.

2. Aim

The present study deals with the issue of designing optimal Integrated Bioethanol Supply Chains (IBSC) for waste management in the process of biofuel production and usage. Tools have been developed for formulation of a mathematical model for description of the parameter, the restrictions and the goal function.

3. Problem statement

The problem addressed in this work can be formally stated as follows. Given are a set of biofuel crops that can be converted to bioethanol. These include agricultural feedstock's e.g. wheat, corn, etc. A planning horizon of one year for government regulations including manufacturing, construction and carbon tax is considered. A IBSC network superstructure including a set of harvesting sites and a set of demand zones, as well as the potential locations of a number of collection facilities and bio refineries are set. Data for biofuel crops production and harvesting are also given. For each demand zone, the biofuel demand is given, and the environmental burden associated with bioethanol distribution in the local region is known. For each transportation link, the transportation capacity, available transportation modes, distance, and emissions of each transportation type are known.

3.1. General Formulation of the Problem

The overall problem can be summarized, as follows:

- Optimal locations of biofuel production centers,
- Demand for petroleum fuel for each of the demand centers,
- The minimum required ratio between petroleum fuel and biofuel for blending,
- Biomass feedstock types and their geographical availability,
- Specific Green House Gas (GHG) emission factors of the biofuel life cycle stages,
- Potential areas where systems for utilization of solid waste from production can be installed.

The objectives are to minimize total cost of a IBSC by optimizing the following decision variables:

- Supply chain network structure,
- Locations and scales of bioethanol production facilities and biomass cultivation sites,
- Flows of each biomass type and bioethanol between regions,
- Modes of transport for delivery for biomass and bioethanol,
- The GHG emissions for each stage in the life cycle,
- Supply strategy for biomass to be delivered to facilities,
- Distribution processes for biofuel to be sent to demand zones.

4. Model formulation

The role of the optimization model is to identify what combination of options is the most efficient approach to supply the facility. The problem for the optimal location of bioethanol production plants

and the efficient use of the available land is formulated as a MILP model with the following notation:

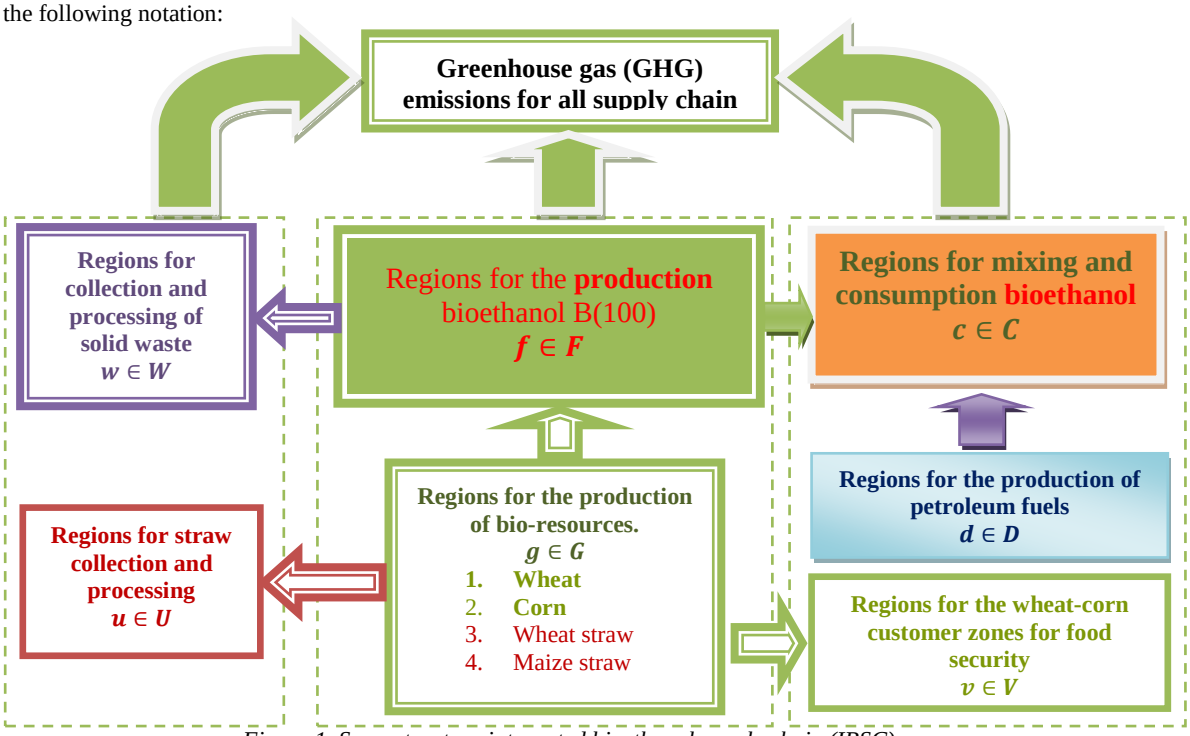


Figure 1. Superstructure integrated bioethanol supply chain (IBSC)

4.1. Mathematical model description

To start with the description of the MILP model, we first introduce the parameters, that are constant and known a priori, and the variables that are subject to optimization. Then we describe step by step the mathematical model by presenting the objective function and all the constraints. First of all, we introduce the set of time intervals of the horizon of planning $t = \{1,2,...,T\}$.

In this article the mathematical model that is used in the network design is described. Before describing the mathematical model, the input parameters, the decision variables, and the sets, subsets and indices are listed below.

4.1.1. Sets, subsets and indices

The following sets and subsets are introduced:

Sets/indices

I Set of biomass types indexed by i;

LF Set of transport modes indexed by lf;

P Set of plant size intervals indexed by $p = \overline{1, N_p}$;

S Set of utilization plant size intervals indexed by $s = \overline{1, N_s}$;

GF Set of regions of the territorial division indexed by gf;

K Set of proportion of bioethanol and gasoline indexed by k;

T Set of time intervals, indexed by t.

Subsets/indices

B Set of transport modes for bioethanol and gasoline is a subset of LF ($B \subset FL$) indexed by b;

L Set of transport modes for biomass is a subset of LF ($L \subset LF$) indexed by l;

M Set of transport modes for solid wastes is a subset of LF ($M \subset LF$) indexed by m;

E Set of transport modes for straw is a subset of LF ($E \subset LF$) indexed by e;

Z Set of transport modes for wheat-corn for food security is a subset of LF ($Z \subset LF$) indexed by z;

F Set of candidate regions for bioethanol plants established, which is a subset of GF ($F \subset GF$) indexed by f;

C Set of bioethanol mixing and customer zones, which is a subset of GF ($C \subset GF$) indexed by c;

D Set for delivery and production gasoline, which is a subset of GF ($D \subset GF$) indexed by d;

W Set for regions for collection and processing of solid waste, which is a subset of GF ($W \subset GF$) indexed by w;

U Set for regions for straw collection and processing, which is a subset of GF ($U \subset GF$) indexed by u;

V Set for regions for the wheat-corn customer zones, which is a subset of GF ($V \subset GF$) indexed by v;

4.1.2. Input parameters for the problem

Environmental parameters:

$EFBP_{ip}$ Emission factor for bioethanol production from biomass type $i \in I$ using technology $p \in P$, [$kg\ CO_2 - eq / ton\ biofuel$];

ESW Emission factor of pollution caused by one tone of solid waste if not used, [$\frac{kg\ CO_2 - eq}{ton\ solid\ waste}$]

$EFDP_d$ Emission factor for gasoline production in region $d \in D$, [$kg\ CO_2 - eq / ton$ gasoline];

$EFTRA_{il}$ Emission factor for biomass $i \in I$ supply via mode $l \in L$, [$kg\ CO_2 - eq / ton$ km];

$EFTRB_b$ Emission factor for bioethanol supply via mode $b \in B$, [$kg\ CO_2 - eq / ton$ km];

$EFTM_{il}$ Emission factor of transportation of biomass $i \in I$ for mode $l \in L$, [$kg\ CO_2 - eq / ton$ km];

$EFTB_b$ Emission factor of transportation of bioethanol and gasoline for mode $b \in B$, [$kg\ CO_2 - eq / ton$ km];

$EFTRW_m$ Emission factor for transport of solid waste with transport $m \in M$, [$kg\ CO_2 - eq / ton$ km];

$EFTRU_e$ Emission factor for transport of straw with transport $e \in E$, [$kg\ CO_2 - eq / ton$ km];

$EFTRV_z$ Emission factor for transport of wheat-corn for food security with transport $z \in Z$, [$kg\ CO_2 - eq / ton$ km];

ECB , ECG Emissions emitted during the combustion of CO_2 unit bioethanol and, gasoline, [$kg\ CO_2 - eq / ton\ bioethanol$] or; [$kg\ CO_2 - eq / ton$ gasoline].

Monetary parameter:

$CosB_p$, $CosW_s$ Capital investment of bioethanol plant size $p \in P$ and capital investment of solid waste plant size $s \in S$, [\$];

C_{CO_2} Carbon tax per unit of carbon emitted from the operation of the IBSC, [$\$ / kg\ CO_2 - eq$];

PG Price of gasoline, [$\$ / ton$];

UTI_{il} , UTB_b , UTG_b , UTS_m , UTU_e , UTV_z , Unit transport cost for biomass $i \in I$, via mode $l \in L$, bioethanol via mode $b \in B$, gasoline via mode $b \in B$, solid wastes via mode $m \in M$, straw via mode $e \in E$, wheat-corn for food security via mode z , [$\$ / ton$ km];

Technical parameters:

PB_p^{MAX} / PB_p^{MIN} Maximum/Minimum annual plant capacity of size $p \in P$ for bioethanol production, [$ton / year$];

ENO , ENB Energy equivalent unit of gasoline&bioethanol, [GJ / ton];

ADD_{dcb} , ADG_{gfl} , ADF_{fcb} , ADU_{gue} , ADW_{fwm} , ADV_{gvz} Actual delivery distance between grids via model of transport ($b \in B$, $l \in L$, $e \in E$, $m \in M$, $z \in Z$), [km];

SW_{ip} The total amount of solid waste generated for production of bioethanol using biomass i for technology p , [$\frac{ton\ solid\ waste}{ton\ biofuel}$];

$JobB_p$, $JobO_p$ The number of jobs needed to build and operation a bio-refinery with size $p \in P$ for year;

$JobG_{ig}$ The number of jobs required to grow a unit of $i \in I$ biosource in the region $g \in G$ per year.

Environmental parameters depending on the time interval:

$EFBC_{igt}$ Emission factor for cultivation of biomass type $i \in I$ in region $g \in G$ for each time interval t , [$kg\ CO_2 - eq / ton\ biomass$];

TEI_t^{MAX} Maximum total environmental impact, [$kg\ CO_2 - eq\ d^{-1}$].

Monetary parameters depending on the time interval

ζ_t Interest rate, % ;

ε_t Discount factor;

M_{ft}^{const} Factor to the change of the base price, depending on the region $f \in F$ where the plant is installed, [*Dimensionless*];

$Cost_{pft}^F$ Capital investment of plant size $p \in P$ for bioethanol production in each zones $f \in F$, [\$];

INS_{ft} The government incentive includes construction incentive and volumetric from region $f \in F$, [$\$ / ton$];

UPC_{igt} Unit production costs for biomass type $i \in I$ in region $g \in G$ for each time interval $t \in T$, [$\$ / ton$];

UPB_{ipft} Unit bioethanol production cost from biomass type $i \in I$ at a biorafinery of scale $p \in P$ installed in region $f \in F$, [$\$ / ton$];

UPD_{dt} Unit gasoline production cost at a rafinery d , [$\$ / ton$].

Technical parameters depending on the time interval

K_{ct}^{mix} Proportion of bioethanol and gasoline subject of mixing for each of the customer zones, [*Dimensionless*];

A_{gt}^S Set-aside area available in region $g \in G$ for biomass production for each time interval $t \in T$, [ha];

A_{gt}^{Food} Set-aside area available in region $g \in G$ for food, [ha];

β_{igt} Production rate of biomass i in region $g \in G$, [ton / ha];

LT_t Duration of time intervals $t \in T$, [$year$];

α_t Operating period for IBSC in a year, [$d / year$];

γ_{ipt} Biomass to bioethanol conversion factor specific for biomass i using technology p , [$ton_bioethanol / ton_biomass$];

YO_{ct} Gasoline demand in customer zones $c \in C$, [$ton / year$];

PBI_{igt}^{MIN} / PBI_{igt}^{MAX} Minimum/ Maximum biomass of type $i \in I$ which can be produced in the region, $g \in G$ per year, [$ton / year$];

QI_{igt}^{MAX} Maximum flow rate of biomass i from region g , [ton / d];

QB_{ft}^{MAX} Maximum flow rate of bioethanol from region f , [ton / d];

QD_{dt}^{MAX} Maximum flow rate of gasoline from region d , [ton / d];

QW_{ft}^{MAX} Maximum flow rate of solid wastes from f , [ton / d];

QU_{gt}^{MAX} Maximum flow rate of srtaw from region $g \in G$, [ton / d];

QV_{gt}^{MAX} Maximum flow rate of wheat-corn from $g \in G$, [ton / d];

4.1.3. Decision variables for the problem X_t

To find the optimal configuration of the IBSC, the following decision variables are required:

A/ Positive continuous variables

PBB_{igt} Biomass i demand in region $g \in G$ at time interval $t \in T$;

QI_{igflt} Flow rate of biomass $i \in I$ via mode $l \in L$ from region $g \in G$ to $f \in F$, for each $t \in T$, [ton / d];

QB_{fcbt} Flow rate of bioethanol produced from all biomass $i \in I$ via mode $b \in B$ from region $f \in F$ to $c \in C$ for each $t \in T$, [ton / d];

QBP_{ifcbpt} Flow rate of bioethanol produced from biomass i via mode b from f to c using technology p for each $t \in T$,[ton / d];

QD_{dcbt} Flow rate of gasoline via mode $b \in B$ from region $d \in D$ to $c \in C$, for each time interval $t \in T$, [ton / d];

QW_{fwmt} Flow rate of solid waste via mode $m \in M$ from region $f \in F$ to $w \in W$, for each $t \in T$, [ton / d];

QU_{guet} Flow rate of straw collection and processing via mode e from region g to u , for each $t \in T$, [ton / d];

QV_{gvzt} Flow rate of wheat-corn for food security via mode $z \in Z$ from region $g \in G$ to $v \in V$, for each $t \in T$,[ton / d];

QED_{ct} Quantity of gasoline to be supplied to meet the energy needs of the region $c \in C$, for each $t \in T$,[$ton / year$];

QEB_{ct} Quantity of bioethanol produced from biomass to be supplied to meet the energy needs of the region $c \in C$, [$ton / year$];

A_{igt} Land occupied by crop $i \in I$ in region $g \in G$, [ha];

A_{igt}^F Land by crops $i \in I$ needed for food security of the population in the region $g \in G$, for each $t \in T$, [ha];

B/ Binary variables

X_{igflt} 0-1 variable, equal to 1 if a biomass type i is transported from region g to f using transport l , and 0 otherwise at $t \in T$;

Y_{fcbt} 0-1 variable, equal to 1 if a bioethanol is transported from region f to c using transport b , l , and 0 otherwise at $t \in T$;

WS_{fwmt} 0-1 variable, equal to 1 if a solid waste is transported from region f to w using transport m and 0 otherwise for each $t \in T$;

WU_{guet} 0-1 variable, equal to 1 if a straw is transported from region g to $u \in U$ using transport $e \in E$ and 0 otherwise for each $t \in T$;

WV_{gvzt} 0-1 variable, equal to 1 if a wheat-corn is transported from region g to v using transport z and 0 otherwise for each $t \in T$;

ZW_{swt} 0-1 variable, equal to 1 if a solid waste utilization plant size s is installed in region w and 0 otherwise at time interval $t \in T$;

ZWF_{swt} 0-1 variable, equal to 1 if a solid waste utilization plant size s is to be working in region w and 0 otherwise at $t \in T$, which includes the plants installed in the previous time and the new ones built during this time which is calculate with equation $ZWF_{swt} = ZWF_{sw(t-1)} + ZW_{swt}$ for first year ($t = 1$) configuration is set by initializing $ZWF_{sw'1'} = ZW_{sw'1'}$;

Z_{pft} 0-1 variable, equal to 1 if a bioethanol production plant size p is to be established in region f and 0 otherwise for each $t \in T$;

ZF_{pft} 0-1 variable, equal to 1 if a bioethanol production plant size $p \in P$ is to be working in region $f \in F$ and 0 otherwise at time interval $t \in T$, which includes the plants installed in the previous time interval and the new ones built during this time interval which is calculate with equation $ZF_{pft} = ZF_{pf(t-1)} + Z_{pft}$ for first year ($t = 1$) configuration is set by initializing $ZF_{sw'1'} = Z_{sw'1'}$;

PD_{dt} 0-1 variable, equal to 1 if a gasoline is manufactured by the region $d \in D$ and 0 otherwise at time interval $t \in T$;

DT_{dcbt} 0-1 variable, equal to 1 if a gasoline is transported from region d to c using transport b and 0 otherwise for each $t \in T$.

4.1. Basic Relationships

As noted above, the assessment of IBSC production and distribution of bioethanol will be made by environmental and economic criteria.

4.1.1. Model of total environmental impact of IBSC

The environmental impact of the IBSC is measured in terms of total GHG emissions ($kg\ CO_2 - eq$) stemming from supply chain activities and the total emissions are converted to carbon credits by multiplying them with the carbon price in the market.

The environmental objective is to minimize the total annual GHG emission resulting from the operations of the IBSC. The formulation of this objective is based on the field-to wheel life cycle analysis, which takes into account the following life cycle stages of biomass-based liquid transportation fuels:

- biomass cultivation, growth and acquisition,
- biomass transportation from source locations to facilities,
- transportation of bioethanol facilities to the demand zones,
- local distribution of liquid transportation fuels in demand zones,
- emissions from bioethanol and gasoline usage.

Ecological assessment criteria will represent the total environmental impact at work on IBSC through the resulting GHG emissions for each time interval t. These emissions are equal to the sum of the impact that each of the stages of life cycle has on the environment. The GHG emission rate is defined as follows for each $t \in T$:

$$TEI_t = ELS_t + ELB_t + ELD_t + ETT_t + ESW_t + ECAR_t, \forall t \quad (1)$$

where

TEI_t Total GHG impact at work on IBSC [$kg\ CO_2 - eq\ d^{-1}$];

$\{ELS_t, ELB_t, ELD_t, ETT_t\}$ GHG impact of life cycle stages;

$ECAR_t$ Emissions from bioethanol and gasoline usage in vehicle operations [$kg\ CO_2 - eq\ d^{-1}$];

ESW_t Emissions from utilization solid waste for each $t \in T$.

Evaluation of environmental impact at every stage of life cycle is:

A. *Growing biomass* ELS_t;

B. *Production of bioethanol* ELB_t;

C. *Production of petroleum* gasoline ELD_t;

D. *Utilization of solid wastes* ESW_t

E. *Transportation biomass* ETA_t;

F. *Transportation bioethanol* ETE_t;

G. *Transportation gasoline* ETD_t;

H. *Transportation of solid waste* ETW_t;

I. *Transportation of straw* ETU_t;

J. *Transportation of wheat-corn for food security* ETV_t;

K. *Usage bioethanol and gasoline* $ECAR_t$.

1/ Greenhouse gases to grow biomass ELS_t, [$kg\ CO_2 - eq\ d^{-1}$]

GHG emissions resulting from the production of biomass depend on the cultivation practice adopted as well as on the geographical region in which the biomass crop has been established [7]. In particular, the actual environmental performance is affected by fertilisers and pesticides usage, irrigation techniques and soil characteristics. The factor may differ strongly from one production region to another. Accordingly, the biomass production stage is defined as follows:

$$ELS_t = \sum_{i \in I} \sum_{g \in G} \left(EFBC_{igt} \frac{\beta_{igt} A_{igt}}{\alpha_t} \right), \ \forall t, \quad (2)$$

2/ Total GHG emissions from bioethanol production ELB_t

The environmental impact of the bioethanol production stage is related to raw materials and the technology employed for the production of bioethanol.

$$ELB_t = \sum_{i \in I} \sum_{f \in F} \sum_{c \in C} \sum_{b \in B} \sum_{p \in P} \left(EFBP_{ip} QBP_{ifcbpt} \right), \ \forall t \quad (3)$$

Since only one of the technologies $p \in P$ can be selected for a region $f \in F$ (which is guaranteed by the condition $\sum_{p \in P} ZF_{pft} \le 1.0 \ \ \forall t, f$), it QBP_{ifcbpt} is equal to "0" for all except $p \in P$ for the selected technology. This is ensured by implementing the inequality $G^{MAX} ZF_{pft} \ge QBP_{ifcbpt}, \ \forall i, f, c, b, p, t$ where G^{MAX} there is a large enough number.

3/ Total GHG emissions from gasoline production ELD_t

$$ELD_t = \sum_{d \in D} \sum_{c \in C} \sum_{b \in B} EDP_{dt} QD_{dcbt}, \ \forall t \quad (4)$$

4/ The environmental impact of transportation ETT_t

The global warming impact related to both biomass supply and fuel distribution depends on the use of different transport means fuelled with fossil energy, typically either conventional oil-based fuels. The resulting GHG emissions of each transport option depend on both the distance run by the specific means and the freight load delivered. As a consequence, the emission factor represents the total carbon dioxide emissions equivalent accordingly:

$$ETT_t = ETA_t + ETB_t + ETD_t + ETW_t + ETU_t + ETV_t \quad (5)$$

where,

$ETA_t = \sum_{i \in I} \sum_{g \in G} \sum_{f \in F} \sum_{l \in L} \left(EFTM_{il} ADG_{gfl} QI_{igftl} \right), \ \forall t$ is environmental impact of transportation biomass **[** $kg\ CO_2 - eq\ d^{-1}$ **]**;

$ETE_t = \sum_{f \in F} \sum_{c \in C} \sum_{b \in B} \left(EFTB_b ADF_{fcb} QB_{fcbt} \right), \ \forall t$ is environmental impact of transportation bioethanol from zones $f \in F$ to $c \in C$ where $QB_{fcbt} = \sum_{i \in I} \sum_{p \in P} QBP_{ifcbpt}$ **[** $kg\ CO_2 - eq\ d^{-1}$ **]**;

$ETD_t = \sum_{d \in D} \sum_{c \in C} \sum_{b \in B} \left(EFTB_b ADD_{dcb} QD_{dcbt} \right), \ \forall t$ is environmental impact of transportation gasoline from zones $d \in D$ to $c \in C$;

$ETW_t = \sum_{f \in F} \sum_{w \in W} \sum_{m \in M} \left(EFTRW_m ADW_{fwm} QW_{fwmt} \right), \ \forall t$ is environmental impact of transportation solid wastes from zones $f \in F$ to $w \in W$;

$ETU_t = \sum_{g \in G} \sum_{u \in U} \sum_{e \in E} \left(EFTRU_e ADU_{gue} QU_{guet} \right), \ \forall t$ is environmental impact of transportation straw from zones $g \in G$ to $u \in U$;

$ETV_t = \sum_{g \in G} \sum_{v \in V} \sum_{z \in Z} \left(EFTRV_z ADV_{gvz} QV_{gvzt} \right), \ \forall t$ is environmental impact of transportation wheat-corn from zones $g \in G$ to $v \in V$;

5/ Total GHG emissions from utilization solid wastes ESW_t

$$ESW_t = \left(\frac{\sum_{i \in I} \sum_{f \in F} \sum_{c \in C} \sum_{b \in B} \sum_{p \in P} SW_{ip} QBP_{ifcbpt} -}{\sum_{f \in F} \sum_{w \in W} \sum_{m \in M} QW_{fwmt}} \right) ESW, \ \forall t, \quad (6)$$

6/ GHG emissions from bioethanol and gasoline usage in vehicle operations $ECAR_t$

$$ECAR_t = ECB\sum_{f\in F}\sum_{c\in C}\sum_{b\in B} QB_{fcbt} + ECG\sum_{d\in D}\sum_{c\in C}\sum_{b\in B} QD_{dcbt}, \quad \forall t, \tag{7}$$

4.1.2. Model of total cost of a IBSC

The annual operational cost includes the biomass feedstock acquisition cost, the local distribution cost of final fuel product, the production costs of final products, and the transportation costs of biomass, and final products. In the production cost, we consider both the fixed annual operating cost, which is given as a percentage of the corresponding total capital investment, and the net variable cost, which is proportional to the processing amount. In the transportation cost, both distance-fixed cost and distance-variable cost are considered. The economic criterion will be the cost of living expenses to include total investment cost of bioethanol production facilities and operation of the IBDS. This price is expressed through the dependence [8] for each time interval $t \in T$ **:**

$$TDC_t = TIC_t + TPC_t + TTC_t + TTAXB_t - TL_t, \quad \forall t \tag{8}$$

where

TDC_t Total cost of a IBSC for year [$ $year^{-1}$];

TIC_t Total investment costs of production capacity of IBSC relative to the operational period per year [$ $year^{-1}$];

TPC_t Production cost for biorefineries [$ $year^{-1}$];

TTC_t Total transportation cost of a IBSC [$ $year^{-1}$];

$TTAXB_t$ A carbon tax levied according to the total amount of CO_2 generated in the work of IBSC [$ $year^{-1}$];

TL_t Government incentives for bioethanol production and use;

1/ Model investment costs for biorefineries by year TIC_t

A rational IBSC planning over the time is based upon the assumption that once a production facility has been built, it will be operating for the remaining time frame.

$$TIC_t = \varepsilon_t \sum_{f\in F}\sum_{p\in P}\left(Cost_{pf}^{F} Z_{pft}\right), \quad \forall t \tag{9}$$

where ε_t is calculate by equation (10):

$$\varepsilon_t = \frac{1}{(1+\varsigma_t)} \tag{10}$$

Capital cost of biorefinery for each region is determined by the equation:

$$Cost_{pf}^{F} = M_f^{cost} Cost_p, \forall p \in P, \forall f \in F, \tag{11}$$

2/ Total production cost model of IBSC TPC_t **[** $ $year^{-1}$ **]**

Total production cost term, TPC_t consists of biomass cultivation TPA_t, bioethanol production costs TPB_t and production cost for gasoline TPD_t as follows for each time interval t :

$$TPC_t = TPA_t + TPB_t + TPD_t, \forall t, \tag{12}$$

where the components of (12) are defined according to the relations:

$$\left.\begin{aligned} TPA_t &= \sum_{i\in I}\sum_{g\in G}\left(UPC_{igt} A_{igt} \beta_{igt}\right) \\ TPB_t &= \sum_{i\in I}\sum_{f\in F}\sum_{c\in C}\sum_{b\in B}\sum_{p\in P}\left(\alpha_t UPB_{ipft} QBP_{ifcbpt}\right) \\ TPD_t &= \sum_{c\in C}\sum_{b\in B}\sum_{d\in D}\left(\alpha_t UPD_{dt} QD_{dcbt}\right) \end{aligned}\right\}, \ \forall t$$

3/ Total transportation cost model TTC_t **[** $ $year^{-1}$ **]**

With regard to transports, both the biomass delivery to conversion plants and the fuel distribution and transport of diesel to blending terminals are treated as an additional service provided by existing actors already operating within the industrial/transport infrastructure. As a consequence, TTC_t is evaluated as follows:

$$TTC_t = TTCA + TTCB_t + TTCD_t +, \forall t \tag{13}$$

where, $TTCA_t = \sum_{l\in L}\sum_{i\in I}\sum_{f\in F}\sum_{g\in G}\left(\alpha_t UTC_{igfl} QI_{igflt}\right), \ \forall t$ is transportation cost for energy crops, $TTCB_t = \sum_{b\in B}\sum_{c\in C}\sum_{f\in F}\left(\alpha_t UTB_{fcb} QB_{fcbt}\right), \ \forall t$, for bioethanol, $TTCD_t = \sum_{b\in B}\sum_{c\in C}\sum_{d\in D}\left(\alpha_t UTD_{dcb} QD_{dcbt}\right), \ \forall t$ and for gasoline, where,

$$\left.\begin{aligned} UTC_{igfl} &= IA_{il} + \left(IB_{il} ADG_{gfl}\right) \\ UTB_{fcb} &= OA_b + \left(OB_b ADF_{fcb}\right) \\ UTD_{dcb} &= OAD_b + \left(OBD_b ADD_{dcb}\right) \end{aligned}\right\},$$

IA_{il} and IB_{il} is fixed and variable cost for transportation biomass type $i \in I$ and (OA_b, OB_b) is fixed and variable cost for transportation bioethanol.

The biomass transportation cost UTC_{igfl} is described by *Börjesson and Gustavsson* **[9]**, for transportation by tractor, truck and train UTB_{fcb}. They are composed of a fixed cost (IA_{il}, OA_b) and a variable cost (IB_{il}, OB_b). Fixed costs include loading and unloading costs. They do not depend on the distance of transport. Variable costs include fuel cost, driver cost, maintenance cost etc.

4/ Government incentives for bioethanol production cost model TL_t **, [** $ $year^{-1}$ **]**

$$TL_t = \sum_{f\in F}\sum_{c\in C}\sum_{b\in B}\left(INS_{ft}\alpha_t QB_{fcbt}\right), \quad \forall t \tag{14}$$

5/ A carbon tax levied cost model $TTAXB_t$ **, [** $ $year^{-1}$ **]**

Many countries are implementing various mechanisms to reduce GHG emissions including incentives or mandatory targets to reduce carbon footprint. Carbon taxes and carbon markets (emissions trading) are recognized as the most cost-effective mechanisms. The basic idea is to put a price tag on carbon emissions and create new investment opportunities to generate a fund for green technology development. There are already a number of active carbon markets for GHG emissions **[10]**.

$$TTAXB_t = \left(\alpha_t TEI_t\right) C_{CO_2}, \quad \forall t \tag{15}$$

4.2. Restrictions

Plants capacity limited by upper and lower constrains

Plants capacity is limited by upper and lower bounds, where the minimal production level in each region is obtained by:

$$\sum_{p\in P}\left(PB_p^{MIN} ZF_{pft}\right) \le \alpha_t \sum_{c\in C}\sum_{b\in B} QB_{fcbt} \le \sum_{p\in P}\left(PB_p^{MAX} ZF_{pft}\right), \forall f, t \tag{16}$$

$$\left.\begin{aligned} &\sum_{m\in M}\sum_{w\in W} QW_{fwmt} \le QW_{ft}^{MAX}, \forall f \\ &\sum_{e\in E}\sum_{u\in U} QU_{guet} \le QU_{gt}^{MAX}, \quad \forall g \\ &\sum_{z\in Z}\sum_{v\in V} QV_{gvzt} \le QV_{gt}^{MAX}, \quad \forall g \end{aligned}\right\}, \ \forall t \tag{17}$$

Constraints balance of bioethanol to be produced from biomass available in the regions

$$\alpha_t \sum_{i\in I}\sum_{f\in F}\sum_{c\in C}\sum_{b\in B}\sum_{p\in P}\left(\frac{QBP_{ifcbpt}}{\beta_{igt}\gamma_{ipt}}\right) = \sum_{i\in I}\sum_{g\in G}\left(A_{igt}\right), \ \forall t \tag{18}$$

A condition that ensures that the total amount of solid waste generated by all bio-refineries can be processed in the plants built for this purpose

$$\sum_{w\in W}\sum_{m\in M} QW_{fwmt} \le \sum_{p\in P}\sum_{i\in I}\sum_{c\in C}\sum_{b\in B}\left(SW_{ip} QBP_{ifcbpt}\right), \forall f, t \tag{19}$$

A restriction that ensures that the amount of solid waste processed at the plant is within its production capacity

$$\left.\begin{aligned} &\sum_{s\in S} P_s^{MIN} ZWF_{swt} \le \alpha_t \sum_{f\in F}\sum_{m\in M} QW_{fwmt} \\ &\alpha_t \sum_{f\in F}\sum_{m\in M} QW_{fwmt} \le \sum_{s\in S} P_s^{MAX} ZWF_{swt} \end{aligned}\right\}, \ \forall t, w \tag{20}$$

Logical Constrains

- Restriction guarantees that a given region $f \in F$ installed power plant with $p \in P$ for bioethanol production.

$$\left.\begin{aligned}\sum_{p\in P} Z_{pft} \le 1\\ \sum_{p\in P} ZF_{pft} \le 1\end{aligned}\right\},\ \forall f,t \tag{21}$$

and for a utilization systems of solid wastes (21):

$$\left.\begin{aligned}\sum_{s\in S} ZW_{swt} \le 1\\ \sum_{s\in S} ZWF_{swt} \le 1\end{aligned}\right\},\ \forall w,t \tag{22}$$

- Limitation ensure the availability of at least one connection to a region of bioresources and region for biofuel

$$\sum_{g\in G}\sum_{l\in L} X_{igflt} \ge \sum_{c\in C}\sum_{b\in B} Y_{fcbt} \ge \sum_{p\in P} ZF_{pft},\ \forall i,f,t \tag{23}$$

- Limit which guarantees that each region will provide only one plant with a biomass type $i \in I$

$$\sum_{f\in F}\sum_{l\in L} X_{igflt} \le 1,\ \forall i,g,t \tag{24}$$

- Limitation of assurance that at least one region $f \in F$ producing bioethanol is connected to a costumer zones $c \in C$

$$\sum_{b\in B}\sum_{f\in F} Y_{fcbt} \le 1,\ \forall c,t \tag{25}$$

- Limitation of assurance that at least one region f is connected to a solid waste utilization plant located in region $w \in W$

$$\sum_{w\in W}\sum_{m\in M} WS_{fwmt} \le 1,\ \forall f,t \tag{26}$$

- Condition ensuring that the solid waste produced from a given bio-refinery will be processed in only one of the plants for use

$$\sum_{m\in M}\sum_{w\in W} WS_{fwmt} = \sum_{p\in P} ZF_{pft},\ \forall f,t \tag{27}$$

- Condition ensuring that a plant used in a given region will be connected to at least one plant in which solid waste is generated

$$\sum_{m\in M}\sum_{f\in F} WS_{fwmt} \ge \sum_{s\in S} ZWF_{swt},\ \forall w,t \tag{28}$$

Transport Links

Restrictions on transportation of biomass are

$$PBI_{ig}^{MIN}\sum_{l\in L} X_{igflt} \le \alpha_t \sum_{l\in L} QI_{igflt} \le PBI_{ig}^{MAX}\sum_{l\in L} X_{igflt},\ \forall i,g,f,t \tag{29}$$

Mass balances between bioethanol plants and biomass regions

The connections between bioethanol plants and biomass regions:

$$\sum_{l\in L}\sum_{g\in G}\sum_{i\in I}\left(QI_{igflt}\right) \le \sum_{p\in P}\left(\frac{PB_p^{MAX} ZF_{pft}}{\gamma_{ipt}}\right),\ \forall f,t \tag{30}$$

Mass balances between bioethanol plants and customer zones

$$\sum_{b\in B}\sum_{f\in F}\left(\alpha_t QB_{fcbt}\right) = QEB_{ct},\ \forall c,t \tag{31}$$

Energy Restriction

- limitation ensuring that the overall energy balance in the region is provided

$$ENO\sum_{c\in C} QEO_{ct} + ENB\sum_{c\in C} QEB_{ct} = ENO\sum_{c\in C} YO_{ct},\ \forall t \tag{32}$$

- limitation ensuring that each region will be provided in the desired proportions with fuels

$$ENB\ QEB_{ct} = K_{ct}^{mix}\ ENO\ YO_{ct},\ \forall c,t \tag{33}$$

4.3. Economic objective function

Objective function associated with the minimization of the economic costs includes all the operating costs of the supply chain, from the purchase of biomass feedstock to transportation of the final product, as well as the investment cost of biorefineries [11]. The costs of the supply chain are: the cost of raw material, the transport of raw material to the facilities, the cost of transport to the biorefineries, the cost of transformation into bioethanol and the cost of final transport to the blending facilities. The economic objective is to minimize the total annual costs. The terms of the cost objective corresponding to the annual operation costs of the IBSC are described in the following equation:

$$COST = \sum_{t\in T}\left(LT_t TDC_t\right) \tag{34}$$

5. Optimization problem formulation

The problem for the optimal design of a IBSC is formulated as a MILP model for the objective function of Minimizing cost.

The task of determining the optimal location of facilities in the regions and their parameters is formulated as follows:

$$\left\{\begin{aligned}&Find: X_t\left[\text{Decision variables}\right]^T\\ &MINIMIZE\left\{COST\right\} \to (Eq.34)\\ &s.t.:\left\{Eq.16 - Eq.33\right\}\end{aligned}\right\} \tag{35}$$

The problem is an ordinary MILP and can thus be solved using MILP techniques. The present model was developed in the commercial software GAMS [12]. The model chooses the less costly pathways from one set of biomass supply points to a specific plant and further to a set of biofuel demand points. The final result of the optimisation problem would then be a set of plants together with their corresponding biomass and biofuel demand points.

6. Discussion and conclusion

This paper studies the interactions among biofuel supply chain design, agricultural land use and local food market equilibrium. The study has been focused on the eco comparable behavior of the stakeholders in the biofuel supply chain incorporating them into the supply chain design model. The model includes the problem of crop rotation and solid waste utilization. The model is believed to be important for practical application and can be used for design and management of similar supply chains.

Acknowledgements

The authors would like to thank Bulgarian National Science Fund for the financial support obtained under contract DN 07-14/15.12.2016.

7. References

[1]. IEA, *World energy outlook 2007*, Paris, France: International Energy Agency, 2007.

[2]. European Commission, Directive 2009/28/EC of the European Parliament and of the Council of 23 April 2009 on the Promotion of the use of energy from renewable sources and Amending and Subsequently Repealing Directives 2001/77/EC and 2003/30/EC. Official J Eur Parliam, Brussels.

[3]. *O. Kitani, Carl HW*. The state of food and agriculture. New York: Food and Agriculture Organization, Rome, Italy: FAO, 2008, vol. 5.

[4]. *Carlos Mireta, Philippe Chazara, Ludovic Montastruc, Stéphane Negny, Serge Domenech.* Design of bioethanol green supply chain: Comparison between first and second generation biomass concerning economic, environmental and social criteria. Computers and Chemical Engineering 85 (2016) 16–35.

[5]. *S. Banerjee, S. Mudliar, R. Sen, L. Giri, D. Satpute, T. Chakrabarti, R.A. Pandey*. Commercializing lignocellulosic bioethanol: technology bottlenecks and possible remedies, Biofuels, Bioproducts and Biorefining 4, pp 77–93, 2010.

[6]. *O. Akgul, A. Zamboni, F. Bezzo, N. Shah, L. Papageorgiou.* Optimization-Based Approaches for Bioethanol Supply Chains, Ind. Eng. Chem. Res., 50, 4927-4938, 2011.

[7]. *Zamboni A., Bezzo F., Shah N.* Spatially explicit static model for the strategic design of future bioethanol production systems, 2. Multi-objective environmental optimization. *Energy and Fuels*, 2009, 23, 5134–5143.

[8]. *Ozlem A., Shah N., Papageorgiou L.*, Economic optimisation of a UK advanced biofuel supply chain, *Biomass and Bioenergy* 2012,41,57-72.

[9]. *Börjesson P., Gustavsson L.,* (1996). Regional Production and Utilization of Biomass in Sweden. *Energy*, 21, 747-764.

[10]. *Johnson E., Heinen R.*. Carbon trading: time for industry involvement. *Environment International*, 2004, 30, 279-288.

[11]. *Atif Osmania, Jun Zhangb.* Multi-period stochastic optimization of a sustainable multi-feedstock second generation bioethanol supply chain − A logistic case study in Midwestern United States , Land Use Policy 61 (2017) 420–450

[12]. *B. McCarl, A. Meeraus, Pvd. Eijk, M. Bussieck, S. Dirkse, P. Steacy*, McCarl Expanded GAMS user Guide, Version 22.9. GAMS Development Corporation, 2008.

ENERGY AND EXERGY ANALYSIS OF SEA WATER PUMP FOR THE MAIN CONDENSER COOLING IN THE LNG CARRIER STEAM PROPULSION SYSTEM

PhD. Mrzljak Vedran[1], Student Žarković Božica[1], PhD Student Eng. Poljak Igor[2]
Faculty of Engineering, University of Rijeka, Vukovarska 58, 51000 Rijeka[1], Rožići 4/3, 51221 Kostrena[2], Croatia
E-mail: vedran.mrzljak@riteh.hr, bozica.zarkovic@gmail.com, igor.poljak2@gmail.com

Abstract: *Energy and exergy analysis of sea water pump which is used for the main condenser cooling at lower steam propulsion system loads on conventional LNG carrier is presented in this paper. By using the measured variables from the exploitation, it is presented different influences of pump used power on cumulative energy and exergy power inputs. Energy and exergy pump power losses are reverse proportional, while pump energy and exergy efficiencies are directly proportional to increase in pump load. The highest obtained pump energy efficiency amounts 59.61 %, while the highest obtained pump exergy efficiency amounts 60.25 %. From the viewpoint of efficiencies and power losses, it will be optimal that analyzed pump operates at the highest possible loads.*

Keywords: *ENERGY EFFICIENCY, ENERGY POWER LOSSES, EXERGY EFFICIENCY, EXERGY DESTRUCTION, SEA WATER PUMP*

1. Introduction

Steam propulsion systems are dominant propulsion systems of LNG carriers [1]. Such steam propulsion systems have many components, not only for ship propulsion, but also for electricity and heat production [2]. One of the constituent components of such marine steam propulsion system is main condenser. Main condenser is cooled with sea water, while the condenser cooling system can be performed in two different ways. First one is cooling with the sea water pump (or more of them) only. Second is combination of cooling with sea water pump at the low steam system loads [3], while on the high steam system loads (at high ship speed) sea water pump is switched off and condenser cooling is performed with the scoop. The scoop is a tube mounted under the ship and it leads sea water directly to main condenser cooling tubes. Condenser cooling with a scoop is very dependable on ship current speed so it cannot be performed under optimal ship speed, defined with scoop producer specifications.

In this paper is analyzed sea water pump from a conventional LNG carrier, which uses main condenser cooling with sea water pump at low and with scoop at high steam system loads. Main characteristics of the LNG carrier in which steam propulsion system is mounted analyzed sea water pump are presented in Table 1.

Table 1. *Main characteristics of the LNG carrier*

Dead weight tonnage	84,812 DWT
Overall length	288 m
Max breadth	44 m
Design draft	9.3 m
Propulsion turbine	Mitsubishi MS40-2 (max. power 29.420 kW)
Turbo-generators	2 x Shinko RGA 92-2 (max. power 3.850 kW each)

The main goal of this paper is to perform analysis of sea water pump during its operation from the aspect of energy and exergy. It was investigated the influences of pump driving power on energy and exergy pump inputs and it was performed analysis of pump energy and exergy power losses, for the entire pump operation range. Based on a measured data from ship exploitation, it was observed the change in pump energy and exergy efficiencies from the lowest to the highest pump load.

2. Sea water pump energy and exergy analysis

2.1. General equations for energy and exergy analysis

The first law of thermodynamics defined energy analysis of any steam system component [4]. Mass and energy balance equations for a standard volume in steady state disregarding potential and kinetic energy can be expressed according to [5]:

$$\sum \dot{m}_{\mathrm{IN}} = \sum \dot{m}_{\mathrm{OUT}} \tag{1}$$

$$\dot{Q} - P = \sum \dot{m}_{\mathrm{OUT}} \cdot h_{\mathrm{OUT}} - \sum \dot{m}_{\mathrm{IN}} \cdot h_{\mathrm{IN}} \tag{2}$$

Energy power of a flow for any fluid stream can be calculated according to the [6] by using the equation:

$$\dot{E}_{\mathrm{en}} = \dot{m} \cdot h \tag{3}$$

Energy efficiency may take different forms and types. Usually, energy efficiency can be written as [7]:

$$\eta_{\mathrm{en}} = \frac{\text{Energy output}}{\text{Energy input}} \tag{4}$$

Second law of thermodynamics defines exergy analysis [8]. The main exergy balance equation for a standard volume in steady state is [9]:

$$\dot{X}_{\mathrm{heat}} - P = \sum \dot{m}_{\mathrm{OUT}} \cdot \varepsilon_{\mathrm{OUT}} - \sum \dot{m}_{\mathrm{IN}} \cdot \varepsilon_{\mathrm{IN}} + \dot{E}_{\mathrm{ex,D}} \tag{5}$$

where the net exergy transfer by heat ($\dot{X}_{\mathrm{heat}}$) at the temperature T is equal to [10]:

$$\dot{X}_{\mathrm{heat}} = \sum (1 - \frac{T_0}{T}) \cdot \dot{Q} \tag{6}$$

Specific exergy was defined according to [11] by an equation:

$$\varepsilon = (h - h_0) - T_0 \cdot (s - s_0) \tag{7}$$

The total exergy of a flow for every fluid stream can be calculated according to [6]:

$$\dot{E}_{\mathrm{ex}} = \dot{m} \cdot \varepsilon = \dot{m} \cdot \left[(h - h_0) - T_0 \cdot (s - s_0) \right] \tag{8}$$

Exergy efficiency is also called second law efficiency or effectiveness [12]. It can be defined as:

$$\eta_{\mathrm{ex}} = \frac{\text{Exergy output}}{\text{Exergy input}} \tag{9}$$

2.2. Sea water pump efficiencies and losses (energy and exergy)

Analyzed sea water pump is used in LNG carrier steam propulsion system for the main condenser cooling at low propulsion system loads. Main condenser cooling on this LNG carrier is performed in two ways: at low propulsion system loads (at low ship speed) main condenser is cooled with pump, while at high propulsion system loads (at high ship speed) main condenser is cooled with the scoop. According to producer specifications [13], main pump characteristics are:

- Pump maximum capacity: 6000 m^3/h
- Pump maximum delivery height: 13 m
- Standard pump operation revolutions: 390 rpm

Power for sea water pump operation, in each operating point, is calculated according to producer specifications [13] by using sea water volume flow at the pump inlet. Sea water volume flow can be calculated by using measured sea parameters at the pump inlet: temperature, pressure and mass flow. Pump used power (P) is approximated by using sixth degree polynomial:

$$\begin{aligned} P = {} & 1.3216361 \cdot 10^{-20} \cdot \dot{V}^6 - 2.4675409 \cdot 10^{-16} \cdot \dot{V}^5 + \\ & + 1.7487692 \cdot 10^{-12} \cdot \dot{V}^4 - 6.0343228 \cdot 10^{-9} \cdot \dot{V}^3 + \\ & + 1.0365022 \cdot 10^{-5} \cdot \dot{V}^2 - 4.2656487 \cdot 10^{-3} \cdot \dot{V} + \\ & + 120.657 \end{aligned} \tag{10}$$

where pump used power P is obtained in (kW) when in equation (10) is placed sea water volume flow at the pump inlet $\dot{V}$ in (m^3/h).

For the analyzed sea water pump, all necessary operating points were presented in Fig. 1. The required specific enthalpies and specific entropies as well as other thermodynamic properties were calculated from measured pressures and temperatures for each fluid stream by using NIST REFPROP software [14].

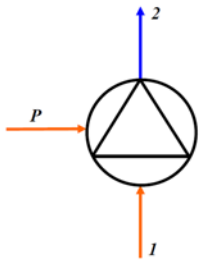


Fig. 1. *Sea water pump symbol with marked inlets (inputs) and outlet (output)*

Mass, energy and exergy balances for the analyzed pump, according to Fig. 1, are:

Mass balance:

$$\dot{m}_1 = \dot{m}_2 \tag{11}$$

Energy balance:

- Energy power input (only sea water flow):

$$\dot{E}_{en,IN,sw} = \dot{m}_1 \cdot h_1 \tag{12}$$

- Energy power input (cumulative):

$$\dot{E}_{en,IN,c} = \dot{m}_1 \cdot h_1 + P \tag{13}$$

- Energy power output:

$$\dot{E}_{en,OUT} = \dot{m}_2 \cdot h_2 \tag{14}$$

- Energy power loss:

$$\dot{E}_{en,PL} = \dot{E}_{en,IN,c} - \dot{E}_{en,OUT} = \dot{m}_1 \cdot h_1 + P - \dot{m}_2 \cdot h_2 \tag{15}$$

- Energy efficiency [15]:

$$\eta_{en} = \frac{\dot{E}_{en,OUT} - \dot{E}_{en,IN,sw}}{P} = \frac{\dot{m}_2 \cdot h_2 - \dot{m}_1 \cdot h_1}{P} \tag{16}$$

Exergy balance:

- Exergy power input (only sea water flow):

$$\dot{E}_{ex,IN,sw} = \dot{m}_1 \cdot \varepsilon_1 \tag{17}$$

- Exergy power input (cumulative):

$$\dot{E}_{ex,IN,c} = \dot{m}_1 \cdot \varepsilon_1 + P \tag{18}$$

- Exergy power output:

$$\dot{E}_{ex,OUT} = \dot{m}_2 \cdot \varepsilon_2 \tag{19}$$

- Exergy power loss (exergy destruction):

$$\dot{E}_{ex,D} = \dot{E}_{ex,IN,c} - \dot{E}_{ex,OUT} = \dot{m}_1 \cdot \varepsilon_1 + P - \dot{m}_2 \cdot \varepsilon_2 \tag{20}$$

- Exergy efficiency [16]:

$$\eta_{ex} = \frac{\dot{E}_{ex,OUT} - \dot{E}_{ex,IN,sw}}{P} = \frac{\dot{m}_2 \cdot \varepsilon_2 - \dot{m}_1 \cdot \varepsilon_1}{P} \tag{21}$$

Ambient conditions during measurements were:

- pressure: p_0 = 0.1 MPa = 1 bar,
- temperature: T_0 = 25 °C = 298.15 K.

3. Measurement results and measuring equipment of the analyzed sea water pump

Measurement results for sea water pump during pump operation are presented in Table 2. Pump operating parameters were presented in relation to propulsion propeller speed. Propulsion propeller speed is directly proportional to steam system load - higher propulsion propeller speed denotes a higher steam system load and vice versa. It also should be noted that the sea water pump load is directly proportional to steam system load, during the entire pump operating time.

Table 2. *Measurement results for sea water pump during its operation*

Propulsion propeller speed (rpm)	Sea water pump - inlet			Sea water pump - outlet	
	Temperature (°C)	Pressure (MPa)	Sea mass flow (kg/h)	Temperature (°C)	Pressure (MPa)
0.00	30	0.1	1120106	30.003	0.223
25.58	22	0.1	1346990	22.002	0.221
34.33	22	0.1	1795986	22.002	0.217
41.78	22	0.1	1795986	22.002	0.218
53.50	22	0.1	2244983	22.002	0.214
56.65	18	0.1	2471535	18.001	0.212

The measurement results were obtained from the existing measuring equipment mounted on the pump inlet and outlet. All measuring equipment is tested and calibrated by producers. List of all used measuring equipment is presented in Table 3.

Table 3. *Used measuring equipment for the pump analysis*

Sea temperature (pump inlet and outlet)	Greisinger GTF 401-Pt100 - Immersion probe [17]
Sea pressure (pump inlet and outlet)	Yamatake JTG940A - pressure transmitter [18]
Sea mass flow (pump inlet)	Promass 80F - Coriolis Mass Flow Measuring System [19]
Propulsion propeller speed	Kyma Shaft Power Meter (KPM-PFS) [20]

4. Results of pump energy and exergy analysis

At each operating point of the analyzed sea water pump is calculated sea volume flow, an essential element for pump used power calculation. Sea water volume flow is calculated for the pump inlet by using measured sea temperature and pressure along with measured sea mass flow, Table 2.

Fig. 2 presents the change in sea water volume flow at the pump inlet for each pump (steam system) load during pump operation. Increase in pump load causes a continuous increase in sea water volume flow from the lowest value (1125 m^3/h at propulsion propeller speed of 0.00 rpm) to the highest value (2475 m^3/h at propulsion propeller speed of 56.65 rpm).

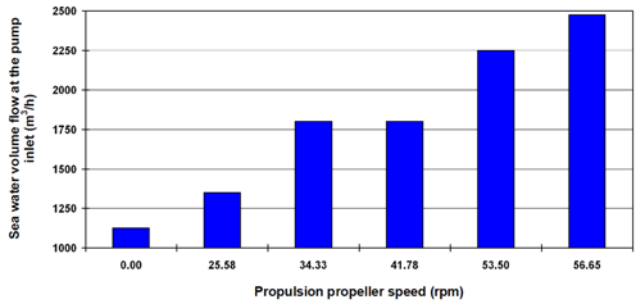


Fig. 2. *Change in sea water volume flow at the pump inlet for various pump loads*

Pump used power is calculated from the sea water volume flow at the pump inlet, according to equation (10). As presented in Fig. 3, pump used power change has the same trend as sea water volume flow. At the lowest load (0.00 rpm of the propulsion propeller) pump uses power of 122.77 kW, while at the highest load (56.65 rpm of the propulsion propeller) pump uses power of 127.85 kW. As expected, sea water pump used power increases during the increase in pump (steam system) load.

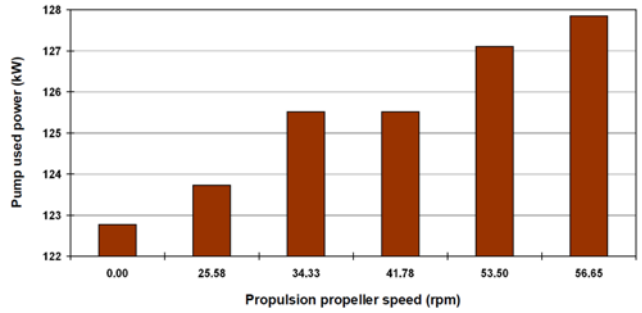


Fig. 3. *Change in a pump used power for various pump loads*

Energy power input and output of the analyzed pump in each observed operating point is presented in Fig. 4. According to equation (13), cumulative energy power input is a sum of only sea water flow power input and pump used power. At each pump operating point, pump used power influence on cumulative energy power input is very small, the dominant element of the cumulative energy power input is sea water flow energy power input. Only sea water flow energy power input amounts from 99.64 % to 99.78 % of cumulative pump energy power input.

In the entire pump operating range, cumulative energy power input amounts from 34686 kW up to 57732 kW, while energy power output amounts from 34608 kW up to 57676 kW. Energy power loss in each observed pump operating point is the difference between cumulative energy power input and energy power output. By taking into account the amount of cumulative energy power input and output, energy power loss for the observed pump will have small values in each operating point, which will not exceed 85 kW.

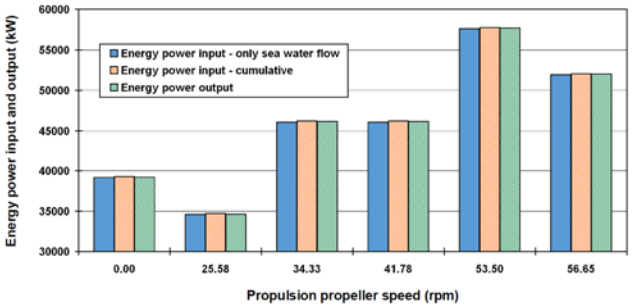


Fig. 4. *Change in pump energy power input and output for various pump loads*

Fig. 5 presents change in sea water pump energy power losses and energy efficiency. At the lowest pump load (0.00 rpm of the propulsion propeller) energy power loss is the highest and amounts 82.32 kW. Pump energy power losses continuously decrease during the increase in pump load and the lowest energy power loss was obtained at the highest pump load (56.65 rpm of the propulsion propeller) and amounts 51.64 kW.

The lowest pump energy efficiency was obtained at the lowest pump load and amounts 32.95 %, while the highest pump energy efficiency was obtained at the highest pump load and amounts 59.61 %. From Fig. 5 can be seen that pump energy efficiency continuously increases during the increase in pump load.

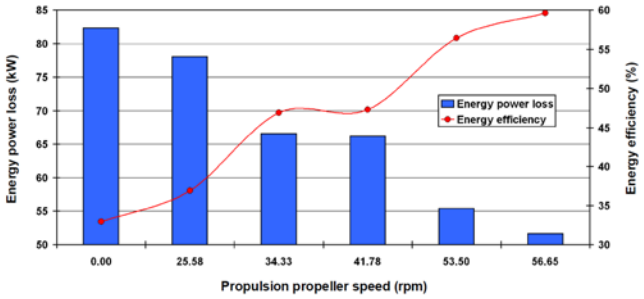


Fig. 5. *Change in pump energy power loss and energy efficiency for various pump loads*

Change in pump exergy power input and output is presented in Fig. 6. Pump used power has a strong influence on pump cumulative exergy power input. Only sea water flow exergy power input amounts from 16.12 % to 30.52 % of cumulative pump exergy power input for all pump operating points except for one at the highest pump load. It can be concluded that pump used power has a strong influence on pump cumulative exergy power input, while its influence on cumulative pump energy power input is low, Fig. 4.

For the whole sea water pump operating range, cumulative pump exergy power input amounts from 147.50 kW up to 367.64 kW, while pump exergy power output amounts from 69.15 kW up to 316.82 kW.

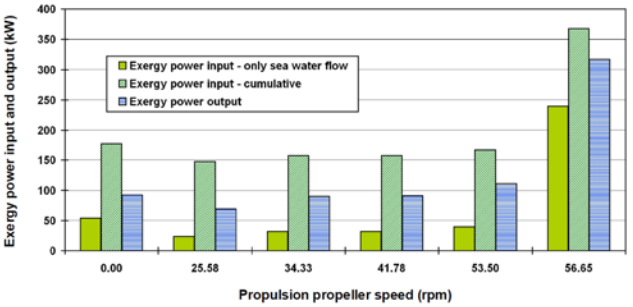


Fig. 6. *Change in pump exergy power input and output for various pump loads*

The change in sea water pump exergy power losses (exergy destruction) and exergy efficiency is presented in Fig. 7. The lowest pump exergy efficiency was obtained at the lowest pump load (0.00 rpm of the propulsion propeller) and amounts 31.31 %, while the highest pump exergy efficiency was obtained at the highest pump load (56.65 rpm of the propulsion propeller) and amounts 60.25 %.

At the lowest pump load exergy destruction has the highest value and amounts 84.33 kW. Pump exergy destruction continuously decreases during the increase in pump load and the lowest exergy destruction was obtained at the highest pump load and amounts 50.83 kW.

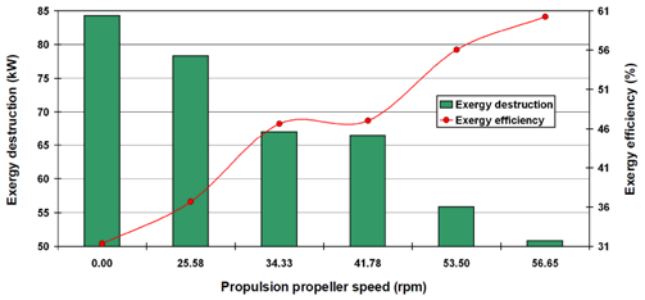


Fig. 7. *Change in pump exergy destruction and exergy efficiency for various pump loads*

5. Conclusions

The paper presents energy and exergy analysis of sea water pump which is used for the main condenser cooling at lower steam propulsion system loads on conventional LNG carrier.

By using the measured variables from the exploitation, it can be concluded that pump used power has a strong influence on pump cumulative exergy power input, while its influence on pump cumulative energy power input is minor, for the whole observed pump operation range.

Pump energy power losses and exergy destruction are reverse proportional to pump load. Increase in pump load also causes a continuous increase in both energy and exergy efficiencies. The highest pump energy efficiency amounts 59.61 %, while the highest pump exergy efficiency amounts 60.25 %. Increase in both efficiencies (and decrease in both power losses at the same time) will be possible if the pump operates at the highest possible loads, higher that presented ones from LNG carrier exploitation.

6. Acknowledgment

The authors would like to extend their appreciations to the main ship-owner office for conceding measuring equipment and for all help during the exploitation measurements. This work was supported by the University of Rijeka (contract no. 13.09.1.1.05) and Croatian Science Foundation-project 8722.

NOMENCLATURE

Abbreviations:

LNG	Liquefied Natural Gas

Latin Symbols:

$\dot{E}$	stream flow power, kJ/s
h	specific enthalpy, kJ/kg
$\dot{m}$	mass flow, kg/s or kg/h
p	pressure, MPa
P	power, kJ/s
$\dot{Q}$	heat transfer, kJ/s
s	specific entropy, kJ/kg·K
$\dot{X}_{heat}$	heat exergy transfer, kJ/s
T	temperature, °C or K
$\dot{V}$	volume flow, m^3/h

Greek symbols:

ε	specific exergy, kJ/kg
η	efficiency, -

Subscripts:

0	ambient state
c	cumulative
D	destruction
en	energy
ex	exergy
IN	inlet
OUT	outlet
PL	power loss
sw	sea water

7. References

[1] Schinas, O., Butler, M.: *Feasibility and commercial considerations of LNG-fueled ships*, Ocean Engineering 122, p. 84–96, 2016. (doi:10.1016/j.oceaneng.2016.04.031)

[2] Baldi, F., Ahlgren, F., Melino, F., Gabrielii, C., Andersson, K.: *Optimal load allocation of complex ship power plants*, Energy Conversion and Management 124, p. 344–356, 2016. (doi:10.1016/j.enconman.2016.07.009)

[3] Fernández, I. A., Gómez, M. R., Gómez, J. R., Insua, A. A. B.: *Review of propulsion systems on LNG carriers*, Renewable and Sustainable Energy Reviews 67, p. 1395–1411, 2017. (doi:10.1016/j.rser.2016.09.095)

[4] Kaushik, S. C., Siva Reddy, V., Tyagi, S. K.: *Energy and exergy analyses of thermal power plants: A review*, Renewable and Sustainable Energy Reviews 15, p. 1857–1872, 2011. (doi:10.1016/j.rser.2010.12.007)

[5] Hafdhi, F., Khir, T., Ben Yahyia, A., Ben Brahim, A.: *Energetic and exergetic analysis of a steam turbine power plant in an existing phosphoric acid factory*, Energy Conversion and Management 106, p. 1230-1241, 2015. (doi:10.1016/j.enconman.2015.10.044)

[6] Mrzljak, V., Poljak, I., Mrakovčić, T.: *Energy and exergy analysis of the turbo-generators and steam turbine for the main feed water pump drive on LNG carrier*, Energy Conversion and Management 140, p. 307–323, 2017. (doi:10.1016/j.enconman.2017.03.007)

[7] Mrzljak, V., Poljak, I., Medica-Viola, V.: *Dual fuel consumption and efficiency of marine steam generators for the propulsion of LNG carrier*, Applied Thermal Engineering 119, p. 331–346, 2017. (doi:10.1016/j.applthermaleng.2017.03.078)

[8] Kanoğlu, M., Çengel, Y.A., Dincer, I.: *Efficiency Evaluation of Energy Systems*, Springer Briefs in Energy, Springer, 2012. (doi:10.1007/978-1-4614-2242-6)

[9] Zisopoulos, F. K., Moejes, S. N., Rossier-Miranda, F. J., Van der Goot, A. J., Boom, R. M.: *Exergetic comparison of food waste valorization in industrial bread production*, Energy 82, p. 640–649, 2015. (doi:10.1016/j.energy.2015.01.073)

[10] Ahmadi, G., Toghraie, D., Azimian, A., Ali Akbari, O.: *Evaluation of synchronous execution of full repowering and solar assisting in a 200 MW steam power plant, a case study*, Applied Thermal Engineering 112, p. 111–123, 2017. (doi:10.1016/j.applthermaleng.2016.10.083)

[11] Ahmadi, G., Toghraie, D., Ali Akbari, O.: *Solar parallel feed water heating repowering of a steam power plant: A case study in Iran*, Renewable and Sustainable Energy Reviews 77, p. 474–485, 2017. (doi:10.1016/j.rser.2017.04.019)

[12] Szargut, J.: *Exergy Method - Technical and Ecological Applications*, WIT Press, 2005.

[13] *Final drawing for Main Sea Water Circulation Pump*, Shinko IND. LTD., Hiroshima, Japan, 2006., ship documentation

[14] Lemmon, E. W., Huber, M. L., McLinden, M. O.: *NIST Reference Fluid Thermodynamic and Transport Properties-REFPROP*, Version 8.0, User's Guide, Colorado, 2007.

[15] Cengel Y., Boles M.: *Thermodynamics an engineering approach*, Eighth edition, McGraw-Hill Education, 2015.

[16] Moran M., Shapiro H., Boettner, D. D., Bailey, M. B.: *Fundamentals of engineering thermodynamics*, Seventh edition, John Wiley and Sons, Inc., 2011.

[17] https://www.greisinger.de (accessed: 18.09.2017.)

[18] http://www.industriascontrolpro.com (accessed: 18.09.2017.)

[19] https://portal.endress.com (accessed: 22.09.2017.)

[20] https://www.kyma.no (accessed: 02.10.2017.)

THE PECULIARITIES OF THE METALLURGICAL DESIGN DEVELOPED THROUGH PROJECT MANAGEMENT PRINCIPLES

Prof.Tontchev N.[1], Assoc. Prof. Dimitrov D.[1] Prof. Hai Hao[2]
[1]«Todor Kableshtov» Higher School of Transport, Sofia, Bulgaria
[2]Dalian University of Technology (DUT): 大连理工大学

Abstract. *The tools for statistical expert evaluation of the influence of alloy composition elements on pre-selected quality indicators are described in order to improve the mechanical properties of the products through the prism of project management. Through the defined approach, it is possible to define a composition providing relatively best meanings of the values of the selected mechanical indices.*

KEY WORDS. SIMULATION, ANN, MODELING, OPTIMIZATION, METALLURGICAL DESIGN.

1. Introduction

At the design stage, the material selection process reflects a whole strand of material science. The traditional alloy development strategy consists of producing multiple samples with varying composition and variations in chemical composition and processing mode to define an alloy with better properties [1]. This approach, known as "trial-error" leads to high experimental costs [2]. In most cases, experimental research may be difficult, too long and unacceptably expensive. An alternative effective approach is the use of previous experience data processed into a statistical model based on a large amount of data associated with composition, processing and properties. Compared to physical models, the advantage of statistical models lies in their ability to obtain complex informative in a peculiar and effective way even when there are no well-established physical theories and models [3], [4].

We develop a system of methods for modeling the properties and optimization of the composition of different alloys. This paper attempts to point to a number of examples with the formulations of which, from various daughter projects, it is possible to develop further and improve the original idea developed in [7]. The formulated task stems directly from the subject of material science and it is already implemented for alloys of iron [7], titanium [9] and magnesium [9] base. In this regard, the graphical visualization of the basic problems of the material science – the basis of the projects for research of the relationship between properties and structure – is depicted in Fig. 1.

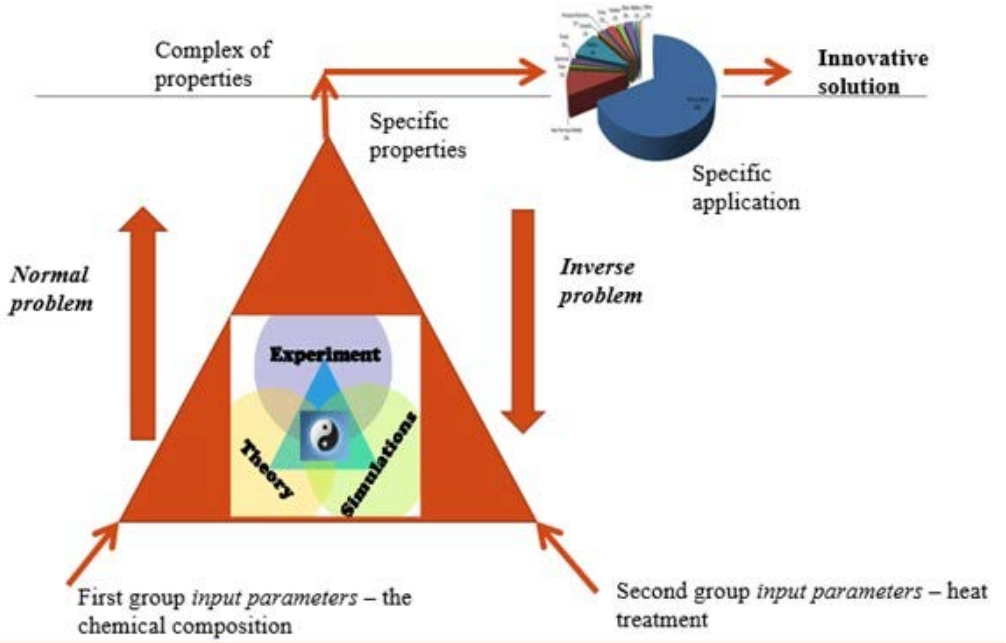


Fig.1. *Relationship between the elements of the problems and the projects from material science.*

The number of all parameters in the project is determined by the sum of the two sets of parameters (the parameters for the type, the number and the quantity of the alloying elements and the parameters of thermal, physical or mechanical impact).

The right task examines the impact of these parameters to synthesize new materials and in the inverse task and a defined and known application or characteristic values of the exploitation behavior, a rational type of material is determined with its composition and processing parameters.

The numeric metallurgical design is not only designing in the base of allying elements by type, number and quantities but also taking into account their synergistic effect. It is necessary to select such a synergistic effect by a combination of elements in which the more expensive elements are in smaller quantities. Along with the accomplishment of this task, the metallurgical design has to fulfill the desired compromise between the properties of the product, depending on the processing parameters. These several groups of parameters should form the overall processing and composition parameters. The complexity of the so formulated problem lies in the large

number of input parameters and in the fact circumstance that the chemical composition participates implicitly via the synergistic effect in the system "composition – processing – structure – properties – price.

Alloy composition design and optimization of process parameters are directly related to resolving the trade-off between measured values relative to defined selected quality indicators for a set of materials in a surveyed group or class.

The process system also optimized the technological parameters of the processes, such as ionization, pouring, post-casting, as well as casting and thermal treatment of aluminum wheels.

With the quoted system, there have been optimized also the technological parameters of the processes such as ionization, plastering, post-casting, as well as casting and thermal treatment of aluminum wheels.

2. Classification of Material-Science Projects

The pursuit of strengthening in defining the specific purpose of a project in the field of material science is associated with its uniqueness. In this subject area, in the development of projects arising from the main task and also from "studying the relationship between the influence of chemical composition and heat treatment on mechanical properties in order to search for new applications", the projects have a unique effect because – as a result of the optimization – a new innovative solution is usually obtained (Fig.1).

The specificity of these tasks is associated with a certain complex of properties, which analyzes several criteria (different qualitative indicators, which are most often contradictory in character), and the optimization of which determines solutions that are inherently effective. This goal is defined in the literature as the SMART goal, and the meaning of this abbreviation is described and explained in more detail in the table below.

Table 1. *Defining the SMART-goal abbreviation*

S	**S**pecific
M	**M**easurable
A	**A**chievable
R	**R**ealistic
T	**T**imed

The specificity of such projects is a consequence of the subject matter of the material science from which the basic relationship "structure-properties" derives. For the definition of qualitative indicators (most often mechanical characteristics) there are standardized methodologies that guarantee a measurable quality result. Many examples from our previous experience prove that the objectives of such a project are achievable. They depend on the database used, and the result of the project is to apply authoring methods that can determine chemical compositions outside the database to exceed the mechanical performance of the database. In this sense, the purpose of the project is realistic.

Determining the project over time depends on the volume of tasks set such as the size and the number of research quantities, and the organization of the implementation of the key activities. The main focus of this organization is at the stage of experimental testing of the prescribed compositions, which are determined by the application of the methodology as optimal.

Since the process of formulating the goal is not an easy process, there are projects that start with an undefined purpose. There is a certain categorization in this sense, which is presented in Fig. 2. It – besides an established or unsettled SMART goal – has also been implemented through known and unknown methods and technologies that will be implemented during the implementation of the project.

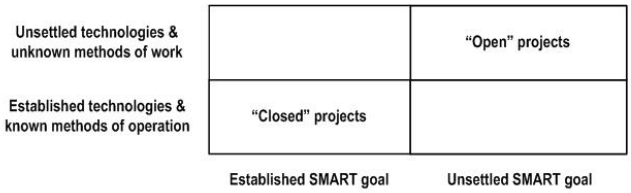


Fig.2. *Classification of projects for clarified goals and used technologies*

"Closed" projects are standard and routine projects. They are most likely to be successful and their performance is associated with the least risk. However, in any organization there is a "narrow" place, shaped as a project where the goal is difficult to be determined and the technology for its solution is unknown.

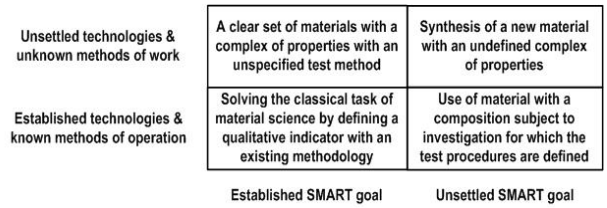


Fig.3. *Specifying the classification from Fig.1 for projects in the field of material science*

In this sense, the project team has never solved such problems, and these projects are called "open" because the issue is open to both the goal and the technologies and methods to be used. The organization balances its activity by accepting to develop both "open" and "closed" projects. "Closed" projects are implemented in a short-term perspective, but similar projects are also being implemented by competitors so they are not very lucrative.

Fig.3 presents a specific application of the above Classification for Material Science projects to elucidate the structure-property relationship in order to provide a more rational application.

In the discovered project of the type described, there is a partial requirement for the material group and the conditions for the operational work in which the workpiece/product will work are known. If it is on a metal base, it is possible to apply a solution theoretically developed by the cited project, consisting of the following:

The existing system of numerical methods, by means of which it is possible to determine optimal thermal processing compositions and parameters, associated with a pre-search complex of properties. Various iterations, specifying shape and size, are performed with CAD / CAE system calculations. The search object in the project does not appear in the CAD system database. The calculations are performed with the material closest to the research class. On the basis of the strength calculations the complex of properties is determined. If there is no standardized test in the **set** of properties, a methodology is developed and experimental research is performed. Project calculations provide optimal formulations for the desired complex of properties. These compositions are validated as being appropriate after an experimental check. Following the verification, the database can be supplemented with the newly defined compositions.

The existing system of numerical methods, by means of which it is possible to determine optimal thermal processing compositions and parameters, associated with a pre-search complex of properties. In various iterations, specifying shape and dimensions, calculations for the strength are performed with the CAD/CAE system. The material being searched for in the project is not included in the CAD system database. The

calculations are performed with the material closest to the research class. On the basis of the strength calculations the complex of properties is determined. If there is no standardized test in the set of properties, a methodology is developed and experimental research is performed. Project calculations provide optimal formulations for the desired complex of properties. These compositions are validated as being appropriate after an experimental check. Following the check, the database with the newly defined compilations can be added.

The Project Life Cycle is related to the full set of stages (phases) of the project, the definition and number of which define the technology of production and the control needs of the organizations involved in the project.

"Open" and "closed" projects differ in their lifecycle approaches. Each project is fragmented in steps. Defining the lifecycle of the "closed project" bears the name "waterfall", because the tasks are done in a top-down sequence and it resembles a cascade of water.

The example of the "closed" project authorizing the classical task "chemical composition – property" according to an approved methodology of the tested indicator is defined by the following phases of the "waterfall" life cycle:

1.Start the project.

2. Collecting existing experience, described by experimental data, expressing the relationship between the different chemical elements of the alloy and the

3.Data processing to obtain a regression [model] or neuronal model.

4. A single-criterion optimization of the derived model, resulting in a composition, guaranteeing an optimal value of the studied property.

5.Experimental examination of the theoretically determined composition.

6.Final of the project with a specified optimal chemical composition.

The definition of the waterfall life cycle model is related to the definition of the main project parameters (content, time, price cost and thus it determines the start of the project. Planning takes place for each project, and some of the phases can be run in parallel. The model is effective when it has a high degree of certainty.

However, the algorithm for "open" projects is [somewhat] different. The first necessary condition is to take steps to clarify the goals and technologies under which these projects will be implemented. However, this condition is not always possible to fulfill in conditions of great uncertainty and a constantly changing external environment. In this case, the "waterfall" life cycle ceases to work. If it is applied, time and resources may be lost and when the project finishes, it can be ascertained that the results obtained are not needed by our applicant.

For open projects where there is a large uncertainty, an iterative life cycle model is being developed. This model involves breaking the content of the project into small iterations. The end of each iteration is controlled by the applicant who has a feedback on the execution of the corresponding intermediate state. Then work continues and begins the next iteration, which in a certain sense is another mini project at the end of which a feedback from our applicant is expected again.

The result of the last stage may be unsatisfactory, which means it is possible to go back [with] a step back before proceeding with the new iteration. After a certain number of iterations, the applicant is fully satisfied with the outcome and this determines the end of the project. This result is ensured at all stages of the project. The end of the project was unknown and it was determined in the course of the work. The great advantage of the iterative approach is to work with a large variability in the external environment.

The iterations ensure the improvement of the resulting product in the course of the project. Planning is performed only for the upcoming iteration. The disadvantage of the iterative approach is that re-expenditures are incurred for the individual iterations of the project itself. The team performs planned actions, some of which the applicant in the process of work may not accept, as a result, and then go another way.

The example of an iteration from the defined in Fig. 2 "open" project is limited to the following:

1. Sequential gradual clarification of the influence of individual elements of the chemical composition on the investigated properties. Determining the synergistic effect of the specified elements and selecting a combination that contains smaller quantities of costly elements. This synergistic effect should relate to the properties of the entire explored complex.

This example is typical for the application of the iterative life cycle, because the simulation uses the idea of a "trial-error" method to elucidate the effect of a combination of individual elements on a sought-after complex of properties.

3. Tools Used to Implement Material Science Projects

In the process of a numerical experiment, the solutions determining the predictive potential of the regression and neural models in the multi-criteria optimization of a number of properties are compared in varying the percentage of the alloying elements or the processing parameters.

The recommended tools are looking for and finding convergent and compromising solutions in the presence of diversity and heterogeneity of the output data. This is also done for the contradiction of the requirements to the designed objects. The influence and the interaction between the alloying elements and their synergistic effect related to the properties of the alloys and in particular their strength and performance properties are monitored.

The methodology of the research project consists of the following stages:

- Preliminary statistical analysis of the research data with visualization of the dependencies between observed quantities. This includes the determination of the basic (descriptive) statistical characteristics, the presence of a correlation of the parameters of the experimental studies.
- Simplification of the dependencies between the participating in the alloy chemical elements and its mechanical properties using neural models.

The most important task at this stage is to find an opportunity to find a possible relation between the independent parameters and the dependent characteristics in the experimental research. The statistical analysis allows determine the uncorrelated input parameters from the experiment that can be used to construct a regression model – the percentage of elements in the composition of the alloy under consideration. The limited number of observations sometimes does not make it possible to draw conclusions on the statistical distribution of the observed variables.

Then with these problems with the construction of the statistical models, approximating the influence of the predictors on the values of the result quantities, most often of Rm and A, there is a need to seek the modeling of the studied relationships with other means. To solve the specific problem, the most commonly used approach is the use of neuronal models of the "multilayer perceptron" (MMP) type. This approach is not a novelty, but it proves to be too effective in cases where classical statistical methods do not work. It allows for the compilation of approximation models in cases where the relations between the

observed values are considerably more complex and sometimes implicit.

In general, neural models are not related to statistical techniques, but they are regarded as self-contained outcomes of machine learning. However, many authors note the computational similarity of these models with the methods of statistical analysis. It is possible to use the Automatic Neural Network of the popular statistic package Statistica. It enables an experiment with more than 2000 models for each of the approximate searches, the selection being made according to the value of the correlation coefficients between the observed and the calculated result values (respectively for the learning, the test and the validation sets).

The analysis of the results of the approximation with the fixed neuronal models can be supplemented by a sensitivity analysis. The latter shows the relative importance of the predictors in the formation of the values of the resultant variables. There is a significant influence of the predictor is if its value is greater than 1.

Following these statistical techniques, it is recommendable to use a Pareto front, which is an established traditional method in multi-criteria research. It makes it possible to assess the appropriateness and the expected effect of combining different preferences regarding the significance of the physico-mechanical parameters of the material, such as the tensile strength Rm and the relative elongation A. The classical formulation of the task of building a set of non-dominated solutions for the multi-criteria selection has the following appearance:

- Basic optimization task - presented in the following form:

$$\max(f_1(x), f_2(x),..., f_m(x)), \quad (1)$$

where:

$f_1(x), f_2(x),..., f_m(x)$ are the private optimization criteria (physico-mechanical characteristics of the material);

$$x \in D \subset R^n, m \le 2, x = (x_1, x_2,..., x) \quad (2)$$

are the conditions defining the decision domain D of the solution vector $x=(x_1,x_2, \ldots, x_n)$. In the specific problem the definition area is set in the form of interval limits:

$$D: x_k \in [l_k, h_k] \subset R, \ k = 1,..,n, \quad (3)$$

where l_k and h_k are respectively the lower and upper bounds of the change interval of each of the arguments (percentage of the chemical element in the material)

- The relation of dominance between a pair of solutions $x^{(1)}$ and $x^{(2)}$ ($x^{(1)} \prec x^{(2)}$) - is expressed as follows:

$$\forall i = 1,..., m \ \ f_i(x^{(1)}) \ge f_i(x^{(2)}),$$
$$\exists j = 1,..., m \ \ f_j(x^{(1)}) > f_j(x^{(2)}). \quad (4)$$

The dominance of $x^{(1)}$ versus $x^{(2)}$ exists when at least one of the criteria has strict inequality (with the indicated orientation) for the two alternative solutions, and for the other criteria is in effect non-steady inequality (or at least equality) .

The Pareto- optimal set is a set of solutions $P^* \subset D$ that are not dominated by any element of the D set. The Pereto-front can be graphically displayed in the space of the considered criteria $f_i(x)$.

The implementation of this experimental-computational approach requires the preliminary ~~study~~ research of the experimental data in order to obtain approximating quantitative relation~~ships~~ between them and subsequently to include the established dependencies in a suitable optimization algorithm.

The steps involved in conducting the research are as follows:

- Creation of approximation models linking the parameters of the alloy composition with the resulting physico-mechanical parameters;
- Selection of a suitable algorithm for building a Pareto front;
- Incorporating the aproximation models into the algorithm and realization as a programming tool.

All numerical approaches for the metallurgical design are set out in [7]

4. Conclusion

An approach has been described to offer a realistic opportunity to significantly reduce the cost and time to predict chemical concentrations for multiple properties of a class of alloys and technological processes so that under new conditions these materials have better properties. The obtained results from our previous research have shown that the proposed methodology can be fully used to determine the essential relations between the extreme values of the mechanical parameters of the investigated alloys.

Any addition to the experimental measurement database would allow the software model to be refined and further refine the results. The proposed approach and established dependencies can be used in engineering practice.

References:

1. Campbell C.E., G.B. Olson, “System design of high performance stainless steels I, Conceptual and computational design”, Journal of Computer-Aided Materials Design 2001, 7:145-17
2. Vitos L., P.A. Korzhavyi and B. Johansson, "Stainless steel optimization from quantum mechanical calculations", Nature Materials 2003, 2:25-28
3. Jones, J. , MacKay, D. J. C., "Neural Network Modeling of the Mechanical Properties of Nickel Base Superalloys", 8th Int. Symposium on Superalloys, Seven Springs, PA, eds. R. D. Kissinger et al., published by TMS, 1996, pp. 417-424.
4. Fujii, MacKay, D. J. C. and Bhadeshia, H. K. D. H., "Bayesian neural Network Analysis of Fatigue Crack Growth Rate in Nickel-Base Superalloys”, ISIJ International, Vol. 36, 1996, pp. 1373-1382.
5. Borst R. de, “Challenges in computational materials science: Multiple scales, multi-physics and evolving discontinuities”, Computational Materials Science 2008, 43:1-15
6. Fischer C.C, K.J. Tibbetts, D. Morgan and G. Cedar, "Predicting crystal structure by merging data mining with quantum mechanics", Nature Materials 2006, 5:641-646
7. Tontchev N. Materials science, Effective solution and technological variants. Lamber, 2014.
8. Razmov T., D. Dimitrov , Laboratory Exercise and Course Design on "Project Management" - Third Edition, Todor Kableshkov University of Technology, 2012.
9. https://www.researchgate.net/profile/N_Tontchev/contributions

ELECTRIC POWER SYSTEMS MODELING AND EDUCATION: HYDRO POWER STATIONS MODELING FRAMEWORK

M.Sc. Trashlieva V. [1], M.Sc. Radeva T. PhD.[1]
Department of Electrical Power Engineering – Technical University of Sofia, Bulgaria
vesselina.trashlieva@gmail.com

Abstract: *In this paper we try to bring a modeling framework in optimization problems for hydro-thermal coordination problems solved in electric power systems. There are certain specifics when dealing with hydro power plants and the reservoirs they are fed from. In many cases these water reservoirs are connected and this involves additional complications in optimization models building. We give guidelines for model size reduction and awareness. This framework is suitable for practitioners willing to be aware of hydro-power modeling and optimization but having no previous mathematical optimization training and experience.*

Keywords: HYDRO-THERMAL COORDINATION, WATER RESERVOIRS MODELING TECHNIQUES

1. Introduction

The unit commitment problem is the procedure for defining the optimal engagement of the units and a plan for optimal operation of the plants in an Electric Power System (EPS). The solution of this problem involves two things: the determination of the operating and reserved units and the output power of each operating unit (an economic dispatch)[1]. The cost function represents in most of the cases a striving to minimize the total operating and production costs while strictly respecting the balance between consumption and production, the reliability and security requirements, according to the constraints arising from the generating units themselves. Due to the nature of the different power stations, often the optimization problems involving the operation of both hydro-power and thermal power plants are subjected to a separate class of problems solved in EPS, called *optimal hydro-thermal coordination*.

2. The HPS and PHPS

Hydro power stations (HPS) use water as a primal source to produce electric power. The cost of water is negligible smaller related to the price for fuels used by the conventional thermal power plants. Water, however, is also a limited resource meaning that the available quantities for the individual planning periods must be used wisely. HPS are the most widely used plants for electricity generation from renewable energy sources, accounting for 16% of global electricity production by 2010, and is projected to grow by an average of 3.2% annually over the next 25 years [2,3]. HPS are used in over 150 countries where China leads with 721 TWh in 2010. There are four HPS with a capacity over 10 GW worldwide.

Since the output level of a hydropower plant depends on the water supply and head, the costs curves are nonlinear as well as in the conventional thermal power stations. The advantages that the HPP provide for the balance of the EPS are not limited only to the possibility of rapid change of their working outputs and fast automated start and stop. Although this flexibility is the main factor determining HPS as peak power plants. HPS also have very low operational (production-dependent) costs, as there are virtually no costs of purchasing and supplying fuel, and the aforementioned operating costs are related to the cost of providing ancillary services, operating and maintenance. Fixed costs, however, include the return of investments for construction and modernization, depreciation of facilities, insurance, etc. Sometimes such fixed costs might be significant, especially for brand new installations. HPS have a very long life cycle and do not require large operating labor costs as HPS are operated automatically. Water dams on the other hand are multifunctional facilities, which are used for the drinking water and domestic water supply purposes, irrigation, industrial water supply, fish-breeding, aquaculture, etc. besides for electricity production purposes (according to most legislations electricity production is of lowest priority among other water purposes). Regarding construction costs, for a hydropower plant the building of the water collection system and its derivative is more expensive than the actual construction and installation of the water turbines. In fact, all deficiencies of HPS are mainly related to water collection and accumulation installments, not to the installed electricity generation apparel. Among the disadvantages the following are often stated: ecosystems damages, habitat fragmentation, land losses in the construction process of large reservoirs, congestion of large areas of land, forests and territories with rich soils, need for relocation of people, reorganization of road infrastructure, flows reduction, methane emissions of rotting organisms and flows risks. Since there is no fossil fuel combustion HPS are considered with no direct carbon dioxide production, except the relatively small quantities produced the construction phase. However, these quantities remain negligible compared to thermal plants.

The electricity production of HPS is determined by the available inlet water quantities. If there is a possibility of accumulation (sufficient useful volume of the water tank), the HPS can produce enough power when needed (under circumstances of electric power shortage). In Bulgaria HPS are mainly used as peak, balance and also accumulation capacities. Pump-storage hydropower plants (PHPS) are capable to accumulate the processed by a water turbine quantities (in the presence of a lower reservoir) and are used for balancing loads, being practically the most flexible and multifunctional elements of the EPS. During high load periods, PHPS operate as generators producing the famine power for the system's balance. During low load periods when the reduction of the power outputs of other generating units is practically impossible, PHPS operate in pumping mode like controllable loads by feeding the excess power to the pumps draining water from the lower into the upper reservoir. In addition to importing the required extra load into the system, they accumulate part of the surplus electricity, which can be later injected during the peak periods at a higher price. This reversible cycle (turbine-pump, load-generator) helps preventing frequent start-stop and the needs for frequent changes in the working levels of nuclear and thermal units.

The operation of PHPS is effective if the income of the operation of the plant is positive. This income is mainly determined by the difference between the sold electricity that is produced and the purchased electricity that is consumed by the pumps [4]. From a financial point of view, the accumulation process is an expense with a future return. If the accumulated energy is not realized in the future at better prices (this condition guarantees a positive revenue), these costs will also include the costs of lost financial benefits as the unit was idle and waited for the respective better financial period. Thus, in the end, the electric power accumulation may prove technically necessary and even crucial from the point of view of the EPS balance but economically unprofitable for the PHPS owner. Sometimes some water wastes from the upper reservoir might be required in order to provide for further load leveling. Energy storage is economically justified when the cost of the electricity used by the pumps is lower than the electricity generated and sold, taking into account the accumulation-generation cycle losses. System load demonstrates daily, weekly and seasonal changes that have to be followed by the power plants. A system operator having a PHPS accumulate the cheaper energy produced during low load

periods and deliver it to the grid during the peak periods when the process is cost-effective. If there is an opportunity to accumulate energy (large dams are built), generation may be postponed. This is not a "*surplus*" energy storage. This power can be used in the balancing market later. Power plants using renewables (except HPS of stored water) can not generally accumulate their primary source and by using their current availability they usually increase the EPS balancing problems [5-7].

With the increase in penetration of power stations using renewable power sources as wind and sun (also considered as stochastic power plants), PHPS become an indispensable element in the balance management of EPS, that present a buffer to reconcile the inconsistency of the renewable generation and load curves. In this paper, some attention is paid to the operation optimization of HPP and PHPS as balancing capacities and a means of minimizing total costs in the EPS[8-14].

3. Modelling interconnected HPS and PHPS

The modeling of the operation of the HPS and PHPS requires modeling of the plant's curve and associated water volumes. Some HPS operate in a cascade mode, i.e. their work is interconnected (consecutive and dependent) within a given terrain. So despite that the cost of the primary energy carrier for HPS is negligible, it is also necessary to model the "*stock*" of water availability. Water reservoirs may be of a complex purpose or electricity production only. The water reservoirs also imply a certain cycles for the water levels management (daily, seasonal, yearly) associated with the so-called water allowances. The inclusion of HPS and PHPS in the EPS optimization leads to two events: HPS allow for *peak shaving* to be adjusted, but also lead to the addition of additional constraints and variables for modeling the work of water power plants. The curve of water waste for a HPS is a function of the water quantity Q fed to the turbine: $P_{k,j} = f(Q)$.

Nomenclature for HPS and PHPS:

r - reservoirs

k - power stations (HPS and PHPS)

$V^{\min}_{r,Usable}, V^{\max}_{r,Usable}$ - minimal and maximal usable water reservoir r volume

$V_{r,j}$ - water reservoir r volume at the end of the time interval j

$F_{r,j}$ - water flow in r during a unit interval j

$R_{r,j}$ - unprocessed water from r in a unit interval j. Unprocesses water quantity includes controllable water release as well as uncontrollable losses such as evaporation.

$P_{Pk,j}$ - power used by the pumps of k in a unit interval j

$P_{Hk,j}$ - power produced by the turbines of k in j

$P^{\min}_{P,k}$, $P^{\max}_{P,k}$ - minimal and maximal pump capacity of k

$P^{\min}_{H,k}$, $P^{\max}_{H,k}$ - minimal and maximal generating capacity of plant k

φ_{Hk} и φ_{Pk} - water consumption (m^3/MWh) for plant k in both generation and accumulation mode

$w_{k,j}$ - artificial binary variable for the operation mode of a PHPS k. $w_{k,j} = 1$ if the mode is pumping in j

The operational curve of a HPS with neglecting the water head may be expressed via the following linear functions:

$Q_{Hk,j} = \varphi_{Hk} P_{Hk,j}$ (1) - processed water quantity by the turbines of plant k in a unit interval j

$Q_{Pk,j} = \varphi_{Pk} P_{Pk,j}$ (2) - processed water quantity by the pumps of plant k in a unit interval j

The output level of all units / plants must be within the technological limits:

$$P^{\min}_{H,k} \le P_{Hk,j} \le P^{\max}_{H,k} \quad \text{and} \quad P^{\min}_{P,k} \le P_{Pk,j} \le P^{\max}_{P,k} \qquad (3)$$

When modeling the PHPS operation, it is necessary to introduce restrictions for non-simultaneous operation of pumping and production capacities for each PSHP in a single interval:

$$P_{Pk,j} - w_{k,j} P^{\max}_{Pk} \le 0 \text{ and } P_{Hk,j} - (1 - w_{k,j}) P^{\max}_{Hk} \le 0 \qquad (4)$$

The volume of each reservoir in every unit interval must be within the actual water level limits:

$$V^{\min}_{r,Usable} \le V_{r,j} \le V^{\max}_{r,Usable} \qquad (5)$$

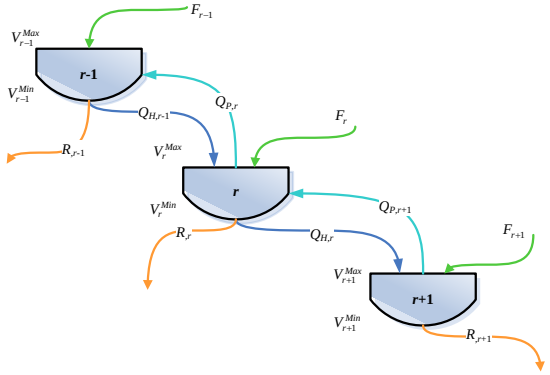
Values for the first (j=1) and last interval (j=$j_{\max}$) might be provided for the water level maintenance cycle:

$$V_{r,j=1} = V_{r,1} \qquad \text{and} \qquad V_{r,j=j\max} = V_{r,N} \qquad (6)$$

General form of the water balance constraints:

$$V_{r,j} = V_{r,j-1} + \left(- \sum_{m \in \Gamma from} \varphi_{Hm} P_{Hm,j} + \sum_{n \in \Gamma in} \varphi_{Hn} P_{Hn,j} - \sum_{q \in \Pi from} \varphi_{Pq} P_{Pq,j} + \sum_{s \in \Pi in} \varphi_{Ps} P_{Ps,j} \right) + F_{r,j} - R_{r,j} + \sum_{\rho \in in} R_{\rho,j} \qquad (7)$$

, where $\Gamma from$ and $\Pi from$ are the sets ot plants (with their pumps and turbines)that drain water from r during j. Γin and Πin are the sets of plants that feed in water in r during j. So $\sum_{\rho \in in} R_{\rho,j}$ is the sum of controlled water wastes associated with the current reservoir r (both in and out) (see figure below).



In a short-term planning (day, week) of HPS and PSHP operation, water balance equations bring more security than complexity in the model, whereas in a medium-term planning (e.g. a year) the modeling of cascade-connected water reservoirs with complex purposes will increase complexity of the model and its size. Different purposes and usage of water volumes may be modeled with so-called quotas. When a large dams with yearly or seasonal water level management is available, a long-term strategy for the possible use of water needs to be applied.

Water balance constraints are build for each interval and each reservoir, i.e. their number depends on the number of unit intervals in the planning horizon. The cycle mater management implies the existence of a certain relationship between the functional dependencies at the beginning and end of the planning horizon. In other words, if modeling of water volumes is performed for a period of one year and the single interval's duration is 1 hour, for each reservoir, 365x24 or a total of 8 760 variables have to be introduced as well as 8 760 of water balance equations, and the constraints (6) must be respected for each equalization cycle.

For large reservoirs with annual management cycle this complication can be avoided by using long-term quotas i.e. by adding availability of water quantities by months, seasons, and even annually. This will result in the introduction of significantly fewer constraints. In the case of cascade-coupled different water volumes, the constraints of the upper and lower reservoirs (8) will keep the levels of the large tanks within their respective limits.

$$Q_r^z \le Q_r^{z-1} + F_r^z + (1/z)V_r^{\max} - \\ -\sum_{k,j} Q_{Hk,j}^r + \sum_{k,j} Q_{Hk,j}^{r-1} + \sum_{k,j} Q_{Pk,j}^{r+1} - \sum_{k,j} Q_{Pk,j}^{r-1} \quad (8)$$

, where Q_r^z is the water volume in m^3 in reservoir r at the end of sub-period z, F_r^z is the flow in the reservoir during the sub-period and $F_r^z + (1/z)V_r^{\max}$ models the available water quantities for the whole sub-period.

The expression $-\sum_{k,j} Q_{Hk,j}^r + \sum_{k,j} Q_{Hk,j}^{r-1} + \sum_{k,j} Q_{Pk,j}^{r+1} - \sum_{k,j} Q_{Pk,j}^{r-1}$ models the operation of the pumps and turbines fed by and feeding in the reservoir r using the respective processed water quantities for the whole sub-period z. Thus, if a one-year horizon is considered for 1 hour single interval duration and seasonal plant operation is modeled, the water balance constraints for a reservoir r are reduced to four from the value 8 760. If an annual quota is used and seasonal interconnectivity is not required (or they are reported with similar indicators in terms of inflows, outflows and maximum volume), the constraint (8) will be only one. Thus, in an optimization problem for an optimal hydro-thermal coordination in which several cascades are modeled and the included water reservoirs are of a different purpose, volume, and management cycle it is possible to model the work of all hydro-power plants in the medium-term planning horizon and this is done without the addition of redundant complexity in the model only by using the appropriate generalization technique. Small reservoirs in the cascades are modeled by water balance equations of type (6) and (7), and the larger ones - with inequalities of the type (8).

4. Conclusion

The general idea of linear programming modelling of hydro-power plants is given including both turbines and pumps (if available), the importance of pump- hydro stations in power balance as well as the specific constraints deriving from the nature of hydro-power generation. Interconnected water reservoirs bring additional complexity and specifics in the optimization modelling. This modelling framework may be used for HPS forecasting, ED or in combination with the thermal framework for optimal coordinated work in an EPS with HPS integration. When the hydro-thermal coordination involves the optimization of PHPS a mixed-integer programming model is required. Some generalisation techniques are proposed for model size reduction that may be handy in many cases of optimization modelling.

5. Bibliography

[1]. Wood A., Wollenberg B., Power Generation Operation and Control, 3rd edition, John Wiley & Sons, New York, 2013, ISBN: 978-0-471-79055-6, 656 pages

[2]. International Hydropower Association, https://www.hydropower.org/

[3]. World Energy Council, www.worldenergy.org/data

[4]. Stoilov D., Yanev K., Electric Power Systems Regimes, Technical University of Sofia, 2011, 315 pages, ISBN 978-954-438-941-3 (in Bulgarian)

[5]. Kaneva M., Popov Z., Stoilov D., Active Power Balance in Electric Power Systems with Significant Use of Wind Power Plants, Ecological Engineering and Environment Protection, 2013г., Issue 1, pp. 60-66, ISSN 1311-8668 (in Bulgarian)

[6]. Stoilov D., Electric Power Systems Balancing and Reservation, Technical University of Sofia, 2013, pages 115, ISBN 978-619-167-084-0 (in Bulgarian)

[7]. Delarue E., Bekaert D., Belmans R., D'haeseleer W., Development of a Comprehensive Electricity Generation Simulation Model Using a Mixed Integer Programming Approach, World Academy of Science, Engineering and Technology, International Journal of Electrical, Computer, Energetic, Electronic and Communication Engineering Vol:1, No:4, 2007, pp. 615 - 620

[8]. Gjelsvik A., Mo B., Haugstad A., Long- and Medium-term Operations Planning and Stochastic Modelling in Hydro-dominated Power Systems Based on Stochastic Dual Dynamic Programming, Handbook of Power Systems I, p. 33-55

[9]. Eid C., Koliou E., Valles M., Reneses J., Hakvoort R., Time-based pricing and electricity demand response: Existing barriers and next steps, Elsevier, Utilities Policy 40 (2016) pp. 15 - 25

[10]. Anagnostopoulos J.S., Papantonis D.E., Pumping station design for a pumped-storage wind-hydro power plant, Energy Conversion and Management, Vol. 48, Issue 11, November 2007, p. 3009-3017

[11]. Chen H., Cong T.N., Yang W., Tan C., Li Y., Ding Y., Progress in electrical energy storage system: A critical review, Progress in Natural Science, Vol. 19, Issue 3, 10 March 2009, p. 291-312

[12]. Dinglin L., Yingjie C., Kun Z. , Ming Z., Economic evaluation of wind-powered pumped storage system, Systems Engineering Procedia, Vol. 4, 2012, Pages 107-115

[13]. Kapsali M., K. Kaldellis J. K., Combining hydro and variable wind power generation by means of pumped-storage under economically viable terms, Applied Energy, Vol. 87, Issue 11, ISSN: 0306-2619, November 2010, Pages 3475-3485

[14]. Siegel N.P., Thermal energy storage for solar power production, Wiley Interdisciplinary Reviews: Energy and Environment, Vol. 1, Issue 2, September/October 2012, p. 119–131

THE SUBJECTIVE MODEL OF RATIONAL CHOICE IN MULTI-AGENT SYSTEMS

Gennady PavlovichVinogradov
Тверской государственный технический университет
Tver
wgp272ng@mail.ru

Abstract: *The paper considers the problem of modeling agent's choice, which allows explaining made decisions, as well as predicting possible options. The approach is based on the ideas of a subjectively rational choice. The subjectively rational choice supposes that a choice motivation is determined by external and internal factors. Internal factors represent the interests of a subject induced by his needs and ethical system he follows. External factors are induced by accepted obligations. The agent can estimate his satisfaction with the current goal-seeking state situation. The estimation might lead to changing a structure of interests, so the agent can choose it. The paper shows that when making decisions the agent uses three sets of alternatives as follows: controlling, structural and identification. This supposes the existence of three virtual sides, which choose relevant alternatives. The selection rules for such alternatives depending on subject's awareness of the situation and the structure of his interests are formed* by finding a compromise.
KEYWORDS: REFLEXIVE CONTROL, DECISION MAKING, MODEL, COMPROMISE.

1 Introduction

Agent's behavior control, when the agent has mentality and will, has become possible after appearing of decision-making models, which take into account his subjective understanding of a choice situation. These models helped estimating control efficiency before controlling [3]. It should be noted, that a decision-making process was an uncontrolled factor in a normative decision-making theory.

The development of the idea of subjective rational choice [3] helped to:

1) explain decision-making by a subject in specific situations; 2) predict possible reactions of the other subject in various situations (for a decision-maker);

3) solve a problem of active prediction when a control side creates an appropriate image of the future for a controlee.

A subjective rational choice supposes that the choice motivation is determined by external and internal factors. Internal factors reflect subject's interests, which are induced by his needs and an ethical system. External factors are connected with obligations. Affective evaluation of the level of subject's satisfaction of current choice situation, as shown in [4], might lead to changing the structure of subject's interests, so he is able to choose it. Subject's preferences in a selection process reflect his interests, thus we can determine a number of G alternatives of a preference structure (structural alternatives according to [1]).

2 Background assumptions

1. Subject's choice is based on his view of a choice situation.

2. The components of his view reflect various aspects of understanding choice situation by the subject and create an information structure of representations. Many optional representations will be X.

3. For many surrounding conditions S a set of observed surrounding conditions meets the condition $S \cap X \neq \varnothing$, i.e. subject's view might include an objective part, as well as a phantom one.

4. The subject chooses structural alternatives depending one valuation of the level of satisfaction of choice situation property values.

5. Formation of the view is based on the procedures of perception, awareness and analysis according to subject's cognitive capabilities.

According to the abovementioned assumptions, the subject uses three sets of alternatives in decision-making: control C (modes of action), structural G and identification X. Therefore, it is possible to assume the existence of three virtual sides, which choose corresponding alternatives. A choice rule for such alternatives depending on understanding of the surrounding and the structure of interests by a subject will be called *strategies* here.

Let us assume that decision-making has several cyclical steps, and modes of action are chosen at each step $n = 1, 2, ...$ from the set C depending on the view of surrounding conditions $x \in X$. This is due to the fact that a joint over conscious (intuitional) and conscious (formal) analysis of surrounding conditions allow firstly accepting a vaguely realizable decision in multiple iterations, then more clear and grounded decision. There are also some restrictions $C_x \subseteq C$ to allow the choice of alternatives depending on the vision of surrounding conditions $x \in X$. Process dynamics in subject's surrounding is out of reach for direct perception, therefore its representations are formed using identification with the idea of choosing a vision alternative depending on the observed conditions. Here there are restrictions $X_s \subseteq X$ to allow representations as identification alternatives depending on the observed conditions $s \in S$.

Proceeding from these assumptions, according to [1], we introduce the strategy determinations.

A single-valued transformation $\lambda : X \to C$ so that $\lambda(x) \in C_x$, $x \in X$, is called a choice or control function; an ordered set $(\lambda_1, ..., \lambda_n) \equiv \lambda_1^n$ is called a choice strategy on the length horizon $n < \infty$; $\lim\{\lambda_1^n\} = \lambda_1^{n\infty}$ when $n \to \infty$ is a strategy directed to achieving a local ideal, which determines subject's reason for existence.

A single-valued monotone transformation $\xi : S \to X$ so that $\xi(s) \in X_s$, $s \in S$, is called an identification function; an ordered set $(\xi_1, ..., \xi_n) \equiv \xi_1^n$ is called an identification strategy on the length horizon $n < \infty$; a consecutive order $\{\xi_1^n, n = 1,2,...\}$ is called an identification strategy on the limited horizon. Due to the fact, that the subject tends to forming useful vision, so there is $\lim\{\xi_1^n\} = \xi^\infty$ при $n \to \infty$.

As the sets S and X meet the condition $|S| > |X|$, therefore a single-valued transformation ξ: $S \to X$ causes separation of the set S on subsets

$$\xi^{-1}(x) = \bigcup\{s \in S : \xi(s) = x\} \subset S, \; x \in X.$$

Subsets $\xi^{-1}(x) \subset S$, $x \in X$ are associated sets, i.e. any element $s \in \xi^{-1}(x)$ uniquely determines appropriate representation $x \in X$. Therefore, it can be said that subsets $\xi^{-1}(x) \subset S$, $x \in X$ form classes of equivalent representations. It allows using the methods of the fuzzy sets theory to formalize subject's representations, e.g. as described in [4].

A structure alternative $\gamma_n \in G$ chosen at the moment n is *a structure choice at* n-th step of decision-making; an ordered set $(\gamma_n, ..., \gamma_1) \equiv \gamma_1^n$ is a *structure choice* strategy on a decision-making horizon of the length $n < \infty$; a consecutive order $\{\gamma_1^n, n = 1, 2, ...\}$ is a structure choice strategy on the limited horizon. As the

subject tends to the correspondence between its structure of interests and requirements of the accepted ethical system, so there is $\lim\{\gamma_1^n\} = \gamma^\infty$ when $n \to \infty$.

3 A decision-making model with changing preference structure

According to [4] a selection criteria for a control strategy have the meaning of a desired specific value of a purposeful condition based on the result with formalization, which has the formula for the utility function $E\varphi^g(C \times S \times X)$ that depends on the structure alternative $g \in G_s$ on a parameter. As the control process starts with a certain situation $x \in X$, then the criterion $E\varphi_n(\lambda_1^n \mid \gamma_1^n)$ will also depend on the situation $x \in X$ as from the initial condition. A number of situation X is finite, so the criterion $E\varphi_n(\lambda_1^n \mid \gamma_1^n)$ will be definitely represented by a vector in the space R^X of the dimension |X|. Its parts will be written as $E\varphi_n(\lambda_1^n \mid \gamma_1^n)(x)$, $x \in X$. According to the choice result, the subjects uffers emotionally, so the quality of the structure choice strategy γ_1^n should be described as a criterion meaning "choice results satisfaction". Therefore, the quality of the structure γ_1^n is natural to describe by a folding of an expected utility vector $E\varphi_n(\lambda_n \mid \gamma_1^n) \in R^X$ in a certain composite function $\mu : R^X \to R^1$. Then a strategy quality criterion γ_1^n might be written as $\mu_n(\lambda_1^n \mid \gamma_1^n) = \mu(E\varphi_n(\lambda_1^n \mid \gamma_1^n)) \in R^1$.

The subject associates its representation quality with evaluation of possibilities of achieving desired conditions when controlling $c \in C$, as well as with the possibility of extending the number of $C\uparrow$ by including efficient alternatives. The paper [6] uses the terms of the linguistic variable "utility", which are based on the values $E\varphi_n(\lambda_1^n \mid \gamma_1^n)$, as a representation estimation criterion. In these conditions utility estimates will depend on control strategies λ_1^n, a structure choice γ_1^n as on postulated conditions. The "utility" criterion will be labeled as follows $\psi_n(\xi_1^n \mid \lambda_1^n, \gamma_1^n)$. As identification starts with a certain state $s \in S$, this criterion will depend on the state $s \in S$, assigned as the initial condition. Here the set of states S is finite, so the identification criterion will be represented by a vector $\psi_n(\xi_1^n \mid \lambda_1^n, \gamma_1^n)$ in the space R^S of the dimension $|S|$.

In a goal-seeking state situation of the quality of control strategies and structure choice is described by criteria $E\varphi_n(\lambda_1^n \mid \gamma_1^n) \in R^X$ and $\mu_n(\gamma_1^n \mid \lambda_1^n) \in R^1$ respectively. They have a meaning of specific value by a result and satisfaction with choice results. The identification strategy quality is described by the criterion $\psi_n(\xi_1^n \mid \lambda_1^n, \gamma_1^n) \in R^S$, which has a meaning of representation utility to achieve desired states. The use of introduced criteria assumes determination of corresponding information structures or models that allow making an appropriate choice.

Let us assume the existence of an information structure of representations I, which reflects subject's knowledge and experience on: modes of action (control), his own interests and preferences, dynamics of surrounding transition into different states. Therefore, it is likely that there is a structural transformation of this structure into an information structure, which enables creating a specific value criterion $E\varphi_n(\lambda_1^n \mid \gamma_1^n)$ and a domain model. Let us call such transformation a *"specific value transformation"*, and the induced information structure will be called "information structure of a specific value of a goal-seeking state situation by a result" and designated as $U = U(I)$.

In a similar way, if there is a structural transformation of the structure I into an information structure, which enables creating an identification criterion $\psi_n(\xi_1^n \mid \lambda_1^n, \gamma_1^n)$ and identification procedure models, then we will call such transformation "identification transformation" and designate it as R, an induced information structure will be called "*identification information structure*" and designated as $R = R(I)$.

Subject's representation about a goal-seeking state situation is subjective and qualitative, based on observations and analysis of the surrounding transition process affected by control $c \in C$ into various states $s \in S$. Let us indicate the rule of such transition using $q^g(S \mid S \times C)$ from $S \times C$ into S. Actually, the subject for estimation of possible result value uses the model $Q^g(X \mid X \times C)$ from $X \times C$ into X constructed by identification strategy results ξ_1^n. When constructing we take in to account control strategies λ_1^n, a structure choice γ_1^n, or it is defined by such strategies. It means that a transformation of the operational function $q^g(S \mid S \times C)$ into function of subject's understanding of the surrounding processes $Q^g(X \mid X \times Y)$ is possible only in the aposterior mode depending on used strategies $(\lambda_1^n, \gamma_1^n, \xi_1^n)$. Such transformation and construction of the desired specific value criterion $E\varphi_n(\lambda \mid \gamma_1^n)$ is possible when "utility" information structures are formed successively depending on used strategies. This condition is written as $U_n = U(\lambda_1^n, \gamma_1^n, \xi_1^n)(I)$, $n = 1,2,...$ As this condition is necessary for forming the desired utility criterion and a domain model, so it should be pointed out every time it is used. Note that the criterion $E\varphi_n(\lambda_1^n \mid \gamma_1^n)$ tacitly depends on the identification strategy ξ_1^n due to introduction an induced structure U_n into the choice model. As it was stated above, the criterion $\mu_n(\gamma_1^n \mid \lambda_1^n) \in R^1$ of the structure choice quality is determined by a criterion folding $E\varphi_n(\lambda_1^n \mid \tau_1^n) \in R^X$. Generality of information structure of their formation allows writing

$$\begin{cases} E\varphi_n(\lambda_1^n \mid \xi_1^n) \\ \mu_n(E\varphi_n(\xi_1^n \mid \lambda_1^n)) \\ U_n = U(\lambda_1^n, \gamma_1^n, \xi_1^n)(I). \end{cases}$$

To construct identification criterion we need to use a specific function, which would have a meaning of "utility". For this purpose it is necessary to construct verbal estimates on the values of a function $E\varphi^g(S \times X \times Y)$. A required transformation exists and might be performed in the aprior mode (i.e. before choosing decisions). Such transformation is determined by the subject as regard to a fuzzy measure, which might be constructed when the defined function is $q^g(S \mid S \times C)$ from $S \times C$ into S. As its analogue has a form of $Q^g(X \mid X \times C)$ in subject's mind, and he can define it in a unique manner in the information structure I, therefore, there is no need in additional transformations. "Representation utility" function construction depletes a necessary structural transformation. We will call it identification structural

transformation and define as *R*. The induced information structure will be called "Representation utility" information structure and defined as $R = R(I)$.

Taking into account these reasons an identification criterion is written as follows:

$$\begin{cases}\psi_n(\xi_1^n \mid \lambda_1^n, \gamma_1^n)\\ R = R(I)\end{cases}$$

The induced definitions and constructions show that quality criteria for strategies are different and interdependent. Therefore the choice problem has game meaning and is reduced to searching as table compromise between aiming at maximizing desired specific value of a goal-seeking state by a result and minimizing possible loss due to wrong actions. Such compromise is called *balance*.

It should be noted that the information structure $U_n = U(\lambda_1^n, \gamma_1^n, \xi_1^n)(I)$, which is a base for the criterion $\mu_n(E\varphi_n(\gamma_1^n \mid \lambda_1^n))$, must be formed consequently depending on used strategies. Thus, required balances will be interdependent not only at each step $n = 1, 2, \ldots$ of forming decisions, but they will also depend on the decisions chosen at the previous steps. Considering this fact, it is natural to call balances *dynamic*.

The triple of strategies $\{\overset{o}{\lambda}{}_1^n, \overset{o}{\gamma}{}_1^n, \overset{o}{\xi}{}_1^n\}$, which meet the conditions

$$\begin{cases}\begin{cases}E\varphi_n(\overset{o}{\lambda}{}_1^n \mid \overset{o}{\gamma}{}_1^n) \geq E\varphi_n(\lambda_1^n \mid \overset{o}{\gamma}{}_1^n) \quad \forall \lambda_1^n,\\ \mu_n(\overset{o}{\gamma}{}_1^n \mid \overset{o}{\lambda}{}_1^n) \geq \mu_n(\gamma_1^n \mid \overset{o}{\lambda}{}_1^n) \quad \forall \gamma_1^n,\\ U_n = U(\overset{o}{\lambda}{}_1^n, \overset{o}{\gamma}{}_1^n, \overset{o}{\xi}{}_1^n)(I)\end{cases}\\ \begin{cases}\psi_n(\overset{o}{\xi}{}_1^n \mid \overset{o}{\gamma}{}_1^n, \overset{o}{\lambda}{}_1^n) \geq \mu_n(\xi_1^n \mid \overset{o}{\gamma}{}_1^n, \overset{o}{\lambda}{}_1^n) \quad \forall \xi_1^n,\\ R = R(I), n = 1,2,.....\end{cases}\end{cases}$$

are called *dynamic balances.*

According to the abovementioned assumptions, the number of cycles that form decisions is unlimited. Therefore, dynamic balances must be meaningful, including the situation when $n \to \infty$.

For this purpose, it is natural to require fulfillment of the following additional conditions:

1) when $n \to \infty$ strategy quality criteria must tend to specific limits;

2) such limits cannot depend on the initial conditions.

As criteria are not assigned in an explicit form, then realization of these properties is not explicit. It requires as signing necessary properties and then indicating criteria in the explicit form, which satisfies these properties.

According to the induced assumptions, quality criteria of stationary strategies $\lambda^n, \gamma^n, \xi^n$ when $n \to \infty$ have limits. Therefore the triple of stationary strategies $(\overset{o}{\lambda}{}^{\infty}, \overset{o}{\gamma}{}^{\infty}, \overset{o}{\xi}{}^{\infty})$ is called stationary balances if there are limits that meet the conditions:

$$\begin{cases}\begin{cases}\varphi(\overset{o}{\lambda}{}^{\infty} \mid \overset{o}{\gamma}{}^{\infty}) \geq \varphi_n(\lambda^{\infty} \mid \overset{o}{\gamma}{}^{\infty}), \forall \lambda^{\infty}\\ \mu(\overset{o}{\gamma}{}^{\infty} \mid \overset{o}{\lambda}{}^{\infty}) \geq \mu_n(\gamma^{\infty} \mid \overset{o}{\lambda}{}^{\infty}), \forall \gamma^{\infty}\\ U = U(\overset{o}{\lambda}{}^{\infty}, \overset{o}{\gamma}{}^{\infty}, \overset{o}{\xi}{}^{\infty})(I)\end{cases}\\ \begin{cases}\psi(\overset{o}{\xi}{}^{\infty} \mid \overset{o}{\lambda}{}^{\infty}, \overset{o}{\gamma}{}^{\infty}) \geq \psi(\xi^{\infty} \mid \overset{o}{\lambda}{}^{\infty}\ \overset{o}{\gamma}{}^{\infty}, \forall \xi^{\infty};\\ R = R(I)\end{cases}\end{cases}$$

As a result, the content of the choice modeling problem consists in finding a compromise between aiming at achieving a maximal desired specific value by a result and minimal loss from wrong representations taking into account their mutual dependence. According to the equilibrium solution principle, compromise must be "un improvable" equally by all parts of interests.

When achieving such compromise it is fair to say that subject's interests are materialized with "the best result". Provided that dynamic balances meet the requirements of asymptotic stationary, it is also fair to say that subject's interests are materialized with "the best result" on the unlimited horizon, including $n \to \infty$. It follows that dynamic balances determine the meaning and the method of interests materializing with "the best result". Thus, dynamic balances naturally determine *internal aim* when making decisions.

4 Information structures in decision-making

The formal descriptions introduced determine not only the conditions of decision-making, but also proper a priori information carriers. Together, they form a set of the following formal properties:

S is an environment state set; $\beta(S)$ is a priori possibility distribution for a state set; *X* is a situation set; $X_S \cap X \neq \varnothing$ stands for the limitations determining the presence of the "right" ideas as diagnostics alternatives depending on $s \in S$ states; *C* is a control alternative set; $C_x \subseteq C$ means control alternative feasibility limitation depending on $x \in X$ situations; *G* is a structural alternative set; $q^g(S \mid S \times C)$ is a transitional function of $S \times C$ to *S*; $E\varphi^g(C \times (S \times X))$ stands for the utility function representing a priori preferences for $c \in C$ alternatives depending on $s \in S$ states, $x \in X$ situations and $g \in G$ structural alternatives.

This set defines an a priori information structure which is to be set according to decision-making rules.

The peculiarity of conditions of an information structure is that it is supposed to include a task of both states and situations, the choice of control actions depending on situations which, being qualitative characteristics, representing relationship to a state, are inaccessible for direct observation and need preventive maintenance.

Under these conditions, the regularity of situation dynamics cannot be set a priori. Therefore, decision-making rules suggest posing the laws of dynamics states only, defined by the $q^g(S \mid S \times C)$ transition function from $S \times C$ to *S*. In this sense, information given a priori is minimal.

In the conditions of a priori information deficiency, the minimum structure can be incomplete. Then it is necessary to introduce plausible assumptions (in the form of hypothesis set Γ) which would allow formulating a problem definition as some approach of the initial task [2]. Let us assume, for example, that in the basic information structure transfer function $q^g(S \mid S \times C)$ is not given, but there is set of hypotheses Γ of it. Then technically it can be assumed that transfer function $q^{(g,\gamma)}(S \mid S \times X)$ depends on some γ parameter getting values from given set Γ, but the true value of the parameter is unknown.

It is obvious that it will also demand the choice of the, in a sense, “best” hypothesis of a transitional function. At the same time expanded information structure completeness can be observed only according to final results of the problem research.

5 Game approach to formalization of the choice problem

Assumptions of the choice specify the existence of two aspects of an agent's interests, one of which is determined by the bias in the management of a desirable object evolution, and the other - by the choice of a preference structure. The purposeful control concept defines the third aspect of interests associated with the need for the diagnostics of the situation depending on the observed condition. In compliance with these three aspects three sets of alternatives are to be assigned: set *C*– action modes, set *G* - structural alternatives and set *X* - diagnostic alternatives. It is also assumed to assign the utility function $E\varphi^{g}(C\times S\times X)$ and the transient function $q^{g}(S\mid S\times C)$ of $S\times C$ to *S*. Assigning these objects suggests the possibility of forming the qualitative mode choice criterion as postulated by the situational control concept that makes sense of expected utility and the purposeful state situation model choice quality criterion that concerns the risk. These criteria are obviously different and in a way interdependent. The natural presumption is that in order to choose structural alternatives the corresponding quality criterion may be introduced. It differs from the rest of the criteria and in some way is dependent on the choice of other alternatives. It is commonly known that in similar conditions the problem of mode choice has a gaming intension [2]. Then each set of alternatives can be formally linked with a party concerned (a player), whose interests are related to the choice of alternatives from the corresponding set of alternatives according to their individual quality criterion. Within a set of alternatives every party has the freedom of choice. Since interests of each party represent a certain component of agent’s interests, parties are to comply with the common to them agent’s interests, when selecting alternatives. Therefore the problem of mode choice acquires a gaming content in relation to corporate interests [6], and the subject of interest plays the role of a center. He can accept the proposed trade-off alternative if it is hardly possible to improve it without infringing at least one component of interests. The compromise that meets this requirement will be called a "corporate stable equilibrium."

Conclusions

The paper considers a decision-making model for an agent, who can form internal aim and uses subjective representations on a choice situation.

It is shown that the aim of choice is to maximize a specific value of the choice situation by a result. The choice result is determined by agent’s representations on the choice situation and on his own interests. When making a decision the agent uses three sets of alternatives: controlling *C* (mode so faction), structural *G* and identification *X*. Therefore, it is possible to assume the existence of three virtual sides, which make a choice of corresponding alternatives that are balanced strategies.

References

[1]. Baranov V.V. Dynamic Equilibria in Problems of Stochastic Control and Decision Making under Uncertainty. *Journ. of Computer and Systems Sciences Int*. 2002, no. 3, pp. 409–425.

[2]. V.V. Baranov, “Methods of static equilibriums in the problems of dynamic decision making under uncertainty about the state,” / V.V. Baranov // Bulletin of RAS. Theory and managerial systems, vol. 5, pp. 45-59, 2001.

[3]. Lefevr V.A. *Konfliktuyushchie struktury* [Conflicting Structures]. Moscow, Sovetskoe radio Publ., 1973, 158 p.

[4]. Vinogradov G.P., Kuznetsov V.N. Modeling agent’s behavior taking into account subjective representations about a choice situation. *Iskusstvenny intellekt i prinyatie resheny* [Artificial Intelligence and Decision-Making].2011, no. 3, pp. 58–72 (in Russ.).

[5]. Vinogradov G.P., Borisov P.A., Semenov N.A. Integration of Neural Network Algorithms, Nonlinear Dynamics Models, and Fuzzy Logic Methods in Prediction Problems. *Journ. of Computer and Systems Sciences Int*. 2008, no. 1, pp. 72–77.

[6]. Vinogradov G.P., Shmatov G.P., Borzov D.A. Formation of agent’s representations of the domain in a situation of choice. *Programmnye produkty i sistemy* [Software & Systems]. 2015, no. 2 (110), pp. 83–94 (in Russ.).

ILLUSTRATION OF MODEL CREATION ON EXAMPLE OF APPROXIMATIONS TO THE STEADY STATE CURRENT OF CHEMICAL CYCLIC PROCESSES

Assoc. Prof. Dimitrov A.G. PhD

Institute of Biophysics and Biomedical Engineering – Bulgarian Academy of Sciences, Sofia, Bulgaria

e-mail: agd@biomed.bas.bg

Abstract: *An approach for creation of biophysically based models for the steady state current of cyclic processes is investigated. When the process (like chemical reactions) can be described by a system of linear ordinary differential equations, an analytic expression for its steady state exists. The analytic expression is especially simple for the current of single cycle processes. In biologic context, concentrations of many substances change in a very restricted (patho)physiological range. This allows neglecting some terms of the analytic expression and thus obtaining biophysically based models that are both simple and adequate for description of currents produced by enzymes, pumps or transporters. The approximations obtained could be reduced to the existing empirical models. A clear way of expanding a specific empirical model for obtaining the desired quality and range of validity is also represented. The described approach is general and can be useful for creating biophysically based models of other types of processes.*

KEYWORDS: MATHEMATICAL MODEL, CYCLIC PROCESSES, STEADY STATE CURRENT, ENZYME, TRANSPORTER, PUMP

1. Introduction

To construct an empirical model of some process one has to fit the parameters of a predefined function to some available experimental data [1]. One could construct many functions that are close to each other for some range of data. The choice of a suitable function is complex and requires taking into account specific information. The range of possibilities spans from a lucky guess to a detailed study of the underlying processes. A comparison of various alternative models may illustrate the advantages and the drawbacks of different approaches. The purpose of this paper is to illustrate important aspects of model creation on the example of the most studied chemical cyclic process – the Na+/K+ ATPase (NKA).

2. Analysis of existing NKA models

2.1. Empirical models

Cyclic processes are abundant in biologic environment. Actions of enzymes, transporters, pumps are all cyclic process. All of them collect some resources, perform the appropriate actions, release the products and then they are ready to start again thus forming a cycle. Typically, one is interested in the cumulative effect of many cycles. As a result, the steady state current or at least the average turning rate is used to characterize the cycle. The first great success was description of the steady state enzyme reaction rate – v, as a function of substrate concentration – [S], performed by Michaelis and Menten (1913) [2] and represented by eq. (1).

$$v = \frac{d[P]}{dt} = \frac{[S]*Vmax}{[S]+Km} \quad (1)$$

where Vmax is the maximal reaction rate, [P] is the product concentration, 1/Km is the substrate's affinity.

The Michaelis – Menten relation becomes a basis for many empirical models of protein kinetics. The models of DiFrancesco and Noble [3] eq. (2) and of Luo and Rudy [4] eq. (3) are those for NKA. The Luo and Rudy model has become the standard model of choice for NKA [5-12]. Empirical equations like eq. (2) and (3) are simple, easy to use and to calculate. Unfortunately it is not clear when the approximation is valid, and how to modify the equation to expand the range of validity.

$$Ipmp = P_0 \frac{[Ko]}{[Ko]+pko} \frac{[Nai]}{[Nai]+pnai} \quad (2)$$

$$Ipmp = P_0 \frac{[Ko]}{[Ko]+pko} \frac{1}{1+\left(\frac{pnai}{[Nai]}\right)^{1.5}} * \\ * \frac{1}{1+0.1245e^{-0.1\frac{FV}{RT}}+0.0365\sigma e^{-\frac{FV}{RT}}} \quad (3)$$

where P_0 is the maximal current, $\sigma = \frac{1}{7}(e^{\frac{[Nao]}{67.3}} - 1)$, [Ko], [Nai] and [Nao] are external potassium, internal and external sodium concentrations, respectively; pko and pnai are corresponding affinities; V is membrane potential; F and R are the Faraday and universal gas constants, T is the absolute temperature.

2.2. ODE models

An approach to modeling the processes that is alternative to creation of empirical models is based on studying and description of the underlying chemical reactions. The chemical reactions are usually described as series of transitions between (often unknown) states. Let us denote the probability of the i-th state by $[T_i]$. Each transition between the states i and j, is described by a rate constant – $\alpha_{i,j}$. This results in a system of linear ordinary differential equations (ODE) that potentially fully describes the reaction – eq. (4).

$$\frac{d[T_i]}{dt} = \sum_j \alpha_{i,j} [T_j] \quad (4)$$

To perform direct numerical integration one must provide all the rate constants that describe transitions between the states.

For cyclic processes it is beneficial to distinguish forward rate constants ($\alpha_{i,j}$) and backward rate constants ($\beta_{i,j}$). For NKA, there are at least 30 rate constants (15 forward and 15 backward ones) [13]. However, only some of them have been estimated [14-18]. The most common approach used in this case is the reduction of the number of states in the cycle [13, 19, 20]. Initially, Chapman et al. [21] constructed a 6-state cycle; however, even in this case, some of the 12 rate constants had to be guessed [21]. Later, a complete set of rate constants was obtained for a 4-state NKA cycle only [13, 19, 22].

The rate constants have a close relation with the thermodynamic force that drives the reaction [23, 24]. For the rate constants that form a complete cycle one could write:

$$\frac{\alpha_{1,2}\alpha_{2,3}\cdots\alpha_{n-1,n}\alpha_{n,1}}{\beta_{1,2}\beta_{2,3}\cdots\beta_{n-1,n}\beta_{n,1}} = \exp(Y/RT) = e^{X} \qquad (5)$$

where Y is the total, associated with the transported substances free energy. Further for clarity we would redefine X=Y/RT and would name X as total (driving) force.

To compensate simplifications, the reduction of the number of states in the cycle should be accompanied by more complex expressions used to define individual rate constants. Attempts were made to increase complexity of the 4-state NKA model as the simplified models faced problems to reflect inter-tissue and inter-species differences [19, 20].

2.3. Analytic models

In the steady state conditions a system of differential equations is transformed into a system of algebraic ones. This allows an exact analytic description of the steady state [23-25]. Some models are based on this observation [26-29].

The steady state current for a cyclic process looks like rational function with two terms above and n^2 terms below the line, where – n is the number of the cycle states. For a 3 – state cycle system the solution is like eq. (6):

$$Ist = \frac{\alpha_{1,2}\alpha_{2,3}\alpha_{3,1} - \beta_{1,2}\beta_{2,3}\beta_{3,1}}{\left(\alpha_{2,3}\alpha_{3,1} + \alpha_{3,1}\beta_{1,2} + \beta_{1,2}\beta_{2,3}\right) + \left(\alpha_{3,1}\alpha_{1,2} + \alpha_{1,2}\beta_{2,3} + \beta_{2,3}\beta_{3,1}\right) + \left(\alpha_{1,2}\alpha_{2,3} + \alpha_{2,3}\beta_{3,1} + \beta_{3,1}\beta_{1,2}\right)} \qquad (6)$$

The general solution for an n-state cycle [23, 24] is a direct expansion of eq. (6):

$$Ist = \frac{\alpha_{1,2}\alpha_{2,3}\cdots\alpha_{n-1,n}\alpha_{n,1} - \beta_{1,2}\beta_{2,3}\cdots\beta_{n-1,n}\beta_{n,1}}{\left(\alpha_{2,3}\cdots\alpha_{n-1,n}\alpha_{n,1} + \alpha_{3,4}\cdots\alpha_{n,1}\beta_{1,2} + (n-2)\text{ other terms in a group}\right) + (n-1)\text{ other groups}} \qquad (7)$$

Where, *Ist* as well as the rate constants have dimension of s^{-1}.

Unfortunately the rate constants in eq. (7) are still mainly unknown. The first approach to this problem is to reduce the number of states in the cycle to 2-6 and then to solve the system of ODE analytically. So obtained approximation is further transferred into an analytical function of concentrations and potential [26-28].

Another approach to the problem is also possible [29]. Instead of decreasing the number of states and complicating the individual rate constants, one could do just the opposite. That is to simplify individual rate constants by using the maximal number of states the transporter can occupy. Then, according to the mass action law, those rate constants would have a linear dependence on concentrations:

$$\alpha_k = \alpha'_k[Sb_k] \quad \beta_l = \beta'_l[Sr_l] \qquad (8)$$

where α'_k and β'_l do not depend on concentrations, $[Sb_k]$ is concentration of the k-th binding substance, $[Sr_l]$ is concentration of the l-th released substance.

Eq. (8) could transform the terms under the line in eq. (7) into a multidimensional polynomial. Then, combining equations (5, 8 and 7) one could obtain for the current:

$$Ist = \frac{e^{X} - 1}{Ae^{X} + B} \qquad (9)$$

$$A = a_0\left(1 + \sum\frac{a_{sbk}([S])}{[Sb_k]} + \sum\frac{[Sr_l]}{a_{srl}([S])}\right)$$

$$B = b_0\left(1 + \sum\frac{b_{srl}([S])}{[Sr_l]} + \sum\frac{[Sb_k]}{b_{sbk}([S])}\right)$$

where a_0, b_0 have dimension of seconds, [S] represents concentrations of all the substances, $a_{sbk}([S])$, $a_{srl}([S])$, $b_{sbk}([S])$ and $b_{srl}([S])$ have dimension of concentration, X is the driving force [29]. For NKA the driving force would be:

$$X = \frac{dGatp}{RT} + \ln\left(\frac{[ATP]}{[ADP][P][H]}\right) - 3\ln\left(\frac{[Na_o]}{[Na_i]}\right) + 2\ln\left(\frac{[K_o]}{[K_i]}\right) + (3zna - 2zk)\frac{FV}{RT} \qquad (10)$$

We see that many different models for a single underlying process could be created.

3. Discussion and recommendations

The steady state current depends on the driving force X, and concentrations of the related substances (eq. 9). Specific approximations would be appropriate in various conditions.

The processes where the driving force is close to zero would be reversible processes, where current could change direction. For them small changes in concentrations could cause large relative changes in the driving force X (eq. 10) and thus in the current. As a result, the effect of the driving force on the current could be significant for reversible processes and should be explicitly present in the model.

For irreversible processes the size of the driving force is significant ($|X| >> 0$). Then the effect of the driving force on the current would be small (eq. 9). As a result it is often neglected like in the cases of empirical models described above (eq. 2, 3).

The driving force calculation should not be a problem. An explicit presence of the driving force in eq. (9) guarantees that the direction of the current would always be correct. So models that explicitly represent the effect of the driving force would have potentially larger range of validity.

In biologic environment, the concentrations of many substances change in very restricted ranges. This could be combined with the observation that the reaction rate in the Michaelis – Menten relation (eq. 1) has a weak sensitivity to the substrate concentration. The rate is 0.1Vmax when [S] = Km/9, and it is 0.9Vmax when [S] =

9Km. In other words an 81-fold increase in substrate concentration is required for increasing the rate from 10% to 90% of the limit [30]. So by neglecting the affinities to substances whose concentrations vary significantly less than 81 times, only a small error would be introduced in a model for the steady state current (eq. 9). If only substances, whose concentrations vary within narrow ranges, are used in the cycle, the current could often be described by a single parameter – its maximal turning rate. This is usually treated as an oversimplification. Therefore, in such cases, the models like those described by eq. (2) and eq. (3) are used, where contributions of the most significant terms are present and contribution of all other terms is neglected.

Concentration of some other substances could vary much more significantly (like 81-fold or similar). That could be intracellular Ca^{++}, pH or other signaling molecules. If that substance is part of the cycle, good reasons should be present to neglect its affinity. That affinity may have complex dependence on concentrations [29].

The processes in the cycle that we have studied so far may have nothing common with the regulation of the cycle. For example, in skeletal muscles, changes in concentration of cyclic adenosine mono phosphate (cAMP) activates the related kinase that in turn, modifies NKA to augment NKA current [31, 32]. Thus to obtain a realistic model, one may need to consider several cycles with possible ligand or voltage gated transitions between them.

A proper system of differential equations could potentially fully describe the chemical processes under study when the necessary states and rate constants are available. However obtaining the states and rate constants could be problematic. When all the substances have rather stable concentrations, the steady state current would be almost equal to its maximal turning rate. Finding many rate constants from what is essentially a single current value is an impossible task. To make situation even more complex external regulation by some signaling molecules or by membrane voltage is likely to be present in that case. To take information on the rate constants, one must perform measurements of the steady state current and of the concentrations of all of the involved substances with great precision. So obtaining rate constants to construct quantitative ODE model may be a very tricky task that is not always possible.

In such complicated cases, when creating quantitative ODE model is not possible, analytic approach that lead to eq. (9) provides a valuable alternative. Thus equation (9), turns out to be a more universal candidate for a quantitative model than a system of ODE. Nevertheless a system of ODE is a great starting point for an analysis of the underlying process [29].

4. Conclusion

Life is more complex than the steady state current of cyclic processes. Models for many processes have to be created. However creation of a useful quantitative model is not an easy task. Different types of models reveal different aspects of the underlying processes. Cyclic chemical processes are sufficiently well studied to illustrate many important aspects of model creation. I hope that the analysis represented here would be helpful in creation of new models.

5. References

1. Press, W.H., et al., *Numerical recipes in C: the art of scientific computing* 1992: Cambridge University Press.
2. Michaelis, L. and M.M.L. Menten, *The kinetics of invertin action.* FEBS letters, 2013. **587**(17): p. 2712-2720.
3. DiFrancesco, D. and D. Noble, *A model of cardiac electrical activity incorporating ionic pumps and concentration changes.* Philos Trans R Soc Lond B Biol Sci, 1985. **307**(1133): p. 353-98.
4. Luo, C.H. and Y. Rudy, *A dynamic model of the cardiac ventricular action potential. I. Simulations of ionic currents and concentration changes.* Circ Res, 1994. **74**(6): p. 1071-96.
5. Wallinga, W., et al., *Modelling action potentials and membrane currents of mammalian skeletal muscle fibres in coherence with potassium concentration changes in the T-tubular system.* Eur Biophys J, 1999. **28**(4): p. 317-29.
6. Pandit, S.V., et al., *A mathematical model of action potential heterogeneity in adult rat left ventricular myocytes.* Biophys J, 2001. **81**(6): p. 3029-51.
7. Bondarenko, V.E., et al., *Computer model of action potential of mouse ventricular myocytes.* Am J Physiol Heart Circ Physiol, 2004. **287**(3): p. H1378-403.
8. Hund, T.J. and Y. Rudy, *Rate dependence and regulation of action potential and calcium transient in a canine cardiac ventricular cell model.* Circulation, 2004. **110**(20): p. 3168-74.
9. Shannon, T.R., et al., *A mathematical treatment of integrated Ca dynamics within the ventricular myocyte.* Biophys J, 2004. **87**(5): p. 3351-71.
10. ten Tusscher, K.H., et al., *A model for human ventricular tissue.* Am J Physiol Heart Circ Physiol, 2004. **286**(4): p. H1573-89.
11. Fortune, E. and M.M. Lowery, *Effect of extracellular potassium accumulation on muscle fiber conduction velocity: a simulation study.* Ann Biomed Eng, 2009. **37**(10): p. 2105-17.
12. Grandi, E., et al., *Interplay of voltage and Ca-dependent inactivation of L-type Ca current.* Prog Biophys Mol Biol, 2010. **103**(1): p. 44-50.
13. Smith, N.P. and E.J. Crampin, *Development of models of active ion transport for whole-cell modelling: cardiac sodium-potassium pump as a case study.* Prog Biophys Mol Biol, 2004. **85**(2-3): p. 387-405.
14. Schulz, S. and H.J. Apell, *Investigation of ion binding to the cytoplasmic binding sites of the Na,K-pump.* Eur Biophys J, 1995. **23**(6): p. 413-21.
15. Schneeberger, A. and H.J. Apell, *Ion selectivity of the cytoplasmic binding sites of the Na,K-ATPase: I. Sodium binding is associated with a conformational rearrangement.* J Membr Biol, 1999. **168**(3): p. 221-8.
16. Holmgren, M., et al., *Three distinct and sequential steps in the release of sodium ions by the Na+/K+-ATPase.* Nature, 2000. **403**(6772): p. 898-901.
17. De Weer, P., D.C. Gadsby, and R.F. Rakowski, *Voltage dependence of the apparent affinity for external Na(+) of the backward-running sodium pump.* J Gen Physiol, 2001. **117**(4): p. 315-28.
18. Gadsby, D.C., et al., *The dynamic relationships between the three events that release individual Na(+) ions from the Na(+)/K(+)-ATPase.* Nat Commun, 2012. **3**: p. 669.
19. Garcia, A., et al., *Kinetic comparisons of heart and kidney Na+,K(+)-ATPases.* Biophys J, 2012. **103**(4): p. 677-88.
20. Lewalle, A., S.A. Niederer, and N.P. Smith, *Species-dependent adaptation of the cardiac Na+/K+ pump kinetics to the intracellular Na+ concentration.* J Physiol, 2014. **592**(24): p. 5355-71.
21. Chapman, J.B., E.A. Johnson, and J.M. Kootsey, *Electrical and biochemical properties of an enzyme model*

of the sodium pump. J Membr Biol, 1983. **74**(2): p. 139-53.
22. Oka, C., C.Y. Cha, and A. Noma, *Characterization of the cardiac Na+/K+ pump by development of a comprehensive and mechanistic model.* J Theor Biol, 2010. **265**(1): p. 68-77.
23. Hill, T.L., *Free energy transduction in biology: the steady-state kinetic and thermodynamic formalism*. 1977, New York: Academic Press. xii, 229 p.
24. Hill, T.L., *Free energy transduction and biochemical cycle kinetics*. 1989, New York: Springer-Verlag. 119 p.
25. King, E.L. and C. Altman, *A Schematic Method of Deriving the Rate Laws for Enzyme-Catalyzed Reactions.* The Journal of Physical Chemistry, 1956. **60**(10): p. 1375-1378.
26. Hernandez, J., J. Fischbarg, and L.S. Liebovitch, *Kinetic model of the effects of electrogenic enzymes on the membrane potential.* J Theor Biol, 1989. **137**(1): p. 113-25.
27. Gadsby, D.C. and M. Nakao, *Steady-state current-voltage relationship of the Na/K pump in guinea pig ventricular myocytes.* J Gen Physiol, 1989. **94**(3): p. 511-37.
28. Sagar, A. and R.F. Rakowski, *Access channel model for the voltage dependence of the forward-running Na+/K+ pump.* J Gen Physiol, 1994. **103**(5): p. 869-93.
29. Dimitrov, A., *An approach to expand description of the pump and co-transporter steady-state current.* Journal of theoretical biology, 2017. **412**: p. 94-99.
30. Cornish-Bowden, A., *Fundamentals of enzyme kinetics.* 2012, Weinheim, Germany: Wiley-Blackwell.
31. Clausen, T., *The sodium pump keeps us going.* Ann N Y Acad Sci, 2003. **986**: p. 595-602.
32. Clausen, T., *Quantification of Na+,K+ pumps and their transport rate in skeletal muscle: functional significance.* J Gen Physiol, 2013. **142**(4): p. 327-45.

STOCHASTIC COMPUTER SIMULATION OF THE IONIC DIFFUSION THROUGH BIOLOGICAL TISSUES UNDER THE EFFECT OF DIRECT ELECTRIC FIELD

MSc. Fawzy HM[1], Associate Prof. Dr. Salem NM[2], Prof. Dr. El Sheikh SM[1] and Prof. Dr. El-Messiery MA[2]

Department of Physics, American University in Cairo, AUC Avenue, P.O. Box 74, New Cairo 11835, Egypt[1]

Department of Engineering Mathematics and Physics, Faculty of Engineering, Cairo University, Giza 12613, Egypt[2]

nmsalem@aucegypt.edu

Abstract: *The effect of the exposure of biological tissues to external electric fields is still a potent source of controversy. This work addresses the diffusion of ions under the effect of an of an external DC electric field. This was done by studying the diffusion coefficient D as an indicating parameter for such effects. The work was based on a stochastic computer simulation in which the tissue was considered as a matrix containing the elements under study. The size of the matrix was up to 30,000 × 30,000. A two-dimensional honey comb cellular pattern was simulated such that it allowed six maximum possible element-to-element communications. The effect of vacancy concentration and annealing time were tested firstly in the absence of electric field. Then different values of the electric field were applied. Moreover, different vacancy concentrations were studied under the effect of the electric field. The results showed that the ionic penetration increases proportionally with the strength of the electric field as well as the percentage of the available vacancies in the host medium.*

.

Keywords: IONIC DIFFUSION, BIOLOGICAL TISSUES, STOCHASTIC SIMULATIONS

1. Introduction

Many theoretical efforts have been devoted to studying diffusion in different media. Electric fields enhance the diffusion of charge carriers in disordered materials. It was shown that the diffusion coefficient in one-dimensional hopping depends linearly on the electric field, while in three dimensions the dependence is quadratic [1].

Diffusion takes place in biological tissues as well. The effective diffusion coefficient, D_{eff}, of salt into a biological tissue due to the application of an electric field at different temperatures showed an increase of ion transport [2]. The effective diffusion coefficients of K+ and Cl− ions are appreciably reduced in narrowing the channel in the cell membrane when subjected to an external field. The extent of the reduction is similar for both the anionic and cationic species [3].

Diffusion in the extracellular space (ECS) is constrained by the volume fraction, hence a modified diffusion equation was proposed to govern the transport behavior of many molecules in the brain [4].

Liu and Shi [5] developed two-dimensional and three-dimensional FEM model to study the transport of ionic species in an externally applied electric field. They found that more chlorides are driven out of samples with increasing direct current density and treatment time.

In the present work we introduce a stochastic model to follow and determine the diffusion coefficient of an ionic tracer through a biological tissue. Hence, the effect of the application of an external DC field on the diffusion and the penetration depth of these ions in biological tissue is studied.

2. Computer Model

The present model simulates the ionic diffusion under the following assumptions: A part of the biological tissue is represented as a 2D matrix of sizes up to 30,000 × 30,000 elements. Each element represents either a host particle, a vacancy or a tracer ion. The diffusants (tracers), are considered as positive ions.

At zero time, the diffusants occupy the first row of the matrix and are in a continuous flow; each particle that leaves the surface into the matrix is replaced by another one. The rest of the matrix is either occupied by the host elements (biological cells) or with vacancies that are randomly distributed throughout the matrix. The characteristics of each element are represented by one byte which contains information of the type (host, vacancy or tracer), spatial location and the time elapsed since diffusion starts. The biological tissue could be simply modeled as a close-packed spherical array of cells as shown in Fig. 1.

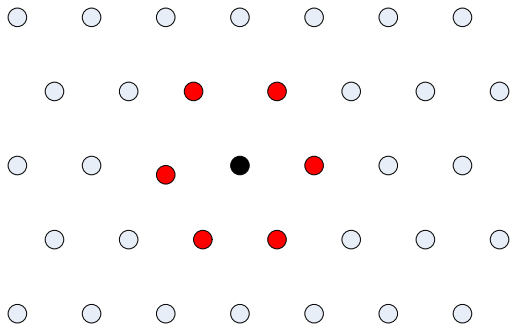


Fig. 1. *The six neighbors' structure in a hexagonal matrix modelling a biological tissue. The middle black element is the tracer with six neighboring vacancies represented by red circles.*

Since the diffusion process follows a random walk procedure, in the present model the tracer ion diffuses through the vacancies available in the nearest sites such that the jump follows a random choice of the accessible vacancies. The effect of the electric field is represented as a controlled bias in the jump direction. The field direction affects the randomization process of jumping so that along the direction of the field there is a higher probability than other directions. Fig. 2 shows a visualization of the system under consideration, for both cases of free diffusion and the diffusion under the effect of a DC electric field.

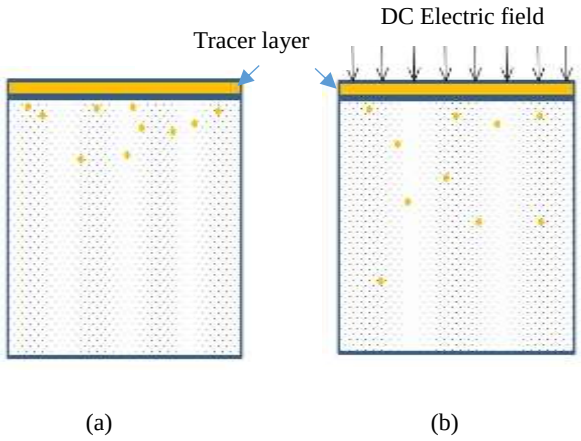


Fig. 2. *The diffusion process (a) in the absence of external field and (b) under the effect of DC electric field. The traces are represented by the larger circles.*

Hence the concentration $c(x,t)$ of the ions/tracer after a certain time t and a location x is obtained from the following

$$c(x,t) = constant \times e^{\frac{-x^2}{4Dt}}$$

The mean squared radius of the diffusion pattern is represented by:

$$< R^2 >= \sum_{i=1}^{N} R_i^2 / N$$

where N is the number of jumps and R_i is the individual displacement.

The diffusion coefficient D can be calculated from the slope of $< R^2 >$ versus the annealing time t:

$$D = < R^2 > / 4t.$$

The concentration is calculated by sectioning the matrix to a certain number of rows and calculating the number of the tracer ions in each section. As the thickness of the layers becomes smaller, the accuracy of the penetration profile which describes the diffusion increases. Plotting the logarithm of the concentration $c(x,t)$ against x^2 for different time steps and different vacancy concentrations is used to obtain the diffusion coefficient D according the equation

$$Slope = -1 / 4Dt.$$

The annealing time is taken as the total number of iterations which is varied up to 500,000 time steps. The vacancies are randomly distributed, and their concentration is varied from 5% to 80%.

3. Results

Firstly, the diffusion pattern is investigated in the absence of an external field and assuming that all the sites are vacant. Figs. 3 and 4 show the relation of the mean squared displacement, $<R^2>$, and the diffusion coefficient, D, as a function of time.

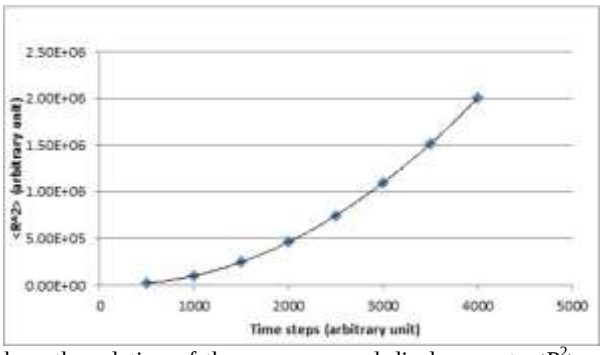


Fig. 3. *Variation of the mean squared radius and time steps in the case of free diffusion.*

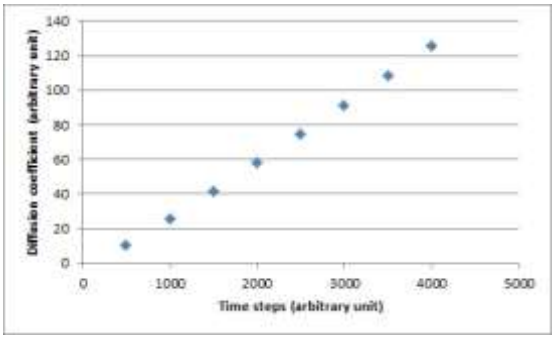


Fig. 4. *The diffusion coefficient with time steps.*

In both figures, the classical pattern of the random walk diffusion in the absence of external field is preserved. The diffusion coefficient increases linearly with annealing time. The penetration depth $< R^2 >$ of the tracers is studied in the presence of randomly distributed vacancies of different ratios in a biological tissue. Fig. 5 shows the increase in the penetration distances of the tracers with annealing time at a vacancy concentration of 50%. In this figure the time steps are increased up to 1.2 millions so that the asymptotic level of the curve is obtained; at this level the penetration distance is about to reach the boundaries of the matrix.

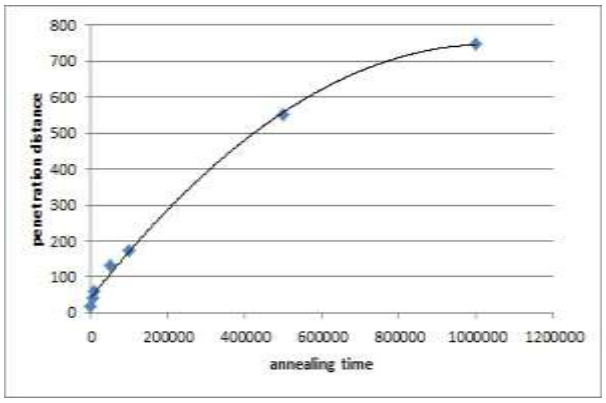


Fig. 5. *The variation of penetration distance (arbitrary units) with the annealing time.*

Fig. 6 show the mean penetration distance with vacancy concentration. It is obvious that at low vacancy percentage up to 20% , the tracers hardly invade the host matrix. Then, $< R^2 >$ increases almost linearly. Similar behavior is observed when the diffusion coefficient is plotted versus the vacancy concentration. Fig. 7 illustrates this relation in absence of external field and for a fixed annealing time.

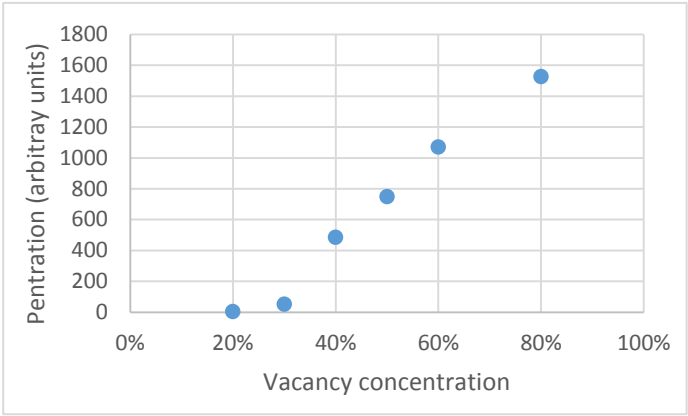


Fig. 6. *The variation of the penetration with vacancy concentration.*

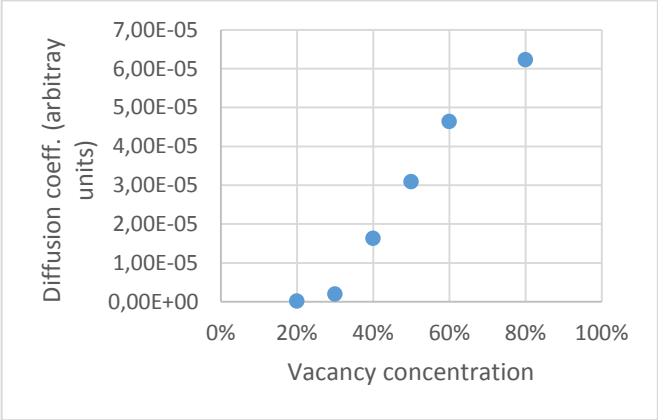


Fig. 7. *The variation diffusion coefficient with vacancy concentration.*

The diffusion of positive ions in a biological host under the effect of DC electric field is then examined for different field strengths, different annealing times and varying vacancy concentrations. Considering the matrix having a 90% vacancy and the DC electric field, EF, is increasing gradually (EF=0 % , 10%, and 70%), the diffusion pattern of the tracer in the host matrix is illustrated in Fig. 8. We infer that the concentration of the diffused ions travels deeper as a result of increasing the electric field strength.

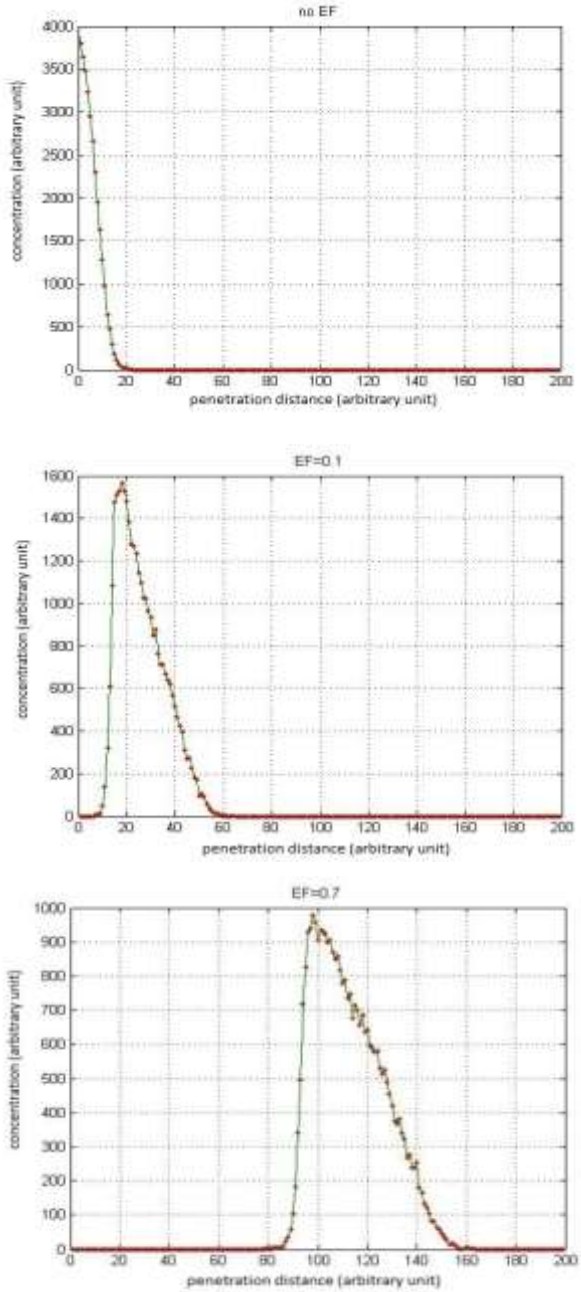


Fig. 8. *Penetration profiles for ions in a 90% vacant matrix under the effect of direct electric field for different strengths, namely, EF=0 %, 10%, and 70% and for constant annealing time.*

Fig. 9 illustrates the increase in the diffusion coefficient with the strength of the external field at a constant vacant percentage and for the annealing time.

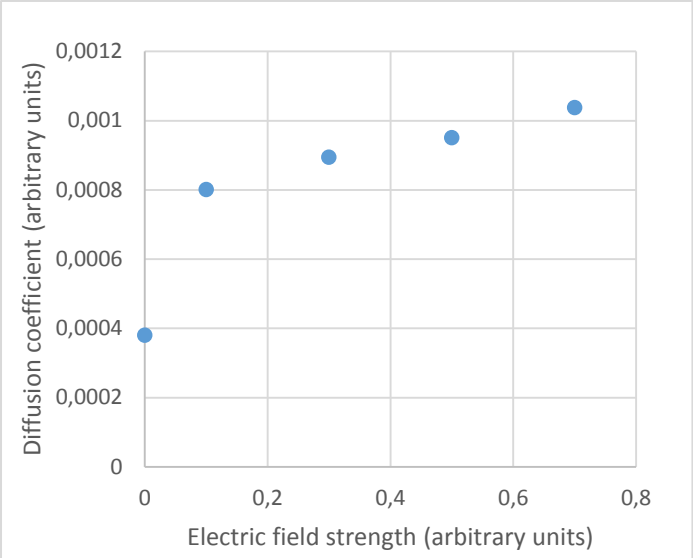


Fig. 9. *Variation of diffusion coefficient with electric field strength.*

4. Discussion and Conclusion

In the present work we have considered the profile of ionic diffusion in a biological tissue under the effect of DC electric fields. Initially, in the absence of an electric field and the vacancies occupy 0-30% of the host tissue, we found that the penetration of diffusing ions and the diffusion coefficient doesn't increase much. As the percentage of vacancies increases more than 30%, the penetration of the diffusing ions and the diffusion coefficient increase linearly with the vacancies concentration.

Preliminary results showed that when the matrix is 50% vacant, as the EF increases the penetration increases up to a point after which it decreases again. This happens because there is no much space for the movement of the ions, they are hindered by the matrix structure. As the percentage of vacancies increases the penetration of the diffusants ions increases. This increase is accelerated with the applications of an external field EF. The positive ions have more space and more probability to jump forwarded aided by the applied field.

In conclusion the present work introduces a stochastic model that tackles the problem of ionic diffusion in a biological tissue. Emphasis is given to the effect of both the existence of different percentage of vacancies available for random jumps and the effect of an external DC field of different strengths.

References

[1] F. Jansson, A.V. Nenashev, S.D. Baranovskii, F. Gebhard, and R. Österbacka, "Effect of electric field on diffusion in disordered materials.," *Annalen der Physik*, vol. 18, pp. 856 – 862, 2010.

[2] C. Kusnadi and S. K. Sastry, "Effect of moderate electric fields on salt diffusion into vegetable tissue.," *Journal of Food Engineering*, vol. 110, no. 3, pp. 329-336, 2012.

[3] G. R. Smith and M. S. P. Sansom, "Effective diffusion coefficients of K+ and Cl− ions in ion channel models. ," *Biophysical Chemistry*, vol. 79, no. 2, pp. 129-151, 1999.

[4] E. Syková and C. Nicholson, "Diffusion in brain extracellular space.," *Physiological Reviews*, vol. 88, no. 4, pp. 1277-1340, 2008.

[5] Y. Liu and X. Shi, "Ionic transport in cementitious materials under an externally applied electric field: Finite element modeling," *Construction and Building Materials*, vol. 27, no. 1, pp. 450-460, 2012.